Energy-efficient PLIA-RWA Algorithms for Transparent Optical Networks

Submitted in fulfilment of the requirements of the degree of Doctor of Engineering: Electrical Engineering in the Faculty of Engineering and the Built Environment at the Durban University of Technology

Andrew Mutsvangwa

OCTOBER 2016

Supervisor: Professor B. Nleya Date:…….

Abstract

The tremendous growth in the volume of telecommunication traffic has undoubtedly triggered an unprecedented information revolution. The emergence of high-speed and bandwidth-hungry applications and services such as high-definition television (HDTV), the internet and online interactive media has forced the telecommunication industry to come up with ingenious and innovative ideas to match the challenges. With the coming of age of purposeful advances in Wavelength Division Multiplexing (WDM) technology, it is inherently practically possible to deploy ultra-high speed all-optical networks to meet the ever-increasing demand for modern telecommunication services. All-optical networks are capable of transmitting data signals entirely in the optical domain from source to destination, and thus eliminate the incorporation of the often bulky and high-energy consuming optical-to-electrical-to-optical (OEO) converters at intermediate nodes. Predictably, all-optical networks consume appreciably low energy as compared to their opaque and translucent counterparts. This low energy consumption results in lower carbon footprint of these networks, and thus a significant reduction in the greenhouse gases (GHGs) emission. In addition, transparent optical networks bring along other additional and favourable rewards such as high bit-rates and overall protocol transparency. Bearing in mind the aforementioned benefits of transparent optical networks, it is vital to point out that there are significant setbacks that accompany these otherwise glamourous rewards. Since OEO conversions are eliminated at intermediate nodes in all-optical networks, the quality of the transmitted signal from source to destination may be severely degraded mainly due to the cumulative effect of physical-layer impairments induced by the passage through the optical fibres and associated network components. It is therefore essential to come up with routing schemes that effectively take into consideration the signal degrading effects of physical-layer impairments so as to safeguard the integrity and health of transmitted signals, and eventually lower blocking probabilities. Furthermore, innovative approaches need to be put in place so as to strike a delicate balance between reduced energy consumption in transparent networks and the quality of transmitted signals. In addition, the incorporation of renewable energy sources in the powering of network devices appears to gain prominence in the design and operation of the next-generation optical networks.

The work presented in this dissertation broadly focuses on physical-layer impairment aware routing and wavelength assignment algorithms (PLIA-RWA) that attempt to: (i) achieve a

sufficiently high quality of transmission by lowering the blocking probability, and (ii) reduce the energy consumption in the optical networks. Our key contributions of this study may be summarized as follows:

Design and development of a Q-factor estimation tool.

Formulation, evaluation and validation of a QoT-based analytical model that computes blocking probabilities.

Proposal and development of IA-RWA algorithms and comparison with established ones.

Design and development of energy-efficient RWA schemes for dynamic optical networks.

Declaration of Originality

I hereby declare that the information presented in this thesis is my original work and has not been submitted for a degree at any other university, and its prior publication was in the form of conference papers and / or journal articles. Any information derived from others and used in this thesis, has, to the best of my knowledge been acknowledged in the text and referenced according to the Durban University of Technology requirements.

Dedication

This work is dedicated to:

My wife, Evernice, and my kids, Edina (Jr.) and Tafara for their unwavering support, love, patience and encouragement.

My mother, Edina (Snr.), who taught me to trust in the Almighty God and to believe in hard work and that so much could be done if you persevere.

My late father, Noel, for the unparalleled support and encouragement to continue seeking knowledge.

Acknowledgements

I would like to express my sincere gratitude to the following people who helped me to complete this work:

My supervisor, Professor B. Nleya, for his professional advice, motivation, guidance and patience. I will forever remain indebted to you and hold you in high esteem. Without your vision and wisdom, this work would not have been completed.

The DUT Financial Aid Scheme for generously funding my studies, I greatly appreciate your kind assistance.

Special acknowledgement goes to Dr M.L. Hove for spending much time editing this thesis and for some insightful suggestions during my course of study. Thank you very much, your effort is greatly appreciated!

Above all, I would like to thank my creator, The Almighty God for the strength and perseverance to complete the studies. Indeed, nothing is impossible in the presence of The Almighty God!

List of Abbreviations and Acronyms

ASE	Amplified Spontaneous Emission
BER	Bit Error Rate
CAPEX	Capital Expenditure
CD	Chromatic Dispersion
DSF	Dispersion Shifted Fibre
EDFA	Erbium Doped Fibre Amplifier
FC	Filter Concatenation
FWM	Four Wave Mixing
GVD	Group Velocity Dispersion
HDTV	High Definition Television
IA-RWA	Impairment Aware Routing and Wavelength Assignment
ICT	Information and Communication Technology
ILP	Integer Linear Programming
ISI	Inter Symbol Interference
LCP	Least Congested Path
LP	Linear Programming
OADM	Optical Add Drop Multiplexer
OEO	Optical Electronic Optical
OPEX	Operational Expenditure
OSNR	Optical Signal to Noise Ratio
OTN	Optical Transport Network
OXC	Optical Cross Connect
PLD	Permanent Lightpath Demand
PLI	Physical Layer Impairments
PLIA-RWA	Physical Layer Impairment Aware Routing and Wavelength Assignment
PMD	Polarization Mode Dispersion
QoS	Quality of Service
QoT	Quality of Transmission
ROADM	Reconfigurable Add Drop Multiplexer
RWA	Routing and Wavelength Assignment
SG	Smart Grid
SPM	Self Phase Modulation

TON	Transparent Optical Network
WDM	Wavelength Division Multiplexing
XPM	Cross Phase Modulation
XT	Crosstalk

Contents

1 Evolution of Optical Telecommunication Networks

1.1 Introduction

The mammoth growth of traffic demand driven largely by the brisk increase in the usage of Internet and emerging online services creates new challenges for communication networks [1]. In order to meet the demand for efficient long-haul telecommunication, optical communication systems have been identified as the vehicle for the realisation of such an important and necessary goal. Amongst a host of available telecommunication systems, optical communication systems are serious contenders for this kind of a task since optical fibres possess unprecedented bandwidth capacity and thus consumers are guaranteed of very fast communication [2].

The development of high speed networks has undoubtedly increased the energy consumption of telecommunication networks and thus the need to reduce their power usage. In the information and communication technology (ICT) sector, telecommunication was the largest electricity consuming category worldwide in 2012. This was mainly due to the increased interconnectivity of digital equipment and substantial growth in the telecom operator networks [3], [4].

Figure 1.1 shows the global ICT energy demand from 2010 and projected to 2030 [5]. It can be clearly seen that the energy demand increases exponentially for the stated period, and it is very vital to put measures in place to curtail an energy consumption of such magnitudes in the ICT sector.

According to researchers at the Centre for Energy-Efficient Telecommunications (CEET) at the University of Melbourne and Bell Labs, the ICT sector annually produces more than 830 million tonnes of carbon dioxide, the main greenhouse gas (GHG). This emission accounts for approximately 2 % of the global carbon dioxide emissions and it is projected that the figure will double by 2020 [6].

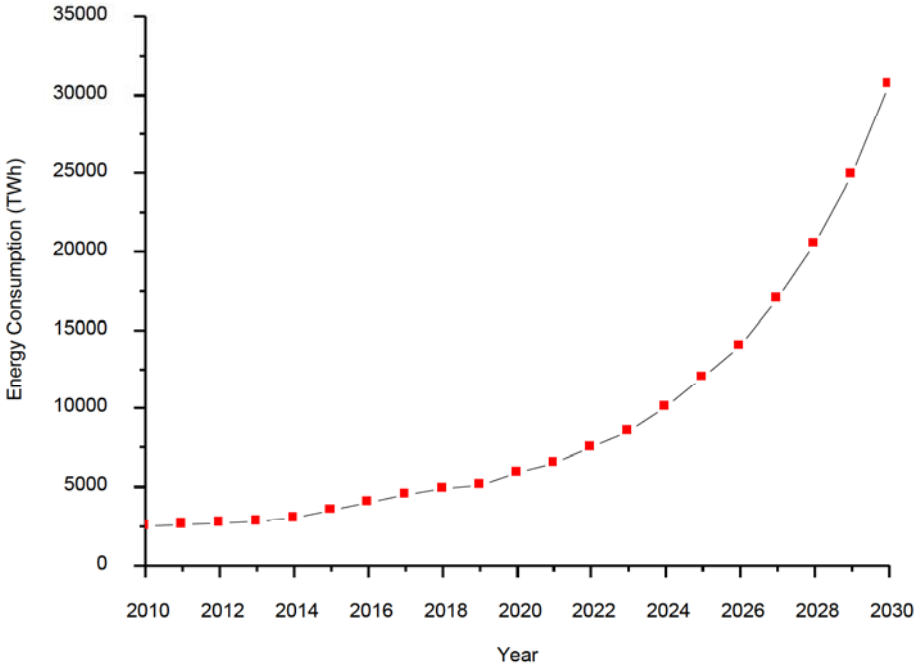

Figure 1.1: Global ICT energy demand

Energy costs are among the largest contributors to high opex for telecommunications network companies, and energy consumption by telecommunications networks significantly leads to increased global GHG emissions. Since there is an upsurge in the number of people worldwide who are becoming connected to fixed and mobile telecommunications networks, the challenges related to providing electricity to these expanding networks have justifiably taken centre-stage and innovative solutions are desperately required to avert potential disasters such as floods. One novel way of reducing the global carbon footprint of telecommunication networks is the use of renewable energy sources in powering pertinent infrastructure such as data centres.

If we consider the general energy consumption of ICT networks, we should examine three crucial factors that influence changes in absolute energy usage, and these are: (i) the number of devices, (ii) the demand for bandwidth and (iii) energy efficiency. By considering ICT traffic projections on the current reposition to cloud services and data-intensive services such as HDTV, traffic is expected to increase by more than 40 % annually, roughly doubling every two years [7]. Unfortunately, network equipment energy efficiency appears to lag behind in this endeavour as it is projected to only improve by 10 – 20 % annually [8]. This implies that more network equipment will be required to sufficiently handle the increased demand in traffic and thus leads to more energy consumption. Currently, energy consumption of devices is not highly prioritized for most network operators and it is expected that this approach will

radically change in the near future. The prevailing state of affairs create an environment in which devices are always powered on and where they consume energy notwithstanding the traffic load. Generally, the basic network infrastructure comprises of three major domains, namely, the access network, the metropolitan network and the core network. The energy consumption of these domains is estimated at 1 % of the total electricity usage in broadband-enabled states [7].

Access networks usually connect end-users to a central office, which is normally connected to a metropolitan or core network. They make up the larger part of the telecommunication network and are thus responsible for a sizeable amount of overall network energy consumption due to the existence of a significant number of power consuming elements. Metropolitan networks are regional networks that typically span cities, and their main function is to aggregate outgoing traffic from and distribute incoming traffic to users. They are either directly connected to big organizations or linked to access networks that are responsible for individual client traffic. A core (or backbone) network normally refers to the cardinal segment of a telecommunication network. The core network connects primary nodes, typically connecting large cities in a nationwide network to allow for long-haul communication and is connected to other core networks and is responsible for transporting large amounts of traffic.

Presently, evidence at hand indicates that access networks dominate data traffic energy consumption and their energy usage is proportional to the number of subscribers [9]. On the other hand, energy consumption of the core network is mainly dependent on traffic volume and it is expected to surpass the zettabyte threshold in the near future. It can therefore be argued that given the projected upsurge of traffic volumes of the future networks, energy consumption of the core networks is certainly most likely to outpace the energy consumption of the access networks [7], [8].

Authors in [8] report in their work that the core network will consume about 34.5 % of the overall network energy as the access network speed per household transcends 100 Mbps, assuming that the annual energy efficiency of network elements increases by 10 %. In related studies, researchers in [10] predict that energy consumption of the core network will exceed that of access networks beyond the year 2020.

To buttress the urgent need to curtail energy usage in core networks, authors in [9] report that energy efficiency in core networks will improve by 64 % in the year 2020 compared to that

of the year 2010, whereas energy efficiencies in the wireless and wired access networks is expected to increase by an impressive 1043 % and 449 % respectively during the same period.

Table 1.1 shows an energy consumption forecast for current and future networks that is mainly driven by unprecedented ubiquity in broadband applications as well as the tremendous growth in mobile devices applications and services [11].

Table 1.1: Energy consumption of key optical devices.

Network Domain	Device	Capacity	Power Consumption
Backbone network	Core router	10 Gbps	25 – 68.5 kW
	Amplifier	1 fibre	46 – 106 W
	Regenerator	Per lightpath	6 – 80 W
	Converter	Per lightpath	0.5 – 2 W
	WDM transponder	40 Gbps	60 – 100 W
	OXC	2-degree	25 – 68.5 W
Metro network	Edge switch	160 Gbps	4.21 kW
	OADM	N/A	450 W
	Ethernet switch	720 Gbps	3.21 kW
	Gateway switch	8 Gbps	1.1 kW
	Edge LAN switch	48000 Mbps	100 – 300 W
Access network	10/100 hub	1200 Mbps	12 – 35 W
	WAP	54 Mbps	8 – 13 W
	OLT	1 Gbps	100 W
	Telephony sub-switch	2000 subscribers	6 kW
	ONU	1 Gbps	5 W
Household network	Modem	Up to 300 Mbps	5.7 W
	Router	Up to 500 Mbps	5.7 W
	Access point	-	1.9 W
	Switch	Up to 500 Mbps	2.6 W
	ONTs	Up to 600 Mbps	16.2 W

It can be clearly observed from Table 1.1 that a core router in a backbone network consumes a substantial amount of energy as compared to other devices in different network domains, and this further cements the need to come up with realistic strategies to contain and reduce energy usage in core networks. Given the abovementioned scenario, it is not surprising therefore that significant strides are being made by research community in seeking redress in as far as energy consumption in backbone networks is concerned. Researchers in [12]-[15] review a number of energy-efficient technologies and energy-aware strategies aimed at reducing energy usage in current and future networks, and the proposed solutions may be classified into the following four broad categories:

1) **Network redesign**: Designing energy-efficient networks using optical and electronic technologies;

2) **Traffic engineering**: Developing energy-aware traffic grooming schemes;

3) **Energy-aware networking**: Powering devices ON/OFF between different operating states;

4) **Load-adaptive operation**: Adopting rate-adaptive and multi-line/link rate techniques.

Since optical networks form the backbone of the telecommunications networks, it is vital to focus our attention on reducing their energy consumption and consequently lower their carbon footprint. With the emergence of the concept called *green telecommunications*, it is prudent to design effective and efficient algorithms that also take care of the energy consumption of optical networks [16].

The use of Wavelength Division Multiplexing (WDM) technology is certainly a clear contender for extensive use in current and next generation optical networks (Figure 1.2). These networks offer a myriad of advantages that include high-speed end-to-end connectivity [17] and fault-tolerance [2], [18]. WDM networks have the capacity of transporting hundreds of wavelength channels on a suitable single optical fibre at bit rates of 10 Gbits/s, 40 Gbits/s or even 100 Gbits/s per channel. Most routing and wavelength assignment (RWA) algorithms generally base their routing decisions on the availability of network resources and thus do not factor in the presence of physical layer impairments [19], [20].

In practice, physical impairments such as Chromatic Dispersion (CD), Polarization Mode Dispersion (PMD) and Four Wave Mixing (FWM) degrade the quality of the propagating optical signal in optical networks. Since future optical networks are expected to be fully transparent, it implies that the optical signals will experience severe physical impairments and thus degrade the quality of the signals [18]. It is therefore imperative that measures are put in place to ensure the provision of acceptable Quality of Service (QoS) and resilience in these networks.

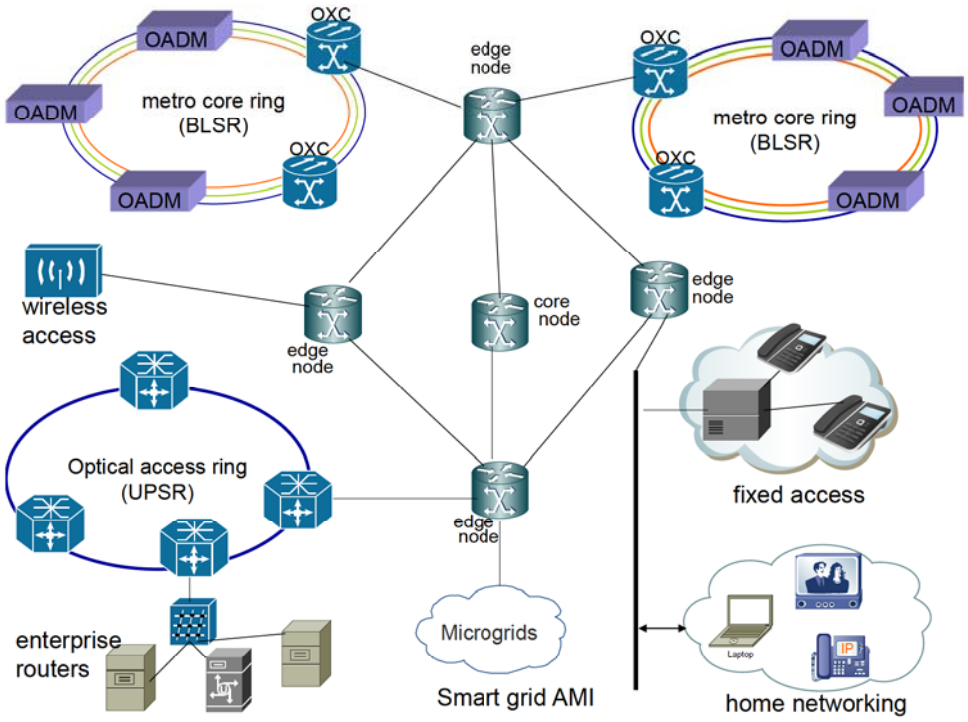

Figure 1.2: A communication network structure

Routing in WDM networks initializes with a connection request and it ideally results in the establishment of a lightpath between a source and a destination node. Path establishment is the process of selecting a distinct path from a pool of available paths and wavelength assignment is the actual selection of a path among a host of wavelengths [21].

1.2 History of Optical fibre communication systems

In September 1970, Corning Glass Works announced that it had successfully developed an optical fibre that had a very low attenuation at the 633 nm wavelength. This development undoubtedly marked the beginning of the era of fast telecommunication systems via the deployment of optical fibres.

With the fabrication of the first Laser in the preceding decade, researchers from leading telecommunications companies and institutions worked tirelessly to come up with building blocks for the first functional optical fibre telecommunications system.
With the development of the ruby and the helium-neon lasers in 1960, lasers went through significant and important evolutions. The arrival of the semiconductor laser on the scene in 1962 was a major turning point in the history of the now multi-billion dollar optical telecommunications sector. These lasers are the type most widely utilized in modern day optical communications networks.

The world's first operational optical fibre communication system was developed in 1977 by General Telephone and Electronics in California and it ran at 6 Mbps. The first generation optical fibre networks could transmit information for a few kilometres and were heavily limited by their optical fibre attenuation rates that were approximately 2.0 dB/km [22], [23].

The deployment of the second generation of optical fibre communication systems was largely enabled by the replacement of multimode fibres by single-mode fibres. The reach of first generation optical communication systems was severely limited due to the undesirable effects of intermodal dispersion which seriously degraded the integrity of propagating signals. Intermodal dispersion arises due to the dependence of the group velocity of a propagating signal in a multimode optical fibre on both the path and optical frequency of the signal. In single-mode fibres, only one path is available and thus intermodal dispersion is eliminated.
Due to rapid advances in the development of semiconductor electronic devices in the 1980s, the first transatlantic system called TAT-8 was developed, and was commissioned in 1988 [24].

The development of dispersion shifted fibres (DSF) together with the evolution of semiconductor lasers with narrow-linewidths spearheaded the deployment of third generation optical communications systems. A DSF is a single-mode fibre that has a modified zero-dispersion wavelength shifted from the 1300 nm to the 1550 nm low-loss window.

With the development of optical amplifiers, it was possible to tap the vast amount of bandwidth offered by the optical fibre via the utilization of the wavelength division multiplexing (WDM) technique. Consequently, it became possible to simultaneously amplify signals without the use of optical-electrical-optical (OEO) conversions on every intermediate node. These developments gave birth to the fourth generation optical fibre communication systems.

The emergence of optical cross-connects (OXC) and reconfigurable optical add-drop multiplexers (ROADM) on the market marked the birth of the fifth generation optical networks. Incorporation of these devices in optical networks facilitates very fast all-optical switching and ultrafast data transmission and modest automation levels and thus a steady departure from traditional manual network configuration [25].

1.3 Elements of Optical Networks

The purposeful design and deployment of advanced optical network elements evidently led to the dramatic evolution of optical communications systems. This evolution inadvertently made optical communication systems networks of choice for the 21st century.

One major trait of the modern optical network elements, is their ability to largely process and allow a signal to traverse the network in the optical domain and thus reduce the number of optical-electrical-optical (OEO) conversions that characterised pioneering optical communication systems. The reduction of the OEO converters in optical networks is a very welcome development since they are generally bulky, expensive, reduce network speeds and consume a lot of energy.

1.3.1 Optical Add-Drop Multiplexers (OADMs)

The transition from single wavelength point-to-point transmission channels to wavelength division multiplexing networks necessitated the need for the development of optical add-drop multiplexers (OADM). These devices are capable of routing or separating different wavelength channels and can be used at different points along an optical link (Figure 1.3). Due to their flexibility, OADMs are widely deployed in WDM metropolitan area networks (MAN) since they are capable of transmitting different data rates in different channels.

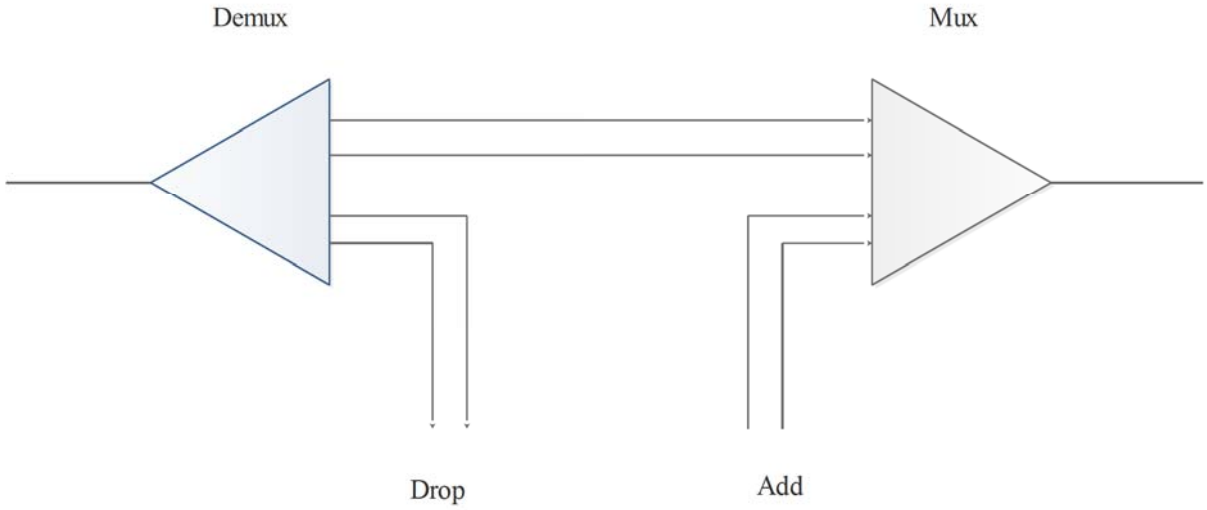

Figure 1.3: Schematic diagram of an optical add-drop multiplexer (OADM)

1.3.2 Reconfigurable Optical Add-Drop Multiplexers (ROADMs)

The initial OADMs were fixed devices and only pre-determined wavelengths could enter or leave the node and thus it was imperative to develop devices that are flexible and able to get rid of inconveniences such as remote programming of the OADMs.

In response to this challenge, reconfigurable optical add-drop multiplexers (ROADMs) were developed that are capable of splitting the incoming optical signal between the drop and straight through paths, and then using wavelength blockers to eliminate individual wavelengths on each path. Advances in the development of tuneable lasers and wavelength-selective switching technology, gave birth to the latest generation of ROADMs. These

ROADMs can handle any wavelength on any port and can connect signals flowing in any direction on any port to any other port [26].

1.3.3 Optical Cross-Connects (OXCs)

Cross-connection of channels is an important function in most communication systems. In typical all-optical networks, optical cross-connects (OXCs) perform the routing and switching functions entirely in the optical domain at each node in the network (Figure 1.4). OXCs are also capable of grooming traffic and can process sophisticated wavelength management tasks in complex network topologies [27].

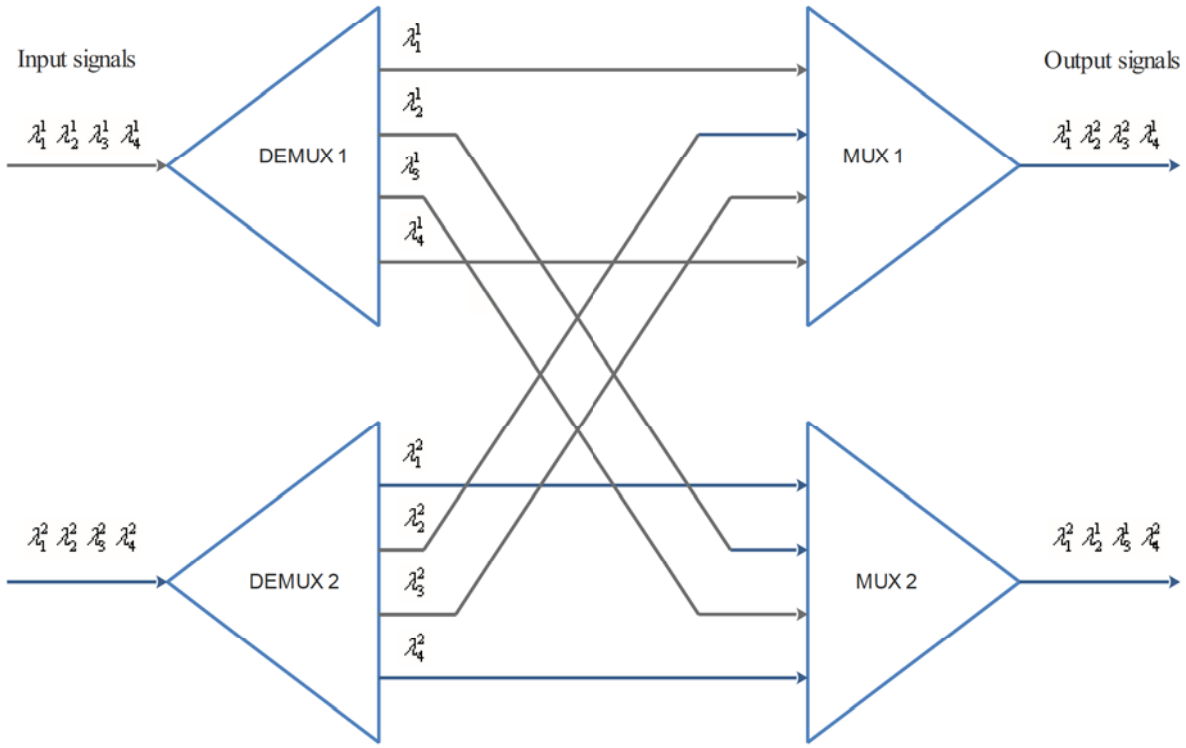

Figure 1.4: Architecture of an optical cross connect

1.3.4 Erbium-doped Fibre Amplifiers

Erbium-doped fibre amplifiers (EDFAs) are the most popular and widely used devices that belong to types of amplifiers that are referred to as doped fibre amplifiers (DFAs) [28].

In DFAs, rare-earth elements such as erbium and neodymium are used to dope some silica fibres during the production process. The use of semiconductor lasers that operate in the 980 and 1480 nm wavelengths ensure efficient pumping in the EDFAs [29]. Sufficient population inversion in EDFAs is attained via the deployment of bi-directional pumps and the usage of co-propagation, counter-propagation techniques. The molecular structure of the doped fibre determines the wavelength-dependent gain spectrum of EDFAs. The main shortcomings of EDFAs arise due to the non-flatness of their gain and a very thin ($\approx 40nm$) wavelength-dependent gain bandwidth [30].

On the other hand, the main advantage of EDFAs is that they inhibit the occurrence of cross-gain saturation and this allows them to achieve high gain with low noise figure. This attribute makes EDFAs attractive and thus their wide deployment in most operational optical networks.

1.3.5 Raman Amplifiers

Modern high-speed backbone optical networks currently deploy Raman amplifiers to compensate for signal attenuation. Raman amplifiers make use of the stimulated Raman scattering (SRS) phenomenon in which energy from a high-power pumping optical beam is transferred to the amplified propagating signal [31], [32]. Although the spontaneous Raman scattering spectrum is wide, the SRS is highly coherent and thus the low-intensity signal radiation becomes coherently amplified in the process. One of the main advantages of the Raman amplifiers is that, they have a broad gain spectrum whose shape can be altered by changing the number of pumps and their respective wavelengths [33]. Another desirable attribute of the Raman amplifiers is their relatively low noise figure that ensures that very little noise is added to the desired amplified signal.

1.4 Types of Optical Networks

Optical networks can be classified into three distinct categories, and these are, opaque, translucent and transparent networks. Early optical networks were basically opaque and there has been an evolution of these networks such that translucent networks have been largely deployed in most operating networks. On the other hand, transparent networks have been

largely confined to laboratories for experimental use, however, these networks will undoubtedly form the core of all future optical networks mainly due to their superior speed and low energy consumption compared to the other two aforementioned networks.

1.4.1 Opaque networks

Opaque networks require the deployment of OEO converters at each node. A propagating signal undergoes regeneration at each and every node in the network so as retain and maintain signal integrity [34]. In opaque networks, the transceivers provide the optical-electrical (OE) and electrical-optical (EO) conversion of the signal. Furthermore, the transceivers provide support for fault detection and isolation, performance monitoring, as well as support for routing and restoration protocols. One of the major shortcomings of opaque networks is the scalability limitations of their transceivers, and thus their deployment in the current high bit-rate networks pose serious financial and operational challenges. In addition, opaque networks switching fabric is generally bulky, slow, expensive and consumes a lot of power. In a nutshell, the deployment of regenerators throughout the network translates into high CAPEX and OPEX for these types of networks [35].

1.4.2 Transparent Optical Networks

Transparent optical networks perform optical switching which enables an optical signal to travel through an entire network without any conversion to the electronic form. These networks aim to maintain a network connection to be in the optical domain from its source to destination, thereby eliminating the often costly and less scalable than optics intermediate electronic circuitry [36].

In these networks, there are no OEO converters and thus, they are currently limited to cover considerably small geographic spaces [37].

Due to the absence of OEO converters, transparent optical networks appear very lucrative since they are relatively cheap and have low carbon footprints [38]. While they offer several notable advantages, transparent networks do present some technical and operational challenges. Some of the key challenges presented by transparent networks include their limitation to passive switching and wavelengths continuity constraints that lead to high levels

of connection blocking. However, recent developments in transparent networks have managed to overcome some of the hurdles that were evident in their earlier systems. The use of Raman amplifiers instead of the traditional EDFA amplifiers has helped modern transparent networks to attain an optical reach of more than 3000 km [39].

The introduction of photonic integrated circuits (PICs) has also boosted the viability of these networks. In PICs, several WDM components are monolithically integrated on a chip, and thus they offer an alternative means of realizing the goals of OEO in transparent networks [40].

In addition, replacement of fixed transponders with tunable ones has greatly reduced the CAPEX costs in modern transparent networks. Another exciting development is the use of waveband-based switching. Waveband switching basically entails that a set of wavelengths are switched as a single unit as opposed to switching individual wavelengths, and this leads to significant cost and energy savings.

A lot of research work is currently under study and is mainly geared towards increasing the optical reach of transparent optical networks. In June 2015, researchers at the University of California's Qualcomm Institute's Photonic Systems Group announced a ground-breaking feat in which they claim signal transmission that spanned an unprecedented 12000 km optical reach in their laboratory experiments [41].

1.4.3 Translucent optical networks

The optical reach is the distance a propagating optical signal can travel before its signal health is degraded to a level that requires regeneration. Translucent optical networks incorporate sparsely located signal regenerators so as to facilitate the transmission of signals that exceed the optical reach [42]. The role of the regenerators is to re-amplify, reshape and re-time (3R) travelling optical signals so as to guarantee an acceptable QoS. One of the key reasons for the deployment of translucent optical networks is to strike a favourable balance between financial costs and satisfactory service provision to clients [43], [44], [45].

Instead of being either purely electronic or purely optical, translucent optical networks are a compromise between all-electronic switching and all-optical switching.

Translucent networks exhibit the following key advantages:

i. They permit a group of regenerators at each OXC node to be accessible to all wavelengths that approach the node and use as required. This sharing of regenerators greatly optimizes regenerator usage.

ii. Since the regenerators have wavelength conversion capabilities, they can be effectively utilized to avoid wavelength collision during the routing process. This leads to significant cost savings because there will not be need to incorporate the costly wavelength converters and the overall resource utilization of the network is significantly improved [45].

Since signal regenerators consume significant amounts of energy, their sparse utilization in translucent networks leads to lower carbon footprints as compared to opaque networks.

1.5 Key Findings

In this chapter, we note that:

- The surging of bandwidth-intensive applications and services is constantly and directly driving the requirement for enabling networking infrastructures to support the extremely high-bandwidths and diverse data traffic flows.
- Optical transmission appears to be an ideal solution towards the provisioning of sufficing transmission as well as switching supporting capability for this information and communication technologies (ICT) infrastructure.
- Because ICT and networking infrastructures (equipment and bandwidth) requirements are trebling every two years, the industry has since been identified as a growing direct contributor to energy consumption as well as greenhouse gases (GHG) emissions worldwide. This has prompted an interest in mitigating better and more energy-efficient ways to design and operate these infrastructures. These measures mainly encompass designing power-efficient end devices, network redesign i.e. designing power-efficient networks, traffic engineering, power-aware networking as well as load-adaptive operation.
- Whereas reasonable strides have been achieved in addressing most of the aforementioned challenges, however, the impact of physical impairments has not been adequately addressed. Since physical impairments accumulation in the optical networks negatively affects the network performance, current strategies employed to tackle this problem generally lead to overall increased energy consumption in the networks. It is thus imperative that we need to strike a balance between energy

efficiency, performance and reliability when addressing impairment-aware routing and wavelength assignment schemes.

- In so addressing this, we take into account that future optical backbone networks will be heterogeneous in nature where a single link may carry various line-rate signals. This Mixed Line Rate (MLR) network architecture will further complicate impairment aware routing and wavelength assignment schemes.

1.6 Problem Formulation

Since the turn of the century, telecommunication networks have witnessed a tremendous increase in traffic due mainly to a surge in demand for bandwidth-intensive services such as the internet and HDTV. The evolution of optical networks aided by key technologies such as WDM and the availability of novel optical devices and switching fabrics such as ROADMs threw a lifeline in as far as meeting the increased traffic demand in modern efficient broadband communication is concerned. In addition, the gradual departure from the traditional opaque networks to translucent and transparent networks provided a solid platform for the provision of sufficiently agile and fast communication. However, despite all these concerted efforts in the design and development of modern networks that are responsive to the ever-increasing demand for faster and reliable networks, new challenges have since emerged that require undivided attention and innovative solutions.

The two key challenges that need to be investigated and addressed are: (i) the accumulation of physical impairments in the backbone optical networks, and (ii) the increased energy consumption of these networks.

1.7 Scope of work

The scope of this research study and the contribution to the body of knowledge are summarized as follows:

- To investigate the main physical layer impairments (PLI) and prevailing impairment-aware routing and wavelength assignment algorithms (IA-RWA) in order to develop novel PLI-RWA algorithms that are anchored on the ones in current existence.

By making use of simulations, the performance of the proposed PLI-RWA algorithms is compared to that of existing models and algorithms that largely ignore impairments effects in their operations.

- To formulate and develop a Q-factor estimation tool that incorporates the effects of physical layer impairments as the link-cost metric. The performance of the proposed tool is then compared with that of existing traditional estimation tools that do not consider impairments such as XT and FC that become more pronounced and problematic in modern high speed core networks.
- To devise and develop a QoT-aware analytical model that computes path wavelength blocking probabilities in core networks. The model is evaluated and validated by using the QoT-aware and QoT-guaranteed wavelength assignments (WA) algorithms.
- To design and develop energy-efficient RWA schemes for core optical networks. Using the shortest-wide path (SWP) and first-fit with ordering (FFwO) algorithms, the results are compared with those of existing schemes that are based on algorithms such as the shortest path (SP) and first fit (FF) algorithms.

1.8 Evaluation Methodology

Several techniques can be employed to evaluate proposed algorithms in optical networking studies. The most effective method makes use of a testbed, where the envisaged energy-efficient network devices and elements are deployed and proposed algorithms are implemented on a real network setup. Appropriate and relevant measurements are then carried out to gauge the performance of the network and conclusions on the effectiveness of the proposed solutions can be made. The major setback of this method is the prohibitive costs that are obviously associated with the setting up of experiments of such a magnitude. Another limitation of using testbeds is that it may be impossible to perform certain experiments because some ideal component features such as the sleep-mode function for several devices may not yet be available on existing devices on the market. Another method for evaluating the behaviour and performance of algorithms is the use of analytical models that represent the system under investigation. Although this technique can be very useful in the description of a behaviour of a network component, or to assess a simple communication network, it becomes challenging to implement on large and complex networks due to the high levels of sophistication of the relevant mathematics and time constraints. Another option for the

evaluation of network performance is through simulations, where replicas that closely represent the functions and behaviours of the network under study are represented in the form of software packages. The main advantages of this method include the appreciably low costs and time effectiveness. On the other hand, the magnitude of the simulated network may be limited by the computational capabilities of the simulation environment. It can therefore be proposed that performance evaluation through simulations may be considered a fairly reasonable choice that provides for cost and time effective assessment of proposed algorithms before they can actually be considered for deployment in real network setups. In this work, simulations are extensively utilized in the evaluation of proposed algorithms due to their flexibility as alluded to in the preceding statement. Analytical modelling is also used in this work, but is essentially limited to RWA algorithms presented in chapter 4.

1.9 Outline of the dissertation

The work presented in this dissertation broadly focuses on the planning and operation of energy efficiency in transparent optical networks (TON), subject to physical layer impairments (PLI). Chapter 1 sets the scene by exploring and reviewing topical issues that characterise the 21st century optical networks such as energy efficiency and consumption. It gives an overview of historic milestones in the evolution of optical fibre communication systems and outlines the types of optical networks. The problem statement, scope of the study and evaluation methodology subsections are clearly presented at the end of the chapter. The remainder of the dissertation is organised as follows:

Chapter 2 reviews relevant literature and provides a detailed description and analysis of the most important PLI. Comprehensive simulations and proposals of limiting the effects of PLI on propagating signals are also provided. The last part of the chapter explores key strategies that are employed to reduce energy consumption in optical core networks.

Chapter 3 focuses on energy efficiency and impairment aware routing and wavelength assignment schemes. It reviews existing energy-aware and efficient algorithms and several algorithms are proposed to enhance and broaden the scope of knowledge in this field.

Chapter 4 presents proposed models and their subsequent evaluation. A Q-factor tool that incorporates most of the pertinent physical layer impairments is presented. The tool is evaluated via simulations to gauge its usefulness and effectiveness. An analytical model to compute the blocking probabilities for RWA with physical impairments in transparent networks is also presented. Numerical examples are also provided to show the performance of the proposed model, and it is validated through the use of simulations.

Chapter 5 presents energy-efficient algorithms that take into effect various parameters in their decision-making processes. In particular, the impact of physical impairments is taken into consideration in the formulation of energy-efficient algorithms and strategies. The proposed algorithms are then compared with the traditional algorithms that do not take cognisance of energy consumption in their computations.

Lastly, Chapter 6 concludes the dissertation by summarizing key findings and aspects of the study, and a brief description of the anticipated future works is also presented.

2 Literature Review

2.1 Introduction

This chapter reviews some important contributions made by scholars in the area of physical impairments that exist in the transmission of signals in optical networks. The physical impairments can be broadly classified into linear and non-linear impairments. The behaviour of different impairments is analysed and described and ways of reducing their effects on transmitted signals are discussed. Lastly, several strategies that are used to reduce energy consumption in core optical networks are presented and discussed.

2.2 Physical Layer Impairments

The integrity and quality of optical signals is lost as they traverse the optical networks and these signal degrading factors are generally referred to as physical layer impairments (PLI). Due to the transparency of optical networks, noise and signal distortion that arise from PLI effects, accumulate along the lightpath and may lead to unacceptably low OSNR that will render the lightpath unusable. PLIs are broadly classified into two main categories, that is, linear and nonlinear effects (Figure 2.1). Linear impairments are independent of the signal power and influence each of the optical channels separately, on the other hand, nonlinear impairments cause disturbance and interference between channels in addition to affecting each optical channel individually [24], [46].

2.3 Linear Impairments

The most prevalent linear impairments that degrade optical signals in optical networks are:

Chromatic Dispersion (CD), *Polarization Mode Dispersion* (*PMD*), *Fibre Attenuation, Polarization Dependant Losses* (*PDL*), *Crosstalk* (*XT*), *Filter Concatenation* (*FC*), *Amplified Spontaneous Emission* (*ASE*) and *Component Insertion Losses* [47]-[51].

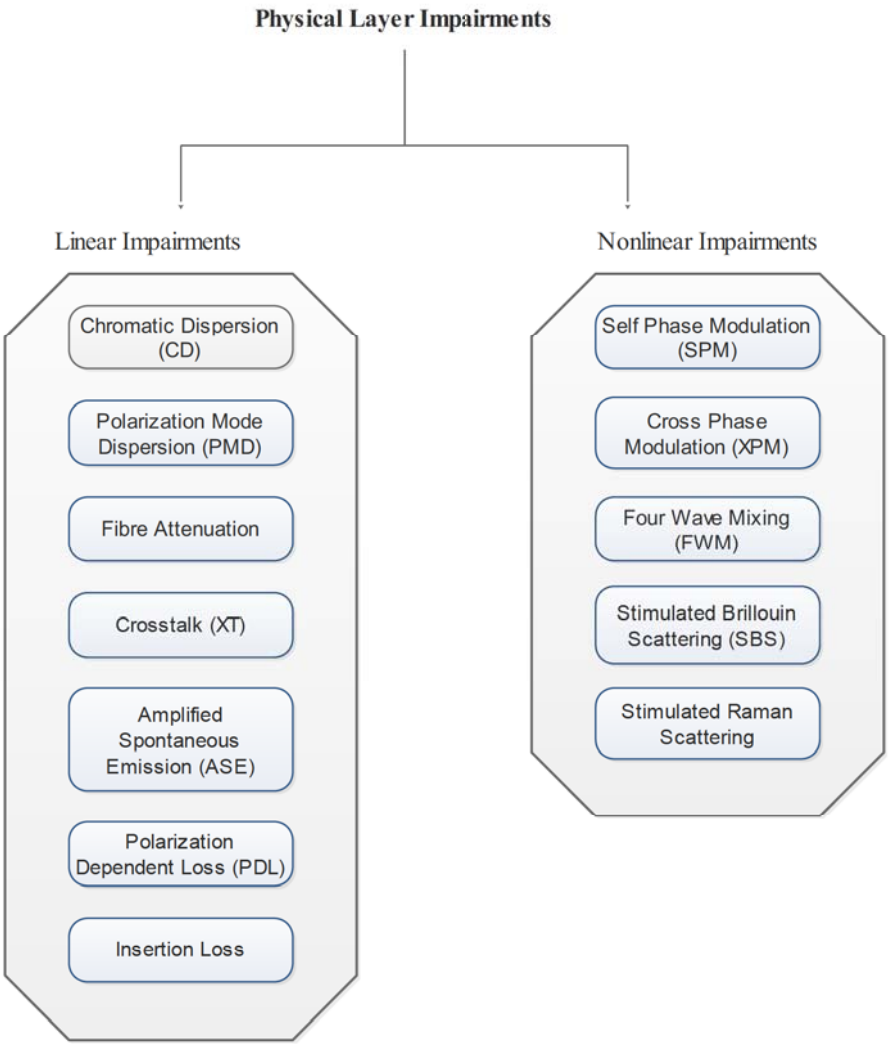

Figure 2.1: Physical layer impairments

2.3.1 Chromatic Dispersion

Chromatic dispersion (CD) affects the bandwidth of high-speed optical communication systems through pulse broadening and nonlinear optical distortion [46], [52]. Basically, the pulse broadening that occurs due to CD arises mainly due to the presence of different wavelengths in the light source and the source modulation. Each distinct wavelength in the light source leads to different phase and group delays along the fibre. If the light source wavelength varies during the pulse, chirping occurs, and this usually leads to pulse broadening.

CD influences the receiver performance by: (1) lowering the pulse energy within the bit slot and (2) expanding the pulse energy above the assigned bit slot causing inter-symbol interference (ISI). The dependence of the propagating pulse speed on wavelength leads to the broadening of the optical pulse shape, which in turn restricts the maximum bit-rate that can traverse through the optical fibre (Figure 2.2) [53], [54].

Figure 2.2: Chromatic Dispersion effects

CD can be mathematically characterized by the Group Velocity Dispersion (GVD) coefficient, usually represented by D.

Suppose τ is the propagation delay at a particular frequency (ω), then:

$$\tau = \frac{L}{v_{gv}} \tag{2.1}$$

$$\frac{\partial \tau}{\partial \omega} = L\left(\frac{1}{v_{gv}}\right) \tag{2.2}$$

Where, L is the fibre length and v_{gv} is the group velocity.

Assuming that a propagating signal has a spectral width of $\Delta\omega$, the propagation time difference between extreme ends of the signal will be;

$$\Delta\tau = \left|\frac{\partial \tau}{\partial \omega}\right| \Delta\omega = \left|\frac{\partial \beta}{\partial \omega}\right| . L . \Delta\omega \tag{2.3}$$

Where β is the propagation constant.

Expressing the pulse spread in terms of the wavelength spectral width $\Delta\lambda$, we obtain the following relationship:

$$\Delta\tau = |D| . L . \Delta\lambda \tag{2.4}$$

Where,

$$D = \frac{1}{L}\frac{\partial \tau}{\partial \lambda} = \frac{1}{L}\frac{\partial \tau}{\partial \omega}\frac{\partial \omega}{\partial \lambda} = -\frac{2\pi c}{\lambda^2}\frac{\partial \beta}{\partial \omega} \tag{2.5}$$

Since,

$$\frac{\partial \omega}{\partial \lambda} = \frac{\partial}{\partial \lambda}\left(\frac{2\pi c}{\lambda}\right) = -\frac{2\pi c}{\lambda^2} \tag{2.6}$$

The GVD is normally measured in ps/(nm.km).

$$\frac{\partial \beta}{\partial \omega} = \frac{\partial}{\partial \omega}\left(\frac{1}{v_{gv}}\right) = -\frac{1}{v_{gv}^2}\frac{\partial v_{gv}}{\partial \omega} \tag{2.7}$$

The above equation implies that at the point of zero dispersion (λ_D), v_{gv} has its minimum value.

Chromatic dispersion is always assumed to be adequately compensated on a per-link basis, however, for high bit-rate systems ($\geq$ 10 Gb/s), dispersion becomes a significant factor that requires appropriate attention [55]. One of the pertinent innovative ways of mitigating the effects of chromatic dispersion on optical networks is the use of dispersion-compensating techniques. Dispersion compensation can be broadly classified into two main categories, viz, (i) passive CD-compensation and (ii) active CD-compensation. Passive CD-compensating techniques that are commonly implemented in modern networks include the use of dispersion-compensating fibres (DCFs), fibre Bragg gratings (FBGs) and incorporation of holey fibres. By far, DCFs have been a favourate choice in CD compensation primarily due to their flexibility. Although DCFs possess lucrative dispersion-compensating abilities, they unfortunately give rise to residual CD whilst compensating CD for the main channel in a given channel plan. Another shortcoming of DCFs is that, they are relatively costly and bulky and this leads to increased capex.

Pre-chirping and soliton transmission are the front-running active CD-compensating techniques that are mostly utilized, and they are poised to be CD-compensating techniques of choice in future optical networks [56].

Signal modulation format is also a significant and vital determinant of CD, and there are four basic modulation techniques that are employed in optical networks. These modulation formats are: (i) on/off keying (OOK), (ii) phase-shift keying (PSK), frequency-shift keying (FSK) and (iv) polarization-shift keying (PolSK). Of these four traditional formats, we will pay our attention only to the two most widely utilized formats (OOK and PSK) and their subsequent variants.

In OOK modulation, a signal is intensity-modulated such that when the light source signal is "on", a "1" bit is generated, and conversely, when the source signal is "off", a "0" bit is generated. Popular variants of OOK modulation include the non-return-to-zero (NRZ) and the return-to-zero (RZ) modulation formats. Although OOK modulation is attractive due to its simplicity and flexibility, it is not suitable for high speed networks because the CD accumulation leads to high BER and thus may render the propagating signal unusable. PSK appears to be an efficient and robust modulation format in which the phase and amplitude of a signal are manipulated during modulation. In PSK, a "1" bit is transmitted by shifting the phase of the carrier through an angle θ relative to the preceding carrier phase. On the other hand, a "0" bit is transmitted by 0 or no phase shift relative to the preceding signal phase. The major setback in PSK modulation is the constant variation of the polarity of the modulator voltage that in turn compromises the purity of the switched signal which unavoidably increases the BER.

Variations of PSK such as differential phase-shift keying (DPSK) and carrier-suppressed RZ (CS-RZ) modulation techniques have appreciably high tolerance of CD, and thus are suitable for high speed optical networks. Advanced modulation formats such as the NRZ-maximum likelihood sequence estimation (NRZ-MLSE) and pulse amplitude modulation (PAM4)-MLSE have been introduced in fairly recent optical networks [57]. Both modulation techniques are moderately tolerant to residual CD, however, they consume more power and their optoelectronic components are expensive as compared to those of traditional modulation formats such as NRZ. It is therefore vital to strike a balance between an acceptable BER, moderate energy consumption and reasonable cost in selecting a modulation format for high speed networks.

2.3.2 Polarization Mode Dispersion

Polarization Mode Dispersion (PMD) is a physical phenomenon that causes light pulses in optical fibres to spread in time. If the dispersion in the optical fibre is severe, adjacent light pulses will overlap and interfere with each other [58]. PMD is directly related to the differential group delay (DGD) that arises due to birefringence in the optical fibres.

The relationship between PMD and DGD is shown in equation 2.8:

$$PMD = \langle \Delta\tau \rangle \tag{2.8}$$

Where $\langle \Delta\tau \rangle$ is the average value of the DGD.

The main causes of PMD include imperfections, external stresses and defects that arise during the fibre manufacturing and cabling processes. External stresses may either be natural or artificial. Examples of natural external stresses include wind, storms and tornadoes. As for artificial external stresses, examples include digging and vibrations that arise due to mobile vehicles. Substantial research effort has been expended in creating methods and ways to reduce PMD, but it is practically impossible to predict the exact value of PMD since it is stochastic in nature. Due to the effects of PMD, polarisation states of various channels get distorted with distance traversed and, in the process, affect other nonlinear effects that are polarization dependent such as four-wave mixing. This will only worsen the situation as it will become increasingly difficult to predict the effective nonlinear effects and their subsequent interactions in propagating signals. PMD becomes problematic in high-speed optical communications such as 10 Gbps and higher and may severely cripple the integrity of an optical network. The gravity of the PMD effects are more serious particularly on links found in older legacy networks. It is a characteristic of a single-mode fibre or an optical component whereby pulse energy at a particular wavelength is resolved into two orthogonal polarization modes with distinct propagation velocities (Figure 2.3).

Figure 2.3: Polarization Mode Dispersion

The following equation relates PMD to the Q-factor of propagating signals:

$$Q_{estimate} \approx \frac{\eta_{PMD} P_{cp}}{\sigma_{total}} \tag{2.9}$$

Where η_{PMD} is PMD multiplication factor, P_{cp} is eye closure penalty for filter concatenation [59].

Generally, birefringent equalizers are usually used to counter the negative effects of PMD in transparent networks. On the other hand, for opaque and translucent networks, PMD is normally compensated for by the use of electrical filters that remove some of the induced distortions. It can be argued that in long-haul networks, the incorporation of these electrical filters will lead to increased energy consumption that may translate to a higher carbon footprint.

In fairly modern systems, digital back-propagation (DBP) has been proposed as one of the techniques that can be employed to tackle the menacing effects of PMD in optical networks [60], [61].

In DBP, the inverse of a nonlinear Schrödinger equation (NLSE) is solved through the optical channel to obtain an estimate of the transmitted signal [62]. However, the main setback of the use of DBP is its extensive computational complexity and difficulty of use due to the presence of other nonlinearities, especially at high bit rates.

Authors in [63], [64] and [65] propose ways of compensating for PMD in fairly modern networks using traditional modulation formats, however, in their works, they do not show how PMD compensation is affected by the utilization of advanced modulation formats such as NRZ-MLSE and PAM4-MLSE.

2.3.3 Fibre Attenuation

Attenuation in optical fibres refers to the reduction in intensity of a propagating light signal with respect to distance travelled through the fibre. The following are the primary causes of attenuation in optical fibres:

i. *Material absorption loss* arises either due to absorption of light by the fibre itself or due to impurities within the optical fibre, and these are commonly referred to as intrinsic and extrinsic absorption respectively. Intrinsic absorption is caused by the interaction of a propagating light signal with silica (or the bulk material of the fibre), and extrinsic absorption is mainly due to absorption of light by transition metal impurities (e.g. Cr, Fe, V) and hydroxyl ions (OH^-).

ii. *Linear scattering loss* occurs due to linear transfer of optical power amongst propagating modes. If the fibre non-homogeneities are of a much smaller size than the wavelength of the transmitted light, Rayleigh's scattering occurs, and it is well pronounced in traditional silica-based optical fibres. Conversely, Mie's scattering occurs when the fibre non-homogeneities are significantly greater than the wavelength of the propagating optical signal.

Suppose a signal that is transmitted through the fibre has an initial power of $P(0)$ and it traverses a fibre of length $x\ km$, its power intensity becomes$P(x)$, and is defined as follows:

$$P(x) = P(0)e^{-\alpha x} \tag{2.10}$$

Where α is the attenuation coefficient.

Modern optical telecommunications systems typically utilize the 1550 nm spectral window mainly due to its relatively favourable low loss attenuation ($\approx 0.2\ db/km$) of silica-based optical fibres. Authors in [66] report that a pure-silica-core fibre (PSCF) that has inherently low transmission loss of less than 0.15 dB/km at 1550 nm has been developed by Sumitomo Electric Industries in Japan. Figure 2.4 shows the relationship between the fibre loss with wavelength for the PSCF optical fibre. This PSCF is poised to become the holy grail of high capacity optical systems that are based on the 100 Gbit/s coherent technologies. Besides their superior low transmission loss traits, the PSCFs also boast of enviable low non-linearity characteristics.

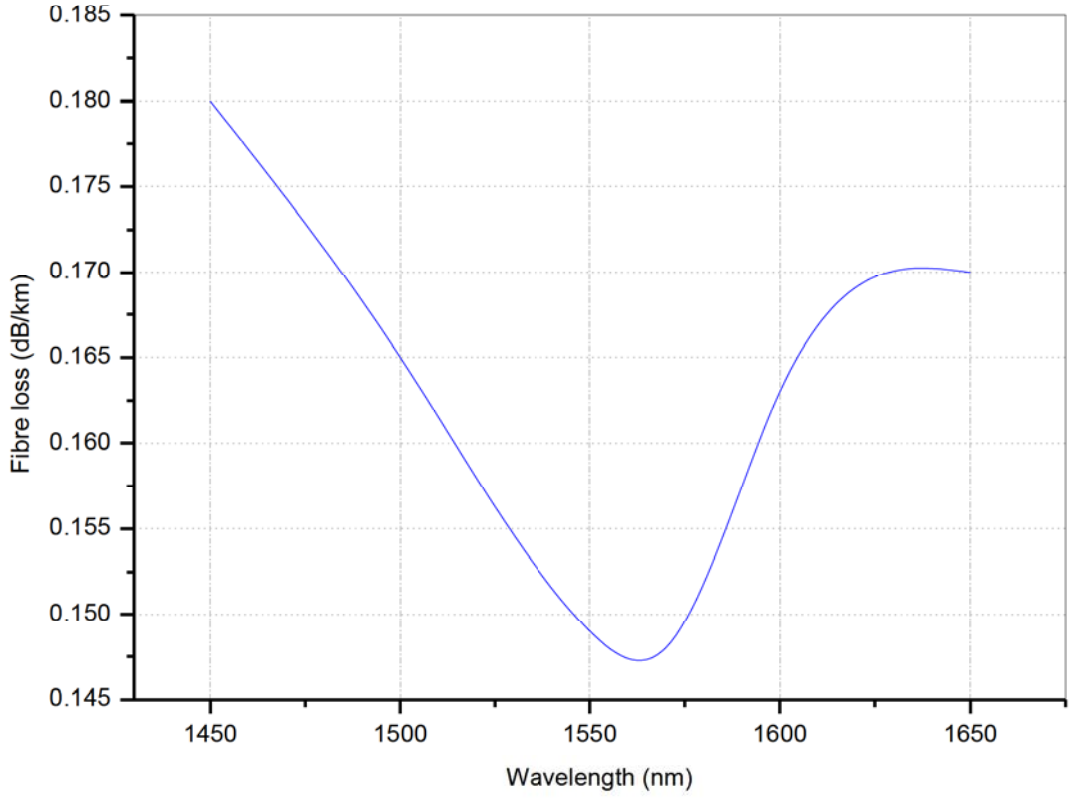

Figure 2.4: Relationship between fibre loss and wavelength for the PSCF fibre

The above-mentioned attributes are highly desirable and they will aid future high capacity ultra-long haul communication systems to significantly improve their overall optical signal-to-noise ratio (OSNR) [66].

2.3.4 Amplified Spontaneous Emission noise (ASE)

ASE noise arises due to the incoherent emission of photons by the optical fibre material that are in turn amplified together with the desired data optical pulse along the communication channel, and this results in the addition of noise to the propagating signal [51].

Assuming the incorporation of erbium-doped fibre amplifiers (EDFA), the output noise power due to ASE can be computed using the following [67]:

$$P_{ase} = 2n_{spon}hf_{o}(G-1)B_{o} \tag{2.11}$$

where n_{spon} is the spontaneous emission factor, h is the Planck constant, f_o is the frequency of the optical signal in the channel, G is the gain of the EDFA and B_o is the bandwidth of the channel. The spontaneous emission factor, n_{spon}, is related to population densities as follows:

$$n_{spon} = \frac{N_2}{N_2 - N_1} \tag{2.12}$$

Where N_1 and N_2 are the population density in the lower state and the population density in the upper state respectively.

We relate the ASE to an important parameter of optical amplifiers known as the noise figure (NF). The noise figure is defined as the ratio of the signal-to-noise ratio (SNR) at the amplifier output to an ideal SNR at the input [68], [69].

The NF can be expressed as follows:

$$NF = 10\ log_{10}\left(\frac{P_{ase}}{hf_oGB_o} + \frac{1}{G}\right) \tag{2.13}$$

Substituting for P_{ase}, we obtain:

$$NF = 10\ log_{10}\left(\frac{2n_{spon}hf_o(G-1)B_o}{hf_oGB_o} + \frac{1}{G}\right) \tag{2.14}$$

By simplifying equation 2.14, we obtain,

$$NF = 10\ log_{10}\left(\frac{2n_{spon}(G-1)+1}{G}\right) \tag{2.15}$$

Further simplification yields the following,

$$NF = 10\ log_{10}\left(2n_{spon} - \frac{2n_{spon}}{G} + \frac{1}{G}\right) \tag{2.16}$$

Modern optical networks now utilize high gain amplifiers such as the wide-band erbium-doped fibre amplifiers (W-EDFA's), therefore, when equation 2.16 is applied to high gain amplifiers it simplifies to equation 2.17:

$$NF = 10\ log_{10}(2n_{spon}) \tag{2.17}$$

Since there is a direct relationship between the NF of an amplifier and the optical network performance, it is paramount that the NF should be kept as low as possible.

The ASE noise variance of the signal on a periodically amplified link of the channel is given by:

$$\sigma_{ase}^2 = 2P_o \sum_{n \in L} ASE(n) \tag{2.18}$$

where P_o is the optical channel power and $ASE(n)$ is the sum of the EDFA generated ASE noise on link n.

We investigate and present the variation of the output noise power due to ASE (P_{ase}) with the spontaneous emission factor (n_{spon}) for different wavelengths as shown in figure 2.5.

It can observed from figure 2.5 that the lowest output noise power due to ASE (P_{ase}), was attained at the wavelength of 1555 nm, and conversely, the maximum value of P_{ase} was achieved at the wavelength of 1580 nm. The amplifier gain in the above scenario was maintained at 40 dB throughout the simulations. It can inferred that P_{ase} is sufficiently low in the C-band, and becomes a serious nightmare for systems that operate in the L-band of the optical communication systems. Figure 2.6 shows the relationship between the noise figure and the spontaneous emission factor for wavelengths that belong to both the C and L-bands of the optical communication systems. It is clearly evident that the NF is independent of the variations of wavelengths. Innovative techniques such amplifier power stabilizing have been proposed and implemented so as to reduce the effects of ASE in amplifiers as suggested by authors in [70], [71] and [72]. However, due to the stochastic nature of the noise, it is practically impossible to fully compensate for ASE. Since ASE noise is a phase noise, it can be argued that its effects are particularly devastating in systems that employ phase modulation formats such DQPSK and DPSK.

ASE noise poses a very grave challenge in high-speed optical networks because it usually results in very low OSNR, and its effects are precisely severe in transparent networks. The profound undesirable effects of ASE primarily lead to limited optical reach and poor bandwidth utilization. We therefore suggest that advanced modulation formats such as the polarization multiplexing, 16-state quadrature amplitude modulation (PM-16QAM) that are not anchored on phase modulation be deployed in high-speed networks so as to minimize the negative effects of ASE. In addition, the incorporation of Raman optical amplifiers will ideally improve the OSNR since they possess ideal characteristics such as low power consumption and enviable spectral efficiencies and seamless integration with existing network infrastructure.

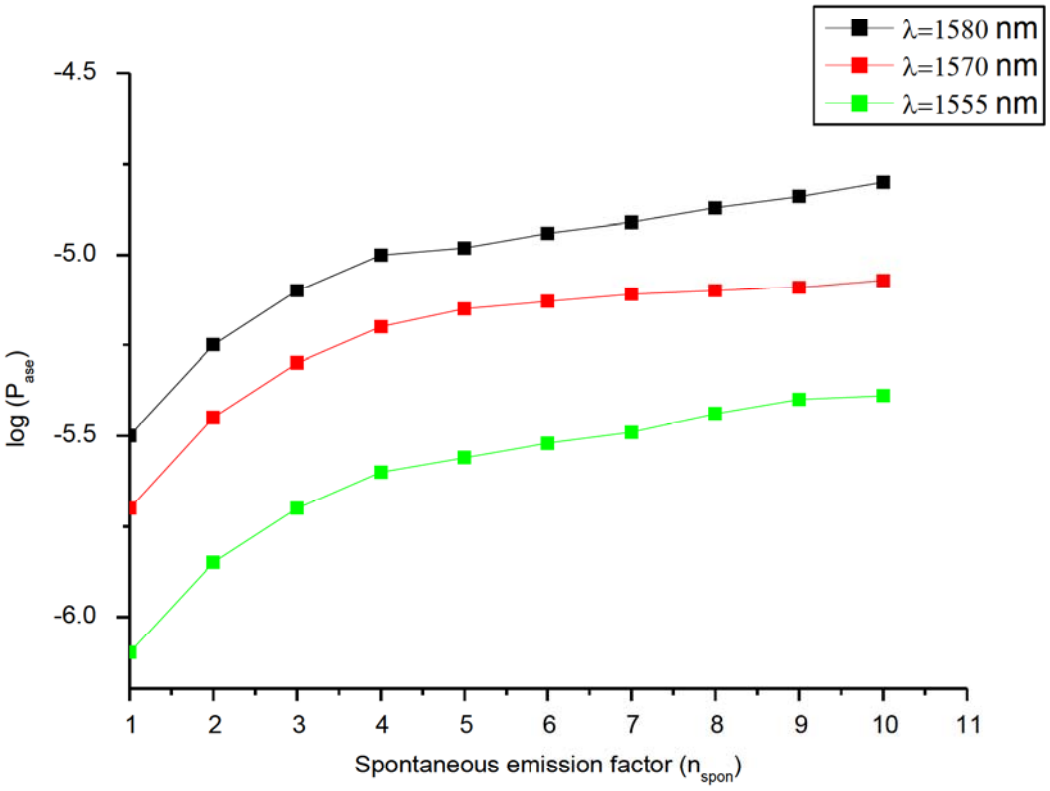

Figure 2.5: Relationship between ASE and spontaneous emission factor

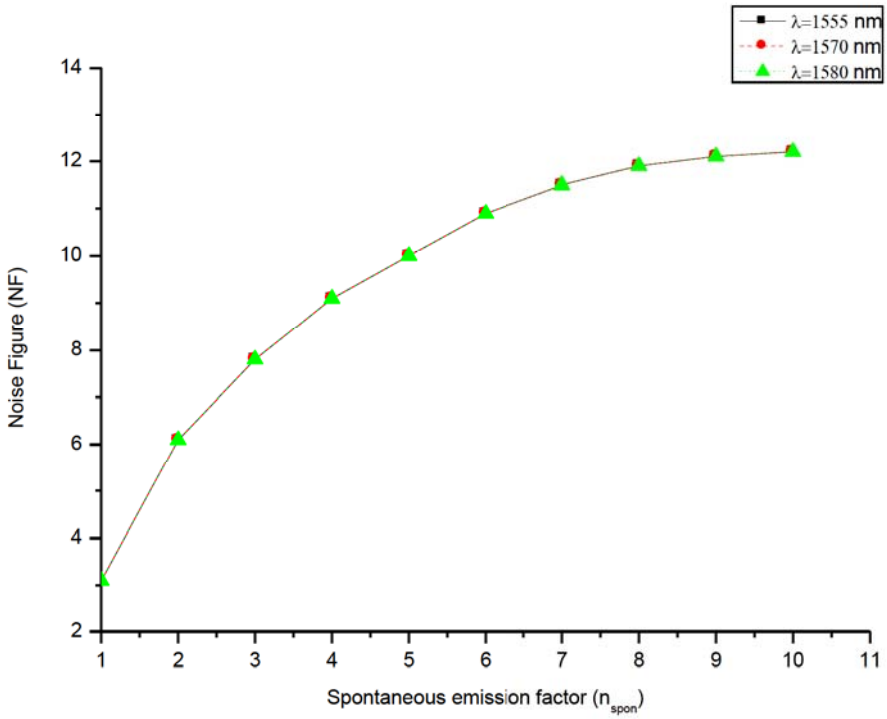

Figure 2.6: Variation of noise figure and spontaneous emission

2.3.5 Filter Concatenation

In WDM optical networks, an optical signal traverses through several optical nodes before it reaches its destination. In transparent optical networks, a signal passes through various vital components such as OXCs and ROADMs. Generally, the OXCs and ROADMs contain several filters that include wavelength blockers (WB) and wavelength selective switches (WSS), and the degradation of the traversing signal through these elements is commonly referred to as filter concatenation [73]. Filter concatenation mainly arises due to device imperfections, temperature fluctuations, operating conditions and deployment duration of the filters [74], [75].

In essence, this implies that the amplitude and phase transfer functions of the optical filters are not ideal. Filter concatenation effect becomes well defined with an increase in the number of optical filters in the channel. The potent transfer function of cascaded filters is the product of each separate filter. Consequently, the tacit transmission bandwidth of cascaded filters is effectively narrower than that of a separate filter. In addition, when the centre frequency of the cascaded filters is misaligned, it leads to spectral narrowing of the effective transfer function, and thus will seriously reduce the effective bandwidth.

The gravity of filter concatenation is usually substantial in transparent networks since a signal may be repeatedly multiplexed and demultiplexed several times before it reaches its final destination. The overall effect of filter concatenation in an optical network is taken into consideration by estimating the eye-closure penalty that is registered at the receiver node.

Authors in [76], [77] and [78] propose ways of limiting the signal degradation of optical signals due to filter concatenation by employing techniques such as intensity modulation and direct detection (IM-DD) optical orthogonal frequency division multiplexing (OOFDM).

In [79], [80] and [81], the filter concatenation effect is further interrogated in coherent orthogonal frequency division multiplexing (CO-OFDM) backbone networks. A comprehensive study of the residual effects of filter concatenation such as group delay ripple and filter-induced dispersion is presented in [82] and [83].

However, in almost all the work alluded to above, the studies and discussions were limited to the use of the standard single-mode fibres (SSMF) and the same types of filters. In our contributions, we extend the work presented in [76] to study and simulate the signal degradation effects that arise due to different types of filters and modulation formats. In

addition, we also focus on the long-haul high speed networks and incorporate the fairly novel and highly attractive PSCF optical fibres instead of the popular SSMFs.

In our model, we explore a 1500 km long-haul network that is made up of 15 spans of 100 km length PSCF fibres. A total of 10 EDFAs with a noise figure of 5 dB and 10 ROADMs are considered. The ROADMs are based on FBG and Chebyshev filters, and an IM-DD OOFDM set up is implemented as shown in figure 2.7.

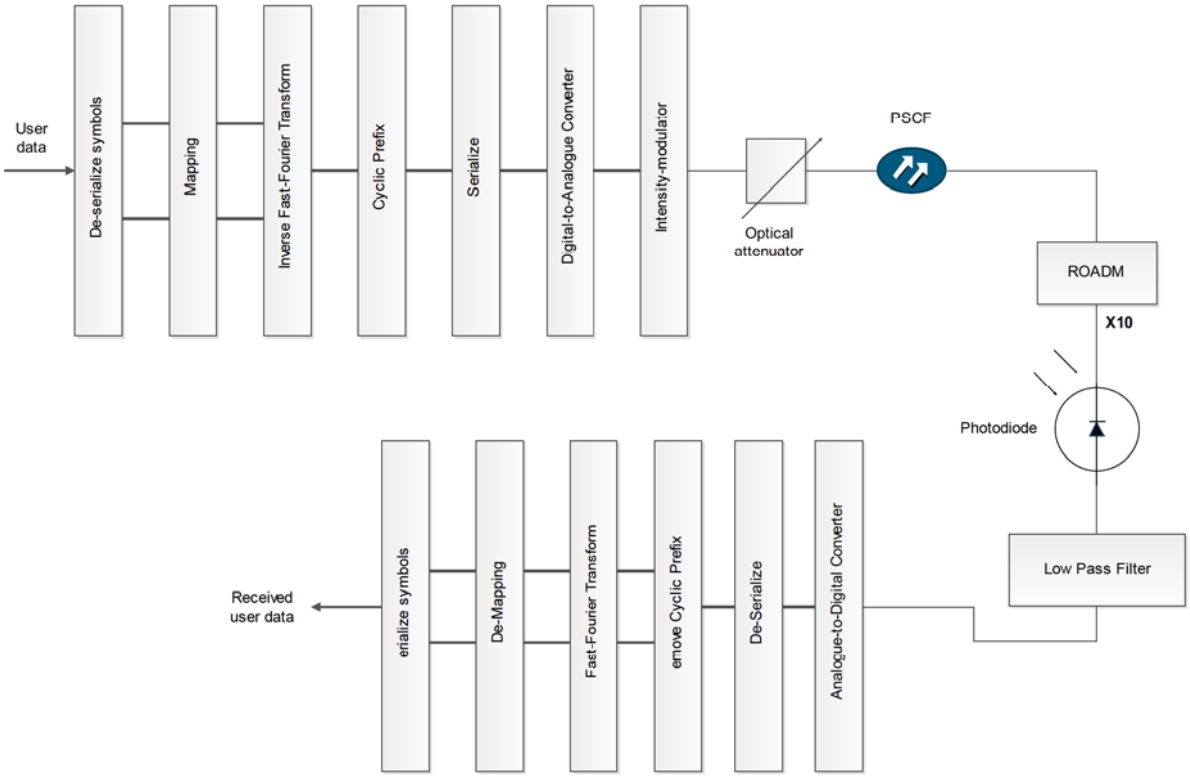

Figure 2. 7: Schematic diagram for the simulation of the IM-DD OOFDM system

Table 2.1 shows some important simulation parameters and their corresponding values for the IM-DD OOFDM system shown in figure 2.7.

Table 2.1: Simulation parameters for the IM-DD OOFDM system

Parameter	Value
Intensity modulator wavelength	1550 nm
Digital-to analogue converter (DAC)/ Analogue-to-digital converter (ADC) resolution	7 bit
Digital-to analogue converter (DAC)/ Analogue-to-digital converter (ADC) sampling rate	12.5 GS/s
Cyclic prefix parameter	25 %
Photodetector sensitivity	-19dBm

The overall effect of cascaded FBG filters for various signal source maximum admissible detuning offsets are shown in figure 2.8 for DBPSK, 16QAM and 128QAM modulation formats.

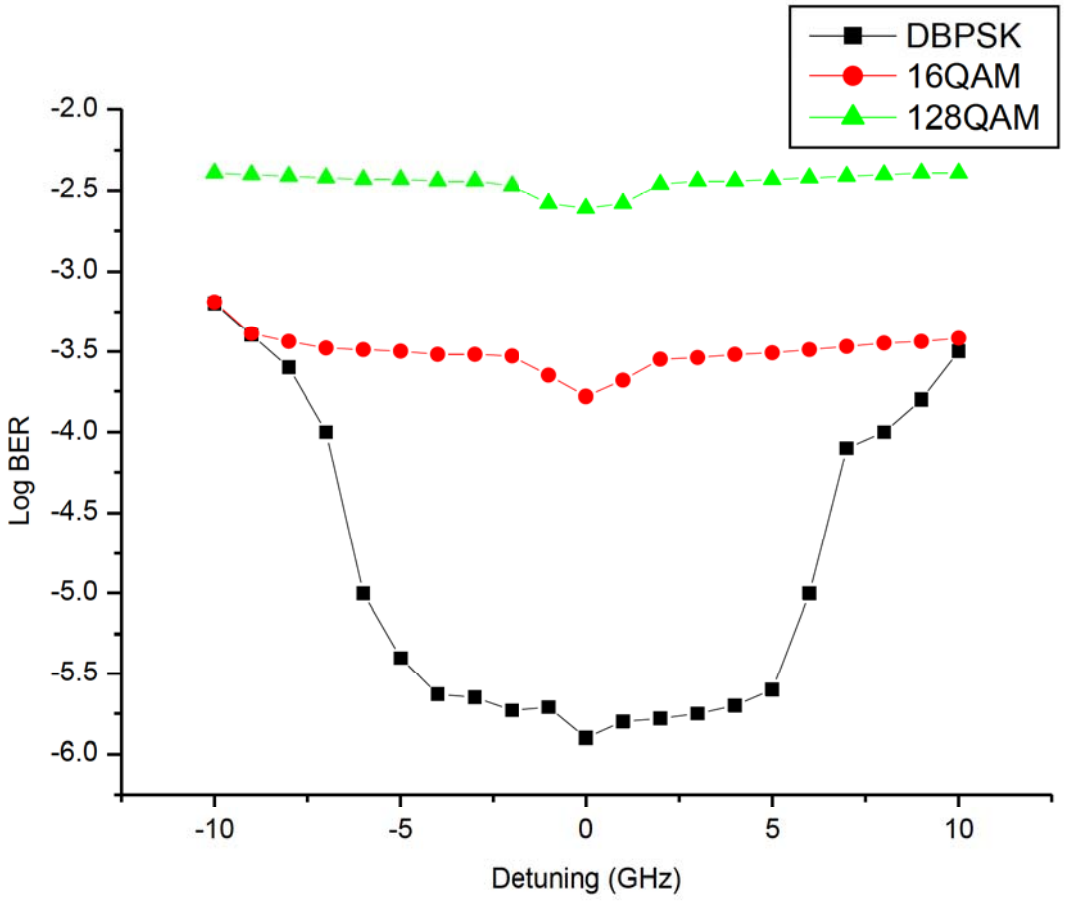

Figure 2.8: Variation of BER with laser source detuning using different modulation formats for 10 FBGs

The filter concatenation manifests itself in the form of the BER for the 10 cascaded FBG filters under simulation study. From figure 2.8, it can be seen that advanced modulation formats (128QAM and 16QAM) lead to higher BERs compared to the DBPSK modest modulation format. This arises mainly due to appreciable loss of optical power triggered by filter concatenation and narrowing, and also due to time-domain distortions that result from the signal spectrum clipping.

Utilizing the same approach as that shown for the FBG filters, figure 2.9 shows the relationship between BER and signal source detuning for 10 Chebychev filters. In this case, the 128QAM modulation format is studied for various ripple factors. It is clearly shown that there is sturdy relationship between the linewidths of the respective ripple regions with BER deterioration.

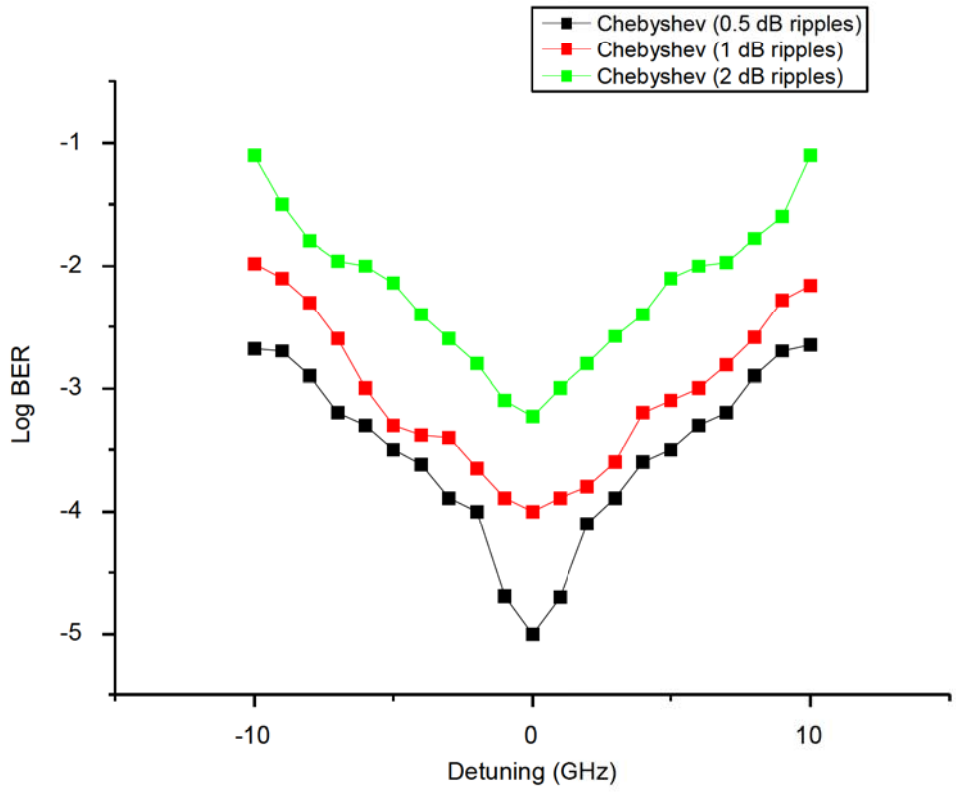

Figure 2.9: The relationship between BER and laser detuning for 10 Chebyshev filters using 128 QAM modulation format for various ripple factors.

From the results obtained above, it may be inferred that advanced modulation formats lead to higher BER and are less tolerant to frequency dips as compared to low signal modulation formats. Therefore, it would be prudent to employ adaptive modulation in long-haul backbone networks so as not to severely compromise the OSNR at the expense of limiting the effects of filter concatenation. Adaptive modulation involves the use of various modulation formats and represents a trade-off between signal degradation, bit rate and energy consumption of the network.

2.3.6 Crosstalk (XT)

Cross talk (XT) in WDM optical networks arises due to insufficient isolation of a channel by optical components such as OXCs, ROADMs and other switching fabric. This leads to signals from one channel to enter into another and thus lead to 'noise'. The interference of channel signals seriously reduce the signal-to-noise ratio (SNR) and normally cause severe signal degradation that leads to unacceptable bit-error rates. XT is generally classified as either in-band (homodyne) or inter-band (heterodyne). In-band crosstalk has the same wavelength as that of the traversing signal and can be further divided into coherent XT and incoherent XT.

Inter-band crosstalk, which is a less severe form of XT, occurs in wavelengths outside the optical bandwidth [84], [85].

Since inter-band crosstalk generally occurs at a wavelength that sufficiently differs from that of the desired signal, it is normally removed by filtering, and thus does not pose a serious threat to the health of the transmitted signal. Conversely, in-band crosstalk cannot be removed by filtering and it severely compromises the performance of an optical network if it is not adequately taken care of [86]. Its effects are even more detrimental in long-haul backbone networks where a significant amount of critical components such as OXCs and ROADMs are cascaded along the communication channel.

Considerable amount of work has been expended in studying and proposing ways of limiting in-band crosstalk, but the studies have been mainly limited to OOK [87], DPSK [88] and other lower modulation formats [89], [90]. The impact of in-band crosstalk on advanced modulation formats such as DQPSK and 128QAM has been largely less investigated and further studies in this regard are therefore necessary.

In our study, we extend the work in [91] to investigate the effects of in-band crosstalk in OXCs for backbone optical networks. An analytical model that considers crosstalk signals with different modulation formats is reviewed. Modulation formats that are considered in the study are DQPSK and 128QAM.

Assuming that P_{io}^{jo} is the input power of a channel, the output power P_{i1}^{out} is given by the following relationship:

$$P_{io1}^{out} = P_{io}^{jo} + P_{io}^{jo}\left\{X_{gate}\left[(M-1)P_i^{jo} + P_i^{jo}\right]\right\} + P_{io}^{j}\begin{Bmatrix}(N-1)R_{gate}\left[1+X_{gate}MP_i^j\right]\\ +(M-1)T_F\left[1+X_{gate}MP_i^j\right]\\ +(N-1)(M-1)^2T_FR_{gate}\end{Bmatrix} -$$

$$2\sqrt{P_{io}^{jo}}\sqrt{P_i^{jo}}\begin{Bmatrix}(N-1)\sqrt{R_{gate}}\\ +(M-1)\sqrt{T_F}\\ +(N-1)(M-1)\sqrt{T_FR_{gate}}\end{Bmatrix} - 2P_{io}^{j}\begin{Bmatrix}(N-1)(M-1)\sqrt{R_{gate}T_F}\\ +(N-1)^2(M-1)R_{gate}\sqrt{T_F}\\ +(N-1)(M-1)^2T_F\sqrt{R_{gate}}\end{Bmatrix} -$$

$$2P_{io}^{j}\left\{R_{gate}\sum_{t=1}^{N-2}t + T_F\sum_{t=1}^{M-2}t + R_{gate}T_F\sum_{t=1}^{(M-1)(N-1)-1}t\right\} \qquad (2.19)$$

Accordingly, the relationship between P_{i0}^{out} and P_{io}^{j} is shown in equation 2.20.

$$P_{io0}^{out} = P_{io}^{j}\begin{Bmatrix}(N-1)R_{gatc}\left[1+X_{gatc}MP_i^j\right]\\ +(M-1)T_F\left[1+X_{gateMP_i^j}\right]\\ +(N-1)(M-1)^2T_FR_{gate}\end{Bmatrix} - 2P_{io}^{j}\begin{Bmatrix}(N-1)(M-1)\sqrt{R_{gate}T_F}\\ +(N-1)^2(M-1)R_{gate}\sqrt{T_F}\\ +(N-1)(M-1)^2T_F\sqrt{R_{gate}}\end{Bmatrix} - 2P_{io}^{j}\left\{R_{gate}\sum_{t=1}^{N-2}t +\right.$$

$$\left.T_F\sum_{t=1}^{M-2}t + R_{gate}T_F\sum_{t=1}^{(M-1)(N-1)-1}t\right\} \qquad (2.20)$$

Where,

P_{io1}^{out} is output power of wavelength channel i_o that includes crosstalk effects.

T_F is the filter transmission factor

R_{gate} is the gate extinction ratio and X_{gate} is the OXC gate crosstalk.

N refers to the number of input fibres to the OXC.

M is the number of wavelengths per input fibre.

P_i^{jo} is the power of a wavelength channel in optical fibre j_o that has wavelength i.

P_{io}^{j} is the power of a wavelength channel in optical fibre j that has a wavelength i_o

P_i^j is the power of a wavelength channel in optical fibre j that has a wavelength i.

The gain of the of the gain-clamped semiconductor optical amplifier (GC-SOA) based OXC is set to N for compensation of the distribution of optical power output.

X_{gate} is a parameter that represents the OXC gate imperfections and is given by, $X_{gate} = P_{gate\,(ref)}/P_{gate}$; where P_{gate} is the output power from the GC-SOA gate and $P_{gate\,(ref)}$ is the GC-SOA gate reference output power.

For an OXC with wavelength conversion capabilities, there is always one gate in the *ON* state for every group of N gates, and thus there are NM gates in the *ON* state at any given time for a total of NM^2 gates, assuming maximum traffic load.

Since we assume that one gate will be in the *ON* state for every group of gates, we define $P_{io}^{out\,(ref)}$ as the output power of the wavelength channel i_o when the OXC only carries wavelength channel i_o. This scenario typically arise when no crosstalk occurs in the channel. $P_{io}^{out\,(ref)}$ is given by the following relationship;

$$P_{io}^{out\,(ref)} = P_{io}^{jo} + X_{gate}\left(P_{io}^{jo}\right)^2 \tag{2.21}$$

If the wavelength channel i_o carries a zero bit, then $P_{io}^{out\,(ref)} = 0$. The crosstalk (XT) for a wavelength channel under review is given by;

$$XT = \frac{\left(P_{io}^{out\,(ref)} - P_{io1}^{out}\right)}{P_{io}^{out\,(ref)}} \tag{2.22}$$

$$XT\ (dB) = 10log_{10}XT \tag{2.23}$$

The crosstalk model for the OXC-based WDM system with wavelength conversion is utilised to derive the BER effects in an IM-DD system as follows:

$$BER_{wc} = \frac{1}{8}\left[erfc\left(\frac{1}{\sqrt{2}}\frac{i_1+i_{XT0}-i_D}{\sigma^2_{1\_0}}\right) + erfc\left(\frac{1}{\sqrt{2}}\frac{i_D-i_0-i_{XT0}}{\sigma^2_{0\_0}}\right) + erfc\left(\frac{1}{\sqrt{2}}\frac{i_1+i_{XT1}-i_D}{\sigma^2_{1\_1}}\right) + erfc\left(\frac{1}{\sqrt{2}}\frac{i_D-i_0-i_{XT1}}{\sigma^2_{0\_1}}\right)\right] \quad (2.24)$$

Where BER_{wc} is the worst case of the BER, i_D is threshold current, i_{XT0} is the current due to crosstalk bit 0, i_{XT1} is the current due to crosstalk bit 1, i_1 is the current due to bit 1 and i_0 is the current due to bit 0.

Equation 2.24 describes the scenario that occur when a bit 1 is interfered by a crosstalk bit 0, bit 0 is interfered by a crosstalk bit 0, bit 1 is interfered by a crosstalk bit 1 and bit 0 is interfered by a crosstalk bit 1 [92].

$$\sigma^2_{1\_0} = \sigma^2_{th} + 2eR_d(P_S + P_{sp} + P_{XT\,0})B + \sigma^2_{S-sp} + \sigma^2_{XT\,0-sp} + \sigma^2_{sp-sp} + \sigma^2_{S-XT\,0} \quad (2.25)$$

$$\sigma^2_{0\_0} = \sigma^2_{th} + 2eR_d(P_{sp} + P_{XT\,0})B + \sigma^2_{XT\,0-sp} + \sigma^2_{sp-sp} \quad (2.26)$$

$$\sigma^2_{1\_1} = \sigma^2_{th} + 2eR_d(P_S + P_{sp} + P_{XT\,1})B + \sigma^2_{S-sp} + \sigma^2_{XT\,1-sp} + \sigma^2_{sp-sp} + \sigma^2_{S-XT\,1} \quad (2.27)$$

$$\sigma^2_{0\_1} = \sigma^2_{th} + 2eR_d(P_{sp} + P_{XT\,1})B + \sigma^2_{XT\,1-sp} + \sigma^2_{sp-sp} \quad (2.28)$$

Equations 2.25 to 2.28 give the variances of the crosstalk interference, where; $\sigma^2_{1\_0}$ is the variance when bit 1 is interfered with by crosstalk due to bit 0, $\sigma^2_{0\_0}$ is the variance when bit 0 is interfered with by crosstalk due to bit 0, $\sigma^2_{1\_1}$ is the variance when bit 1 is interfered with by crosstalk due to bit 1 and $\sigma^2_{0\_1}$ is the variance when bit 0 is interfered with by crosstalk due to bit 1.

σ^2_{th} is the thermal noise variance, R_d is the receiver responsivity, B is the bandwidth of the receiver filter and P_S is the signal power. P_{sp} is the ASE power.

The photocurrent for a transmitted bit 1 is given by $i_1 = 2R_dP_S$, and that for a transmitted bit 0, is $i_0 = 0$ where P_S is assumed to be 0.

Other parameters included in the above equations are defined as follows:

σ^2_{S-sp} is the beat power due to the signal and ASE,

$\sigma^2_{XT\,0-sp}$ is the beat power of crosstalk and ASE due to bit 0,

$\sigma^2_{XT\,1-sp}$ is the beat power of crosstalk and ASE due to bit 1,

$\sigma^2_{S-XT\,0}$ is the beat power of the signal and crosstalk due to bit 0,

$\sigma^2_{S-XT\,1}$ is the beat power due to the signal and crosstalk for bit 1,

σ^2_{sp-sp} is the beat power due to ASE and ASE.

Figure 2.10 shows the variation of BER and gate input power for an OXC set at two distinct R_{gate} values. It can be observed from the graph that an optimum gate input power of approximately -18dBm gives a highly favourable BER under the conditions specified in Table 2.2. This desirable result is achieved by meticulously improving the filter transmission factor of the OXC and hence the crosstalk of the system should be kept as low as is possible so as to attain a modest BER. In a nutshell, high resolution filters should be incorporated in the switching fabric of the network so as to limit the effects of crosstalk on the quality of the transmitted signals.

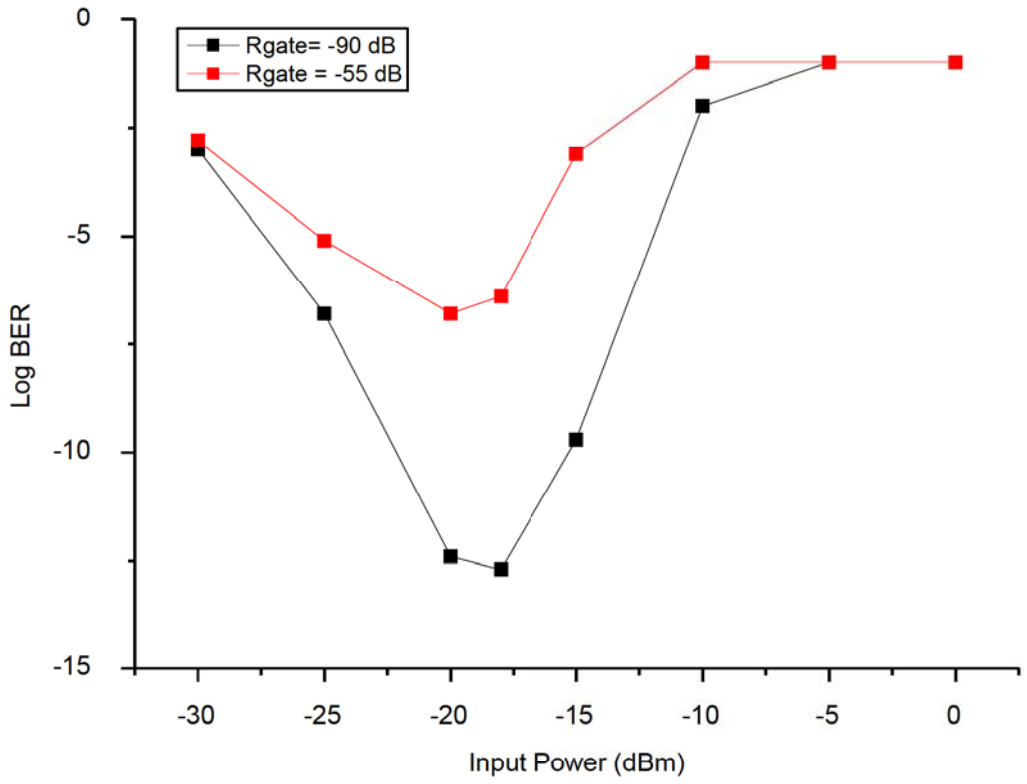

Figure 2.10: The relationship between BER and gate input power for an OXC

Table 2.2: Assumption parameters used in computing the BER due to XT in OXCs

Parameter	**Value**
Temperature	$300\ °K$
Bandwidth (B)	10
Responsivity ($\boldsymbol{R_d}$)	$1\ AW^{-1}$
Amplifier gain (G)	260
Operating frequency (f)	$2 \times 10^{14} Hz$

2.3.7 Polarization Dependent Loss (PDL)

Polarization dependent loss (PDL) refers to the ratio of minimum to maximum coefficient of optical transmission of a device when the input totally polarized light sweeps all states of polarization [93].

Although PDL is almost negligible in optical fibres, it is significant in other pertinent optical network devices such as connectors, multiplexers, demultiplexers and couplers. PDL accumulates as we move from one component to the other and it causes significant variations of the SNR and may lead to very high BER along the optical channel. In particular, PDL generally leads to an imbalance in the OSNR of the two polarization states, and its effects are overtly profound in ultrafast transmission systems that are based on the polarization division multiplexing (PDM) technique.

Considering the probability density function of the coefficient of transmission ($P_x(X)$) in an optical network (X), we find that it depends on the state of polarization of the incoming signal and the transmission function of each fibre along the channel [93].

$$P_x(X) = \frac{1-K}{\sqrt{2\prod n\{(1-K)^2-K(lnK)^2\}}} exp\left[-\frac{\{(1-k)lnX+n(1-K+KlnK)\}^2}{2n\{(1-K)^2-K(lnK)^2\}}\right]\frac{1}{X} \qquad (2.29)$$

Where n is the number of PDL devices in the optical transmission network and K is the PDL value of each PDL component in the network. To gain some insight into the effects of PDL, it is vital to look into the theories and related statistics that characterize its impact on transmitted signals. Authors in [94], [95] and [96] thoroughly investigated the relevant theories on the effects of PDL and explored the concept of principal states of polarization (PSP) in networks that are affected by PDL.

Utilizing the Jones space, states of polarization are related by the 2-d complex column "ket" vector, $|s\rangle \equiv \begin{pmatrix} s_x \\ s_y \end{pmatrix}$ and the corresponding "bra" $\langle s| \equiv (s_x^*, s_y^*)$ conjugate row vector [88].

For PDL considerations, the Jones vectors are assumed to be not normalized, thus,

$$\langle s|s\rangle \equiv (s_x^* s_x, s_y^* s_y) \qquad (2.30)$$

The cognate Stokes vector, $\hat{s} = (s_1, s_2, s_3)$ is defined by $\hat{s} \equiv \langle s|\vec{\sigma}|s\rangle / \langle s|s\rangle$, where $\vec{\sigma} \equiv (\sigma_1, \sigma_2, \sigma_3)$ is the Pauli matrix vector whose respective components are the Pauli matrices [97]:

$$\sigma_1 \equiv \begin{pmatrix} 1 & 0 \\ 0 & -1 \end{pmatrix}, \sigma_2 \equiv \begin{pmatrix} 0 & 1 \\ 1 & 0 \end{pmatrix}, \sigma_3 \equiv \begin{pmatrix} 0 & -i \\ i & 0 \end{pmatrix} \tag{2.31}$$

The Pauli matrices are defined according to the Stokes space, where the Stokes parameter $s_3 \equiv \langle s|\sigma_3|s\rangle / \langle s|s\rangle$ is non-negative and equal to unity. It should be noted that the Stokes vector $\hat{s}$ is real and it is of unit length. Accordingly, the Stokes vector's last point rests on the surface of the Poincaré sphere. The state of polarization is completely characterized either by the Stokes parameters s_1, s_2 and s_3, or by the equivalent angles of the Poincaré sphere 2Ψ and 2χ.

A parameter known as the power transmission coefficient (τ) of a network with PDL, describes the extent of the PDL effects and it relies on the initial state of polarization. The maximum transmission coefficient is denoted by τ_{max}, and the smallest transmission coefficient is represented by τ_{min}, and it is further assumed that the corresponding Stokes space vectors are not automatically linear. The Stokes vectors' degree of polarization (DOP) is unity and the vectors are mutually orthogonal ($\hat{s}_{max} = -\hat{s}_{min}$). For unpolarized light (DOP=0), the transmission coefficient is given by:

$$\tau_{unpol} = (\tau_{max} + \tau_{min})/2 \tag{2.32}$$

The parameters τ_{max}, τ_{min} and $\hat{s}_{max}$ completely characterize the PDL in a system. The footprint of a PDL element is given by the Jones vector:

$$|t\rangle = \sqrt{\tau_{max}} e^{(-\frac{\alpha}{2})} e^{(\frac{\vec{\alpha}}{2}\vec{\sigma})} |s\rangle \tag{2.33}$$

Where $\vec{\alpha}$ is the differential loss vector. Further simplification of equation 2.33 leads to:

$$|t\rangle = \sqrt{\tau_{max}} e^{(-\frac{\alpha}{2})} \left[cosh(\alpha/2) \begin{pmatrix} 1 & 0 \\ 0 & 1 \end{pmatrix} + sinh(\alpha/2) \begin{pmatrix} e_1 & e_2 - ie_3 \\ e_2 + ie_3 & -e_1 \end{pmatrix} \right] |s\rangle \tag{2.34}$$

Where e_1, e_2 and e_3 refer to the orientation of minimal attenuated SOP.

In our study, we assume that τ_{max}/τ_{min} is greater than 0.5 and thus we can expect the differential loss and PDL to be equally distributed.

Figure 2.11 shows the variation of total PDL with the number of PDL elements in optical network. It can be observed that the probability density function (PDF), in dB, emulates a Maxwellian distribution. This implies that PDL becomes particularly problematic for long-haul backbone optical networks where there is a significant number of switching fabrics that are inherently prone to PDL effects. Generally, dynamic polarization controllers are normally used to minimize the PDL effects in various optical components. These controllers' deployment increase the energy consumption of optical networks and it is necessary to limit and manage their operation so as to utilize energy efficiently.

In order to limit the effects of PDL in such networks, high purity and low loss optical fibres such as the PSCF should be deployed together with switching fabrics that introduce sufficiently low PDL in the networks. This will ideally result in the overall reduction of switching fabrics and thus lower energy consumption and acceptable OSNR.

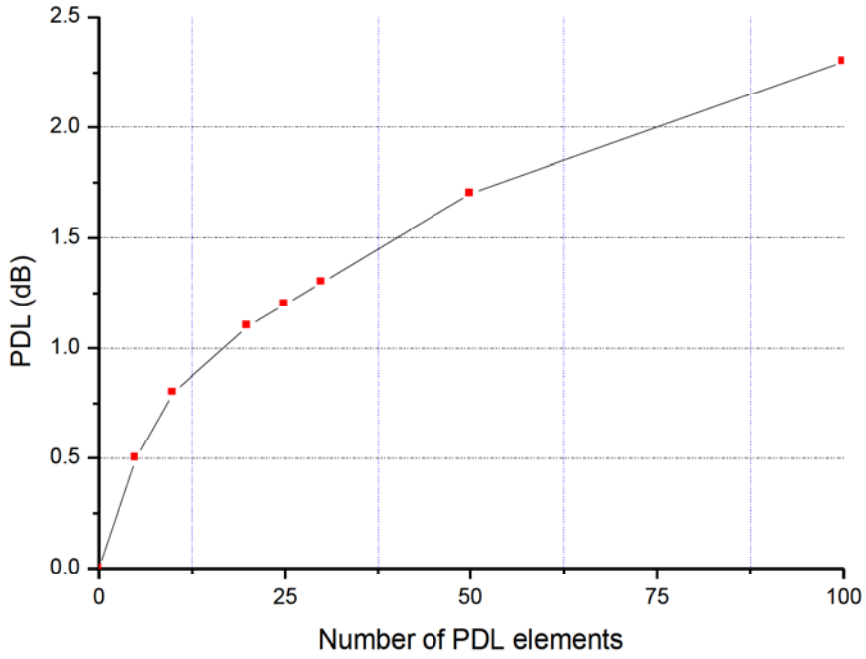

Figure 2.11: Relationship between PDL and number of PDL elements

2.4 Non-linear impairments

Pertinent non-linear impairments that adversely degrade optical signals are: self-phase modulation (SPM), cross-phase modulation (XPM), four-wave mixing (FWM), stimulated brillouin scattering (SBS), and stimulated Raman scattering (SRS) [35].

2.4.1 Self-Phase Modulation (SPM)

SPM is an important nonlinear effect that arises due to the refractive index's dependence on the intensity of propagating optical signals in the communication channel (Figure 2.12). SPM occurs when the phase of the signal is modulated by its own intensity and leads to pulse broadening.

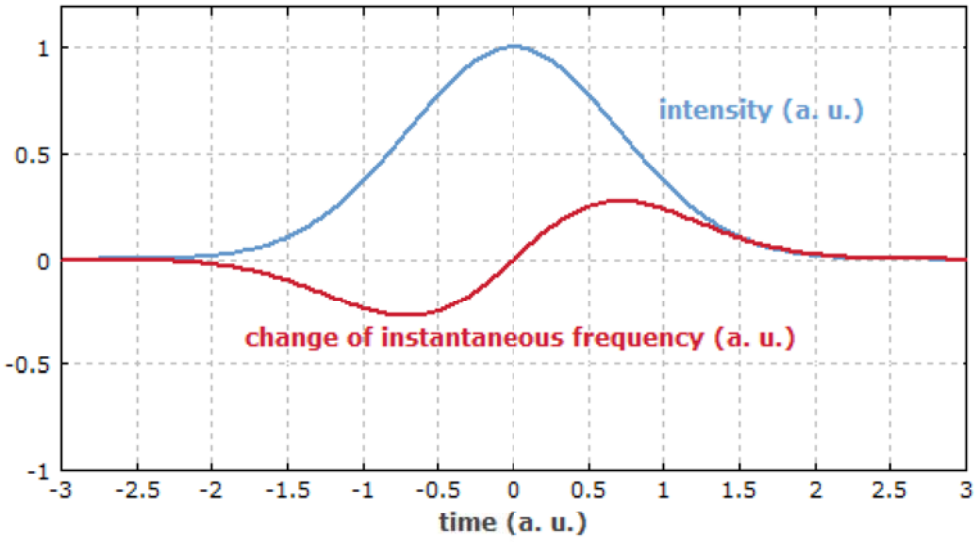

Figure 2.12: Self-phase modulation of an initially unchirped pulse

For an optical signal that traverses through the optical fibre, the higher intensity segment of the pulse experiences a higher refractive index compared to its lower intensity counterpart [98].

Consequently, the front section of a pulse encounters a positive refractive index gradient $\left(\frac{dn}{dt}\right)$, and the tail-end of the pulse experiences a negative refractive index gradient $\left(-\frac{dn}{dt}\right)$. This change in the refractive indices gradient leads to temporally altering phase changes that are dependent on the pulse intensity. We denote the phase introduced by the electric field (E) as φ, and it can be expressed as follows:

$$\varphi = \frac{2\pi}{\lambda} nL \tag{2.35}$$

Where, n, λ and L are the refractive index, wavelength of the propagating signal and the length of the fibre respectively. Assuming that the power transmitted into the optical fibre is sufficiently high, the phase may be expressed by the following relationship:

$$\varphi = \frac{2\pi}{\lambda} n_{eff} L_{eff} = \frac{2\pi}{\lambda} (n_l + n_{nl} I) L_{eff} \tag{2.36}$$

Where, n_{eff} is the effective refractive index, L_{eff} is the effective fibre length, n_l is the linear refractive index, n_{nl} is the non-linear refractive index, and I is the optical intensity of the pulse. It is important to note that the variation of phase with respect to time results in the modification of the frequency spectrum (ω), and can be represented by the following relationship:

$$\omega = \frac{d\varphi}{dt} \tag{2.37}$$

The temporal spectrum change causes a change in the pulse variation, and if we consider a Gaussian pulse that modifies an optical carrier frequency (ω_0), another instantaneous frequency (ω') is created, and is represented by:

$$\omega' = \omega_0 + \frac{d\varphi}{dt} \tag{2.38}$$

The phase change due to SPM is negative, and the frequency expression may be written as follows:

$$\omega' = \omega_0 - \frac{2\pi}{\lambda} n_{nl} L_{eff} \frac{dI}{dt} \tag{2.39}$$

SPM is very problematic for networks that operate above 10 Gbps because its effects result in high BER that manifest as low OSNR. It is therefore vital to consider their contribution in routing and wavelength assignment decision-making processes so as lower blocking probabilities. One way of reducing the effect of SPM in modern networks is to employ the technique of offset filtering transmitted signals. This occurs via the all-optical regeneration of signals where a chirping effect that is opposite to the one introduced by SPM is induced so as offset the undesirable pulse broadening caused by SPM. Another innovative way of reducing the effects of SPM in networks is the use of non-linear optical loop mirrors (NOLMs). The NOLMs are essentially optical bidirectional couplers that utilize interferometry to offset the effects of SPM on transmitted signals. However, these seemingly ingenious techniques to curtail the effects of SPM are power hungry and lead to increased energy consumption and thus higher carbon footprints of the networks. The use of low-loss and dispersion compensated optical fibres that are capable of containing high power pulses may be a cost-effective and long term solution to the effects of SPM in optical networks.

2.4.2 Cross-Phase Modulation (XPM)

XPM originates from the nonlinear phase shift of signal induced by a co-propagating signal at a disparate wavelength. One crucial way of analysing the effects of XPM in WDM systems is anchored on intensity and phase modulation of propagating pulses [99]. In this kind of a model, the Q-factor is an important parameter in the analysis of XPM-induced power penalty in IM-DD systems and can be expressed as follows:

$$Q = \frac{2k\bar{P}(r-1)/(r+1)}{\sqrt{\frac{2k_{sp}r\bar{P}}{r+1}+\left(\frac{2kr\bar{P}}{r+1}\right)^2.\sigma_n^2}+\sqrt{\frac{2k_{sp}\bar{P}}{r+1}}} \quad (2.40)$$

Where, k and k_{sp} are constants that depend on the receiver type, r is the extinction ratio, $\overline{P}$ is the average optical power at the receiver, and σ_n^2 is the variance of the XPM-induced intensity modulation.

The effective XPM noise power can be evaluated by using the following equation:

$$\sigma_{xpm}^2 = \overline{P(0)}^2 \sum_{i\in N} \frac{1}{2\pi} \int_{-\infty}^{\infty} \left|H_{xpm,i}(\omega)\right|^2 \left|H_{filter}(\omega)\right|^2 PSD_i(\omega) \quad (2.41)$$

Where, $\overline{P(0)}$ is the initial link average power of probe channel, N is the number of probe channels, $H_{xpm,i}(\omega)$ is the transfer function of XPM, $H_{filter}(\omega)$ is the transfer function of the optical filter and $PSD_i(\omega)$ is the power spectrum density of the i^{th} channel respectively [100].

XPM is commonly minimized by appropriately managing channel spacing in WDM systems. This is ideally implemented by leaving unused wavelength channels between lightpaths so as reduce the impact of XPM in the systems [101]. Although this approach appears lucrative and simple, it may not be prudent to implement it for long-haul high speed optical networks. If the technique is applied in such networks, it would translate to higher capex and increased energy consumption due to the need for the deployment of more optical fibres and other necessary ancillary switching fabrics so as to cater for the unused channels on the optical fibres. The use of ultra-low loss and DCF fibres may assist in the reduction of XPM effects in long-haul optical networks.

2.4.3 Four Wave Mixing (FWM)

FWM arises due to the Kerr effect and it occurs when at least two signals of different wavelengths traverse the same optical channel. Assuming just two input signals with wavelengths λ_1 and λ_2, a refractive index modulation at the difference wavelength occurs, which creates two additional wavelength components. In essence, two new wavelength components are generated, and these are [102]:

$$\lambda_3 = \lambda_1 - (\lambda_2 - \lambda_1) = 2\lambda_1 - \lambda_2, \tag{2.42}$$

and

$$\lambda_4 = \lambda_2 + (\lambda_2 - \lambda_1) = 2\lambda_2 - \lambda_1 \tag{2.43}$$

The total power of the FWM signal can be calculated by employing equation 2.44:

$$P_{fwm} = \sum_{a,b,c} P_{(a,b,c)} \tag{2.44}$$

Where, P_{fwm} is the power of any FWM signal generated by any multiple combinations with wavelengths λ_a, λ_b and λ_c.

The noise that arises due to FWM can be evaluated using the following equation:

$$\sigma^2{}_{fwm} = 2P_0 P_{fwm} \tag{2.45}$$

One technique of suppressing FWM impact on the quality of transmission is to increase the channel spacing. The increase in channel spacing ideally leads to an arrangement where the new generated wavelengths components fall outside the useful range of optical channels, and thus the decreased likelihood of intra-channel interference [103].

Suppose that four input signals are launched in a WDM system at 193.175 THz, 193.225 THz, 193.275 THz and 193.325 THz respectively. We assume that the channel spacing is uniform at 100 GHz, 50 GHz, 25 GHz and 12.5 GHz respectively. Figure 2.13 shows the relationship between the BER and equal channel spacing for the four different channels. It can be seen from Figure 2.13 that the BER significantly decreases as the channel spacing is increased. This may be due to the decrease in interference between the input signals that result in a reduction in FWM in the system.

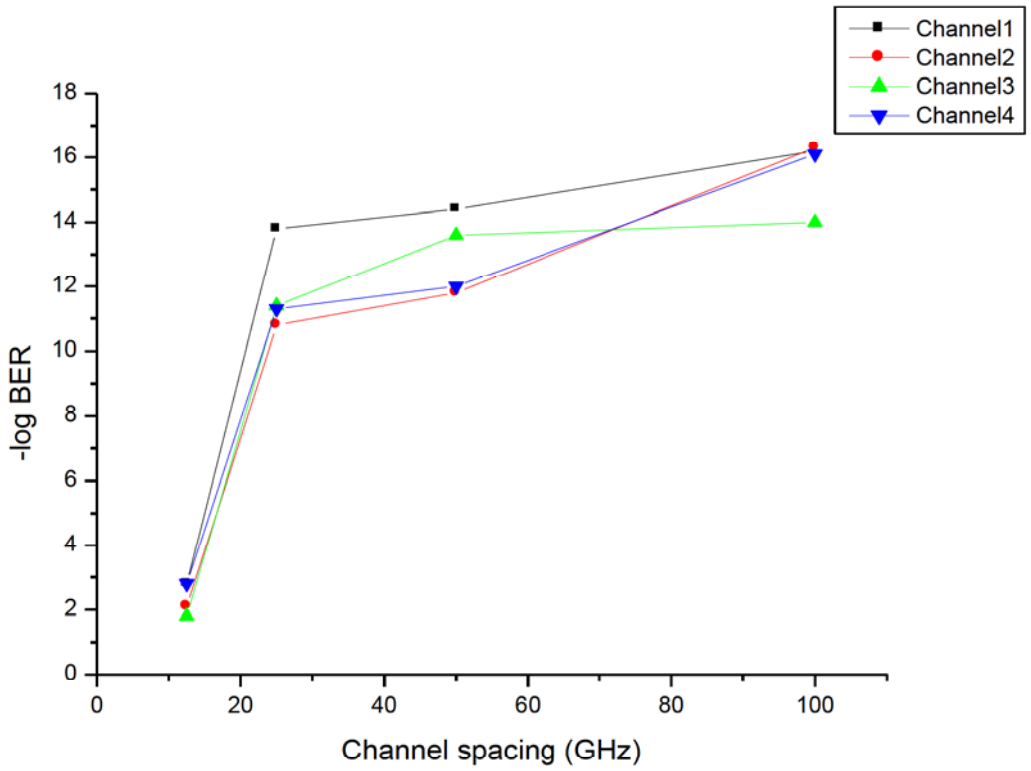

Figure 2.13. Relationship between BER and uniform channel spacing for four different channels

We now consider the scenario presented above with the same parameters but making use of unequal channel spacing for the four signals at 193.190 THz, 193.255 THz, 193.305 THz and 193.370 THz. It can be observed from figure 2.14 that the BER greatly improves with the non-uniform channel spacing compared with its uniform channel spacing counterpart.

This implies that in non-uniform channel spacing, intra-channel interference of input signals is profoundly lowered and thus FWM impact is less pronounced.

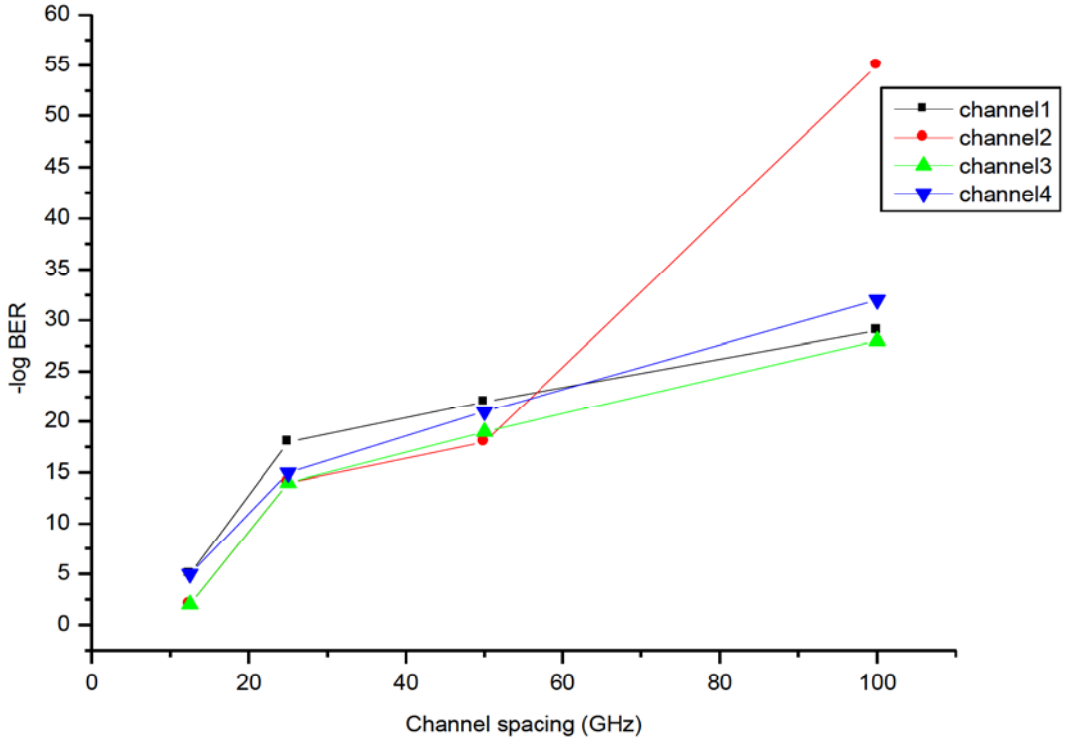

Figure 2.14: Relationship between BER and non-uniform channel spacing for four different channels

The model presented above for Q-factor estimation takes into consideration cardinal linear and non-linear physical layer impairments in optical networks. By employing analytical techniques to numerically compute the Q-factor, this model can provide a satisfactory estimation of the extent of signal health degradation due to physical layer impairments.

2.4.4 Stimulated Brillouin Scattering (SBS)

Nonlinear scattering in optical fibres arise due to the inelastic scattering of photons. Thermal phonons are created as a propagating optical signal in a fibre compresses the dielectric material when its intensity exceeds a particular threshold. A wave known as Stokes wave is

generated due to the inelastic interaction between a propagating optical signal and a diffracted wave in the optical waveguide. The Brillouin shift is the frequency shift between these two waves. Stimulated Brillouin scattering is typically observed at low signal power levels in the order of a few mW [104], [105].

Suppose an electric field oscillates at a pump frequency ω_P, an acoustic wave with a frequency ω_B is generated. Assuming spontaneous Brillouin scattering, the pump photon is annihilated, and the both a Stokes photon and an acoustic phonon are simultaneously generated. Application of the conservation laws of energy and momentum to the process yields the following [106]:

Conservation of energy:
ω_B must be equal to $(\omega_P - \omega_s)$, where ω_s is the Stokes wave frequency.

Conservation of momentum:

$$K_A = (K_P - K_S) \tag{2.46}$$

Where K_A is the momentum vector of the acoustic wave, K_P is the momentum vector of the pump wave and K_S is the momentum vector of the Stokes wave.

Taking v_A as the acoustic wave velocity, the dispersion relationship can be written as follows:

$$\omega_B = v_A \left|\overrightarrow{K_A}\right| = v_A \left|\overrightarrow{K_P} - \overrightarrow{K_S}\right| \tag{2.47}$$

or

$$\omega_B = 2v_A \left|\overrightarrow{K_P}\right| sin\frac{\theta}{2} \tag{2.48}$$

Where θ is the angle between the pump and Stokes momentum, and the modulas of K_P and K_S is assumed to be nearly equal.

The maximum backward frequency shift is obtained when $v_B = \frac{2nv_A}{\lambda_P}$

Where n is the mode index.

SBS challenges can be sufficiently addressed by increasing the linewidth of propagating signals in order to overcome the power threshold limitations that they impose on optical signals.

2.4.5 Stimulated Raman Scattering (SRS)

The main difference between SRS and SBS is that acoustic phonons bring about SBS, whereas optical phonons are responsible for SRS. Degradation of optical signals is generally not severely affected by SRS and thus SRS is not a very critical nonlinear impairment as compared to some of the impairments discussed above.

2.5 Strategies of reducing energy consumption in core networks

Due to the purposeful global campaigns aimed at mitigating factors that cause environmental pollution, the telecommunication sector joined the bandwagon in the quest to protect our environment by adopting initiatives that are geared towards energy-efficient communication networks [107]. In addition, the current departure from the traditional technologies and strategies does not only result in the reduction of harmful gases released into the environment, but also lead to substantially low opex for network operators. As previously stated in the preceding chapter, a significant number of scholars have focused their attention in conducting research in this important niche area in order to come up with energy-efficient solutions for backbone communication networks. The proposed energy-efficient solutions can be broadly classified into the following four approaches:

i. **Network redesign**: Designing energy-efficient networks using optical and electronic technologies;
ii. **Traffic engineering**: Developing energy-aware traffic grooming schemes;
iii. **Energy-aware networking**: Powering devices ON/OFF between different operating states;

iv. **Load-adaptive operation**: Adopting rate-adaptive and multi-line/link rate techniques.

In this section, an overview of each of the aforementioned approaches is carried out.

2.5.1 Network Redesign

Generally, the energy usage of the core network can be significantly lowered by redesigning the physical links and the core nodes. Traditionally, the physical links rely on optical technologies, whereas the core nodes have essentially been based on electronic technology [8]. Since electronic devices are slower than their optical components, there is a need to gradually replace most electronic switching components by optical switching devices [108]. Through the technique of "multiple-shelves", the speed of an electronic core router can be improved, but at the expense of increased energy consumption [109]. However, the replacement of a core electronic router by an OXC provides opportunities for very fast switching due to the elimination of bottlenecks that arise due to slow electronic processing. In addition, potential energy savings will be realized as well [110]. Table 2.3 shows some vital information about various core network devices and their respective energy consumptions [111].

Table 2.3: Power consumption values of key core network devices

Device	Product	Capacity	Power consumption
Core router	Cisco CRS-1	1.2 Tbps	9.63 kW
	Cisco CRS-3	4.4 Tbps	12.3 kW
	Juniper T1600	1.6 Tbps	8.35 kW
	Juniper T4000	4 Tbps	9.83 kW
Transponder	Fujitsu Flashwave 7200	10 Gbps	68.5 W
	Transmode 10 G tunable	10 Gbps	25 W
OXC	Cisco 40-Channel OXC	2-degree	400 W
	Cisco 80-Channel OXC	2-degree	550 W
Amplifiers	Cisco ONS 1454 PrA	1 fibre	78 W
	Alcatel LM1600 ILA	1 fibre	52 W
	Cisco ONS 1454 ILA	1 fibre	46 W
	Infira EDFA	1 fibre	106 W
Regenerator	Cisco optical regenerator	2.5 Gbps	100 W
	iLynx regenerator	2.5 Gbps	8 W
	40 G electronic regenerator	40 Gbps	126 W
Converter	All-optical regenerator	1 wavelength	6 – 80 W
	Tunable wavelength converter (TWC)	1 wavelength	500 – 800 mW
	Fixed wavelength converter (FWC)	1 wavelength	600 mW
	All-optical wavelength converter (AOWC)	1 wavelength	2 W

By redesigning the physical topology of the core networks via the optimization of available links, massive energy savings may also be realized [112]. Since the capex of an optical core network is mainly determined by link deployment costs, it is therefore prudent and logical to interconnect core nodes through as fewer number of links as is possible. However, it is crucial to strike a balance between the number of links and energy consumption as some topologies may contain fewer links but end up consuming significantly large amounts of energy. Figures 2.15 (a) and 2.15 (b) show two different topologies designed to reduce cost and energy consumption respectively.

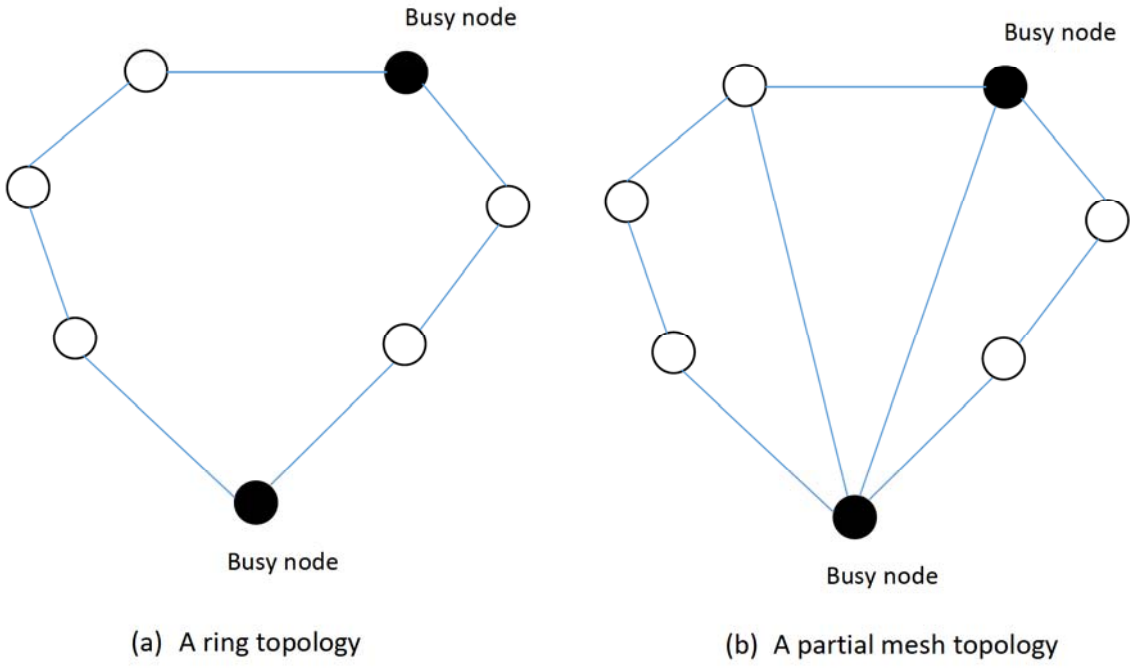

Figure 2.15: Two distinct topologies connecting 7 core nodes

2.5.2 Traffic Engineering

Another way of reducing energy consumption of core networks is to limit the use of network devices such as ports and fibres, by utilizing traffic grooming techniques [8], [113]. If several low-granularity traffic movement is aggregated into a few, high-granularity traffic flow, the number of wavelengths that traverse the core network will be drastically reduced and this leads to a reduction in demand of network resources [114], [115].

Wavelength grooming occurs when several sub-wavelength traffic is aggregated into a single wavelength, and waveband grooming arises when several wavelengths are aggregated into a single waveband.

Since a large portion of modern backbone network traffic is for internet services, it implies that the connection requests arrive randomly and their durations vary over different time periods. Several energy-reducing approaches have been proposed for such kinds of dynamic traffic, and some of the most effective dynamic grooming approaches include the Power-Efficient Grooming Algorithm (PEGA) and the Time-Aware Traffic Grooming (TATG) [116] - [119]. In PEGA, new lightpaths are only established in the event of capacity constraints on existing lightpaths, otherwise, the new requests are incorporated into lightpaths already in existence. The TATG approach uses appreciably less energy at low traffic loads, but uses up more energy at high traffic loads.

In a nutshell, traffic grooming is essential in modern backbone networks as it aids in reducing energy consumption by optimizing resource usage via minimization of network devices usage.

2.5.3 Energy-aware networking

In general, network elements in core networks are configured to support peak-period traffic and thus during off-peak periods, significant amounts of energy are unwisely wasted since most devices will not be performing any functions [13], [120], [121]. Due to the increased sizes of current networks, and hence several energy consuming devices, it has become very critical and important to switch off some devices during low traffic periods, and this in turn calls for the adjustment of routing schemes to be fully optimized to become energy-efficient. A number of scholars have proposed and developed several schemes that are responsive to the energy demands of the networks, and these schemes can be subdivided into energy-aware routing and energy-aware network design [28], [122], [123].

Energy-aware routing can be accomplished by exploiting the technique of multilayer traffic engineering (MLTE) whereby routing is optimized and logical topology adaption is enabled by the creation of a virtual mesh layer and the subsequent computation of the most energy-efficient route.

This results in the rerouting and grooming of traffic and adaptation of the topology results in switching off devices that will not be in use. Through the use of energy-aware routing techniques, several approaches may be implemented to switch off the network nodes, and these include:

i. When a node is completely redundant.
ii. When the traffic passing through a node falls below a preset level.

It is important to note that each approach may lead to some undesirable network management challenges such as a compromised QoS, and therefore a trade-off between potential energy savings and network performance should be considered.

A fairly novel and exciting innovative approach to energy-aware routing involves the concept of *green routing* whereby network nodes are mindful of the source of their power [13]. In such schemes, routing can be optimized to utilize as much energy from renewable sources as is possible, thereby leading to lower GHG emissions that arise from powering communication networks.

Energy-aware networking schemes such as the sleep mode operation, were initially conceived for Ethernet and LANs and their development was made possible by considering daily traffic variations of several networks [124], [125]. The results from the dedicated studies showed that a significant number of specific links provided an opportunity for energy savings and guaranteed network robustness against link failures [126]. It is essential to bear in mind that in the noble quest of developing energy-aware schemes, greater emphasis need to be placed on reducing network disruptions and configurations.

2.5.4 Load-adaptive Operation

The bulk of most active core networks operate on a single line rate (SLR) such as a 10 Gbps despite different capacity demands that actually exist between traffic nodes [127]. It is not surprising therefore that core networks that operate on SLR exhibit poor utilization of network resources and consequently use more energy than would be essential in their operations [128]. In order to intelligently manage and utilize energy efficiently, it is desirable to use a minimum number of network elements that are capacitated to meet the actual demand of the network.

For example, it would be logical and effective to deploy a single 40 Gbps transponder if a 37 Gbps traffic exists between two nodes than to deploy four 10 Gbps transponders to accomplish the same task. The deployment of links that support mixed line rates (MLR) appear to be an important step in the right direction in as far as energy-efficiency is concerned in future networks. MLR are capable of adjusting network bandwidth to that required by individual lines and thus lead to appreciable energy savings as opposed to the networks that only support SLR [129]. Networks that support also referred to as elastic optical networks (EON) and are destined to lead the revolution of the next generation ultrafast backbone networks. Despite directly lowering energy consumption due to their adaptability to variable lightpath patterns, EONs also improve the overall spectral efficiency of links and thus impact positively on the general energy efficiency of the entire backbone network [130].

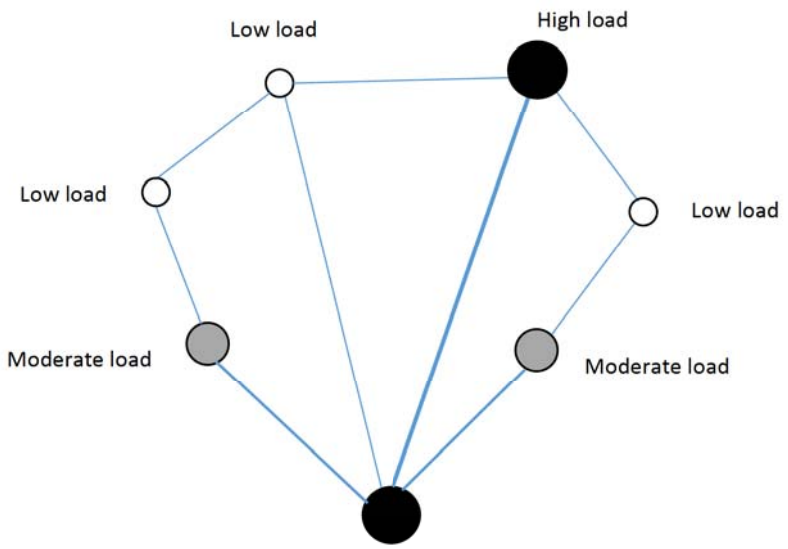

Figure 2:16: A core network that employs the MLR technique

Figure 2.16 depicts a schematic diagram of a core network that employs the MLR technique. The core nodes are represented by circles and their traffic capacities are illustrated by the sizes of the respective circles. In addition, the line thicknesses indicate the extent of utilization of the core edges.

2.6 Summary

Physical layer impairments that compromise the quality of transmitted optical signals are discussed in this chapter. The impairments are broadly divided into linear and non-linear impairments. Linear impairments are independent of the signal power and influence each of the optical channels separately, on the other hand, nonlinear impairments result in interference between channels in addition to affecting each optical channel individually. The linear impairments discussed include CD, PMD, fibre attenuation, PDL and XT. On the other hand, the non-linear impairments reviewed include SPM, XPM, FWM, and SBS. It is found out that the effects of impairments such as FC and SBS become prominent in high speed networks and may not be ignored in formulating RWA algorithms of these core networks.

Strategies employed to curb energy consumption in backbone networks are also presented, and these are: (i) Network redesign, (ii) Traffic engineering, (iii) Energy-aware networking, and (iv) Load-adaptive operation. It is shown that these techniques are capable of significantly lowering the energy use of core networks when applied in various traffic contexts and topologies.

3 Energy efficiency and Impairment Aware-Routing and Wavelength Assignment

3.1 Introduction

The issue of the efficient utilization of energy has undoubtedly taken centre stage in the 21st century due to a myriad number of reasons. There are concerted and coordinated efforts globally to prioritize energy conservation and the scientific research community has been at the forefront of spearheading this noble cause. According to the International Energy Agency, 13371 Mtoe (million tonnes of oil equivalent) of energy was supplied to the whole world in 2012 [131]. Figure 3.1 shows the energy supplied in 2012 by type of fuel.

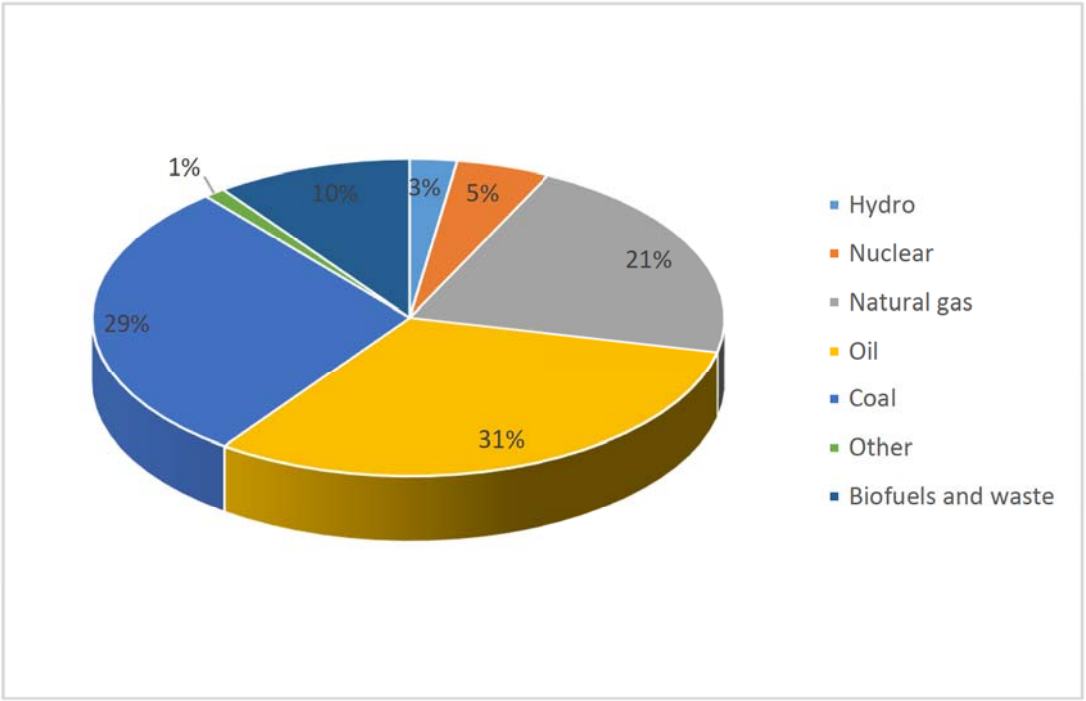

Figure 3.1: World energy supplied in 2012

It is evident from the data given above that traditional energy sources such as oil and coal are still widely preferred for energy generation. These energy sources are non-renewable and thus may eventually get used up in the near future. In addition, these non-renewable energy sources pose serious global environmental and health challenges since they produce large quantities of the so-called greenhouse gases (GHG). GHGs are a major cause of global

warming and their adverse effects include higher average global temperatures that lead to natural disasters like droughts and floods.

It is without doubt that the carbon footprint of the ICT sector has drastically increased over the past decade. This is mainly so due to the deployment of high speed telecommunications networks to meet the ever-increasing demand for efficient and bandwidth hungry applications such as video streaming [132], [133], [134].

Authors in [135], [136] point out that the growth rate of electricity consumption in telecommunication networks outpaces the overall electricity usage. The increase in the traffic volume of telecommunications networks has imperatively led to increased energy consumption by these networks [137], [138]. Figure 3.2 shows a projection of energy consumption by telecommunication networks in the next few coming years [139].

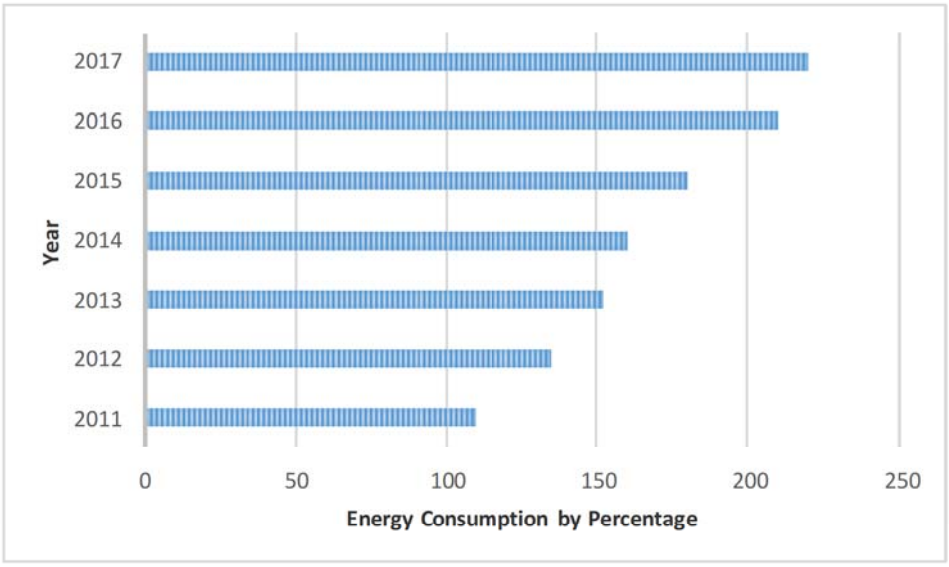

Figure 3.2: Energy consumption prediction of telecommunication networks

The advent of smart grids (SGs) has opened up glamorous opportunities for the exploitation of vast renewable energy sources for the powering of high-speed telecommunication networks. In simple terms, a smart grid (SG) is an intricately integrated hybrid power generating system that allows bidirectional flow of both energy and data between devices and power generators. An important aspect of a SG is the ability to incorporate power generation

from diverse sources such as wind and the sun. Predictably, the benefits derived from such distributed generation are immense and some of them include, improved energy system reliability and flexibility. In addition, energy efficiency is greatly enhanced, and in the process the GHG emissions are significantly reduced due to the effective use of renewable energy sources such as solar and wind [140].

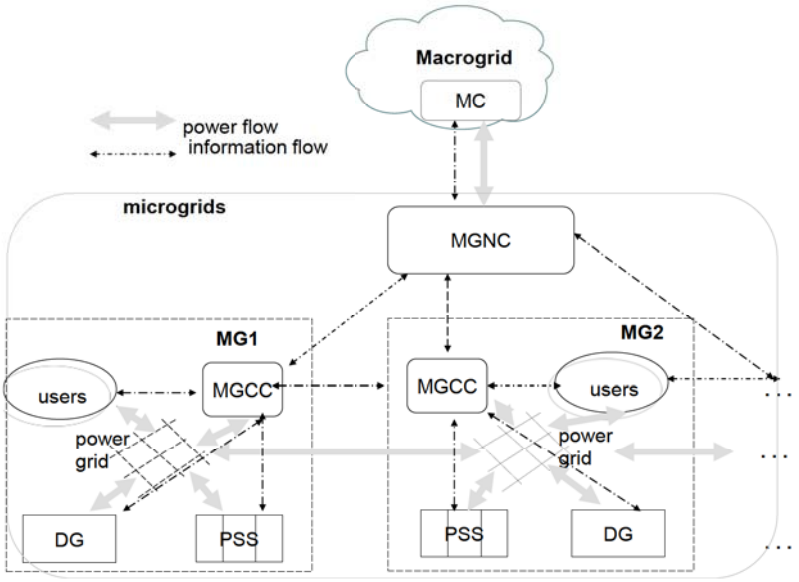

Figure 3.3: A Smart Grid model

Figure 3.3 shows a model of a typical SG. This model consists of a single macrogrid and several microgrids (MGs) such that the macrogrid can supply power to MGs that may require it. In the same vein, the MGs can always supply excess power to the macrogrid in a formal trading arrangement. The macrogrid is essentially equipped with traditional power generating sources such as hydro and coal-fired stations. A macrogrid controller (MC) ensures optimal power distribution to all the users within the macrogrid, and it also facilitates external power trade with MGs and other macrogrids through the MG control center (MGCC). A typical MG consists of several distributed generation (DG) sources, a power storage system (PSS), smart infrastructure, a set of users and a single MGCC. A MG network controller (MGNC) acts as an interface between the macrogrid and the MGCCs [141].

Taking into the cognisance the importance of reducing global warming, it is therefore logical and noble to design and develop energy-efficient next generation telecommunication networks. Since modern backbone telecommunication networks heavily rely on optical networks due to their superior speed and capacity, it becomes vital to study and come up with ingenious ideas to reduce energy consumption in these networks. Although a number of scholars have shown interest in pursuing studies in energy consumption of optical networks, the research area of energy-efficient optical networks is fairly novel and in its infancy.
The reduction of energy use in optical networks can be generally solved at four main levels, viz: component, transmission, network and application [134].

The deployment of all-optical components such as OXCs and related switching fabrics will evidently reduce energy consumption at the component level [142]. The introduction of low-loss and low-dispersion optical fibres and energy-efficient transponders has the potential to improve energy utilization during the transmission stage [142]. Energy-aware and efficient resource allocation strategies and green routing have been earmarked to be the front running techniques for the reduction of energy consumption at the networking level [143]. Green cloud computing has been proposed as a key innovative way of energy consumption reduction at the application stage in optical networks [144].

3.2 Energy Consumption in Optical Networks

This section shows the computation of energy consumption in all-optical networks. The main components considered in the calculations include, OXCs and EDFA amplifiers. Energy may be defined as the product of power and time, and in optical networks, there are two main types of energy that are normally considered. These are, (i) Energy consumed during the transmission of one bit over an optical fibre, and (ii) Energy consumed during the optical signal switching process. The average bit rate (B) is the inverse of the average time to transmit an optical bit over an optical fibre, and is given by the following equation:

$$B = \frac{1}{T_{bit}} \tag{3.1}$$

Where T_{bit} is the time taken to transmit one optical bit over the fibre.
The energy consumed per bit is given by:

$$E_{bit} = P_T T_{bit} \tag{3.2}$$

Where E_{bit} is the energy consumed per bit over a distance of l km, and P_T is the power dissipated.
Assuming that a path is made up of a transmitter, several EDFAs, OXCs and a receiver, then P_T may be expressed as follows:

$$P_T = P_{Tx} + P_{EDFA} + P_{OXC} + P_{Rx} \tag{3.3}$$

Where P_{Tx}, P_{EDFA}, P_{OXC} , P_{Rx} are the total powers consumed by the transmitter, EDFAs, OXCs and receiver respectively.

If an optical bit traverses J hops with each hop consisting of k in-line EDFAs, the total energy consumed due to the OXCs and EDFAs is given by,

$$(J+1)E_{bit}^{OXC} + kJE_{bit}^{EDFA} \text{ for } J > 1 \tag{3.4}$$

Taking use of the network architecture given in [145], the energy per bit consumed for a given source-destination pair is expressed by,

$$E_{bit\langle s,d\rangle} = (P_{Tx} + P_{Rx})T_{bit} + \sum_{\forall i \in Z} k_i E_{bit}^{EDFA} + (J+1)E_{bit}^{OXC} \tag{3.5}$$

Where Z is the shortest path for the source-destination pair.

A relationship between E_{bit} and BER is now derived for a typical On-Off Keying (OOK) modulation format. For an OOK scheme, the BER is given by the following equation:

$$BER = Q\left(\frac{\langle I_1\rangle - \langle I_0\rangle}{\sigma_1 + \sigma_0}\right) \tag{3.6}$$

Where, $Q(x) = \frac{1}{\sqrt{2\pi}} \int_x^{\infty} e^{-\frac{y^2}{2}} dy$

$\langle I_1 \rangle$ and $\langle I_0 \rangle$ are the mean photocurrent values of high and low signal levels respectively

σ_1 and σ_0 are the standard deviations of high and low signal noise levels respectively.

Given that P_0 *and* P_1 are the received optical powers when "low" and "high" bits are transmitted respectively, we formulate a relationship between received optical powers and mean photocurrents as follows,

If $\mathcal{R}$ is the responsivity of the photodetector, then,
$I_1 = \mathcal{R}P_1$ and $I_0 = \mathcal{R}P_0$.

The standard deviation of the photocurrent is given by,

$$\sigma_1 = \sqrt{2qI_1B_e + 4k_BTB_e/R_L} \tag{3.7}$$

$$\sigma_0 = \sqrt{2qI_0B_e + 4k_BTB_e/R_L} \tag{3.8}$$

Where, q is the electronic charge, B_e is the electrical bandwidth, k_B is the Boltzmann constant, T is the temperature in $°K$, and R_L is the load resistance.

P_0 *and* I_0 are assumed to be both zero for an ideal OOK modulation scheme, therefore,

$$I_1 = \mathcal{R}L_tP_T \tag{3.9}$$

Where, $P_1 = L_tP_T$

P_T is the transmitted power, L_t is the loss incurred by signal during transmission.
The loss incurred for one hop is given by,

$$L_t = e^{\alpha l}L_{mux}L_sL_{demux} \tag{3.10}$$

Where, α is the optical fibre attenuation, l is the length of the fibre. L_{mux}, L_s *and* L_{demux} are the multiplexer, switch and demultiplexer losses respectively.

Combining the above equations yield,

$$BER = Q\left(\frac{\mathcal{R}e^{\alpha l}L_{mux}L_sL_{demux}P_T}{\sigma_0+\sqrt{2q\mathcal{R}(L_tP_T)B_e+4k_BTB_e/R_L}}\right) \tag{3.11}$$

Assuming, $\varphi = Q^{-1}$ and substituting into equation 3.11, and taking E_{bit} as the subject of the formula, we obtain;

$$E_{bit} = \frac{\left(\frac{2\mathcal{R}L_tB}{\varphi\sigma_0}\right)+\left(\frac{2qR_LBB_e}{\sigma_0^2}\right)}{\left(\frac{\mathcal{R}L_tB}{\varphi\sigma_0}\right)^2} \tag{3.12}$$

Where, $B = \frac{1}{T_{bit}}$

Equation 3.12 shows the energy needed to transmit an optical bit over an optical fibre for a distance of $l\ km$. The necessary specifications utilized to calculate E_{bit} are provided in Table 3.1.

Table 3.1: Parameters for the calculation of $\boldsymbol{E_{bit}}$

Item	Value
Signal input power	1 mW
Electrical bandwidth ($\boldsymbol{B_e}$)	$B/2$
Bit rate (b)	10 Gbps
Mux/demux loss	3 dB
Fibre coupling loss	1.5 dB
Optical fibre attenuation coefficient ($\boldsymbol{\alpha}$)	0.18 dB/km
Plank's constant ($\boldsymbol{h}$)	$6.63 \times 10^{-34} Js$
Wavelength ($\boldsymbol{\lambda}$)	1550 nm
Fibre length ($\boldsymbol{l}$)	70 km
$\boldsymbol{\varphi}$	8
Photodetector responsivity ($\boldsymbol{\mathcal{R}}$)	1.20 A/W
$\boldsymbol{\sigma^2_{thermal} = 4k_BTB_eR_L}$	$3.3 \times 10^{-22} B_eA^2$
Switch insertion loss ($\boldsymbol{L_s}$)	0.5 dB

In Figure 3.4, the relationship between energy and BER is shown. It can be observed that more energy is required to transmit signals at low BER values. This implies that a delicate balance should be sought and struck between the quality of the transmitted signal and the energy consumed per bit.

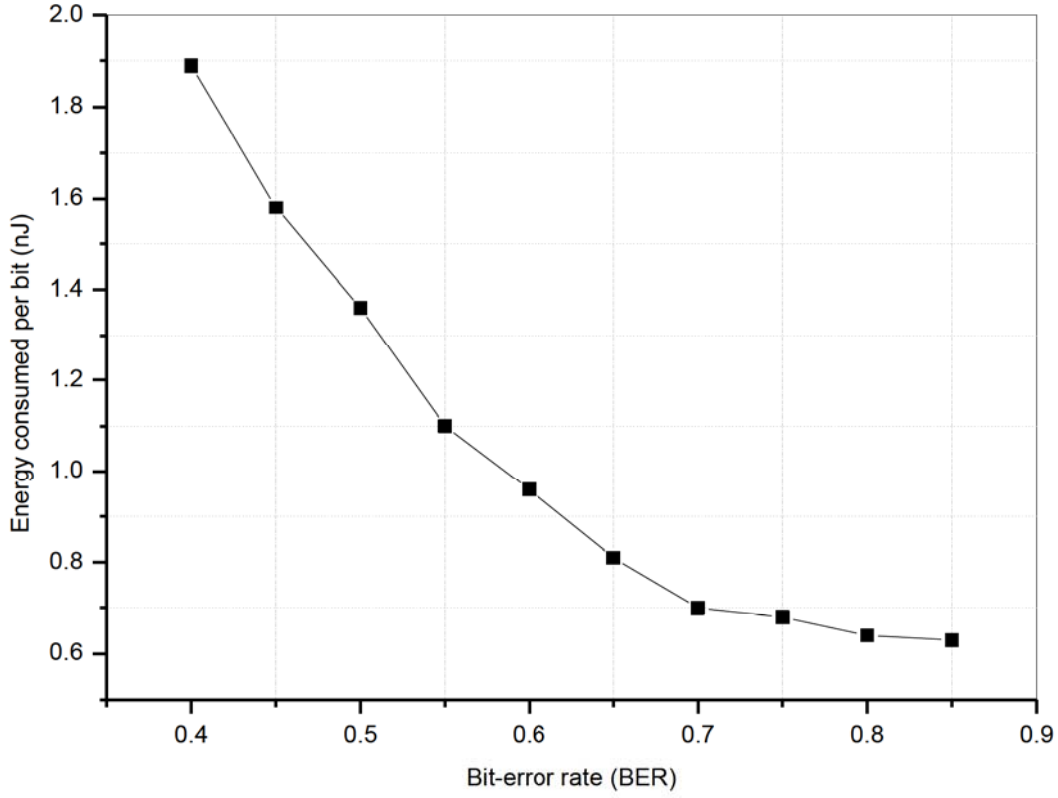

Figure 3.4: The relationship between E_{bit} and BER

Figure 3.5 gives the relationship between energy used per bit and the optical fibre length. For optical fibre lengths that are above 97 km, we can see that there is a sudden increase in the required energy per bit. However, in most existing networks, EDFAs are normally placed at interval distances of about 70 km to alleviate the challenges posed by optical fibre attenuation. This implies that the overall uncompensated length of the optical fibre becomes less than 70 km, in which case the energy consumed is approximately 1 nJ as observed in Figure 3.5.

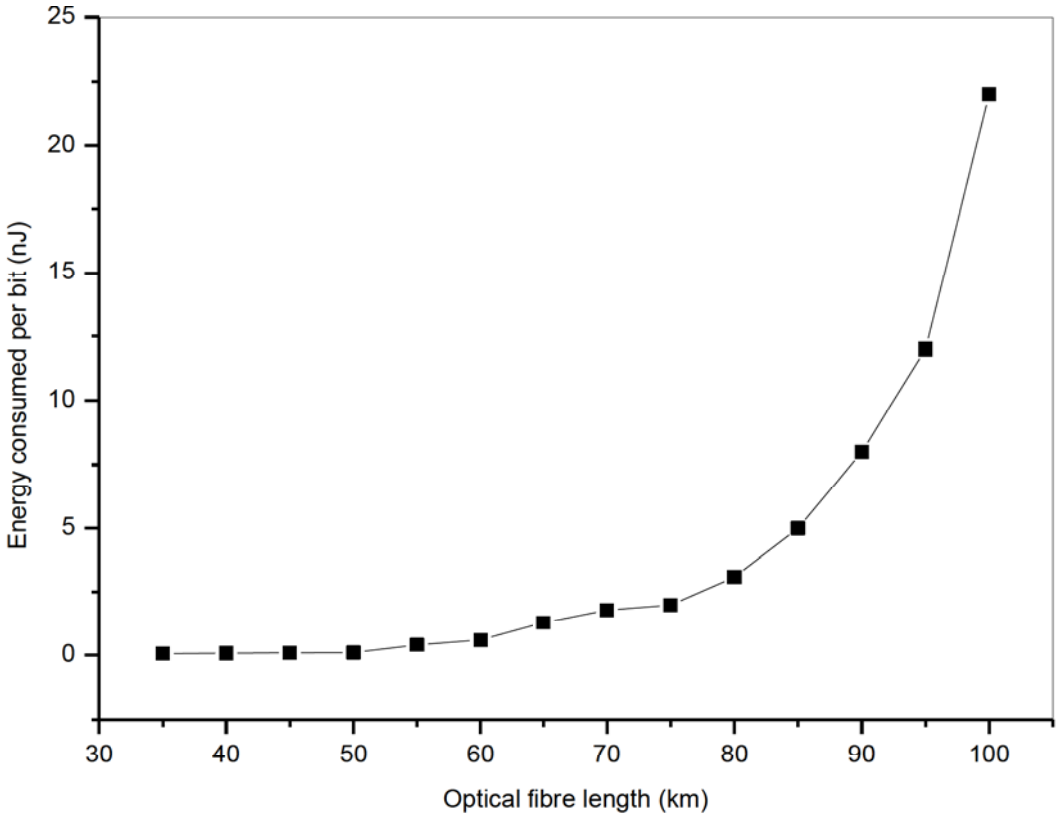

Figure 3.5: Energy consumed per bit versus optical fibre length for OOK

3.3 Impairment Aware-Routing and Wavelength Assignment (IA-RWA)

WDM transparent optical networks are favourite candidates for high speed next-generation telecommunications networks due mainly to their ideal superior bandwidth provision. In addition, transparent optical networks make it possible to transmit and switch signals entirely in the optical domain without the inclusion of the bulky and costly OEO converters. However, the absence of OEO converters at intermediate nodes in these networks generally lead to undesirable signal degradation due to physical impairments caused by optical fibres and associated optical components. This necessitates the inclusion of the effects of physical-layer impairments in the decision-making process of routing and wavelength assignment (RWA). Traditional RWA algorithms assume that the optical network waveguides and related

components are ideal. This, however, is not true since the quality of the travelling optical signal is degraded as it traverses the optical network. It is therefore imperative to take into consideration the effects of physical layer impairments during network design and subsequent operation phases in order to guarantee acceptable QoS.

In optical network planning, individual lightpath establishment requests can be classified as either permanent lightpath demands (PLD) or static lightpath demands (SLD). Further classifications of demands are known as dynamic lightpath demands (DLD) whereby each individual lightpath request has a defined specific lifetime. Two types of DLD exist and these are scheduled lightpath demands (SLD) and ad-hoc ligthpath demands (ALD). For SLD, the activation time and lifetime of the individual requests are known in advance and thus it is possible to consider the entire demands during network planning or operation phases. As for ALD, both the arrival time and lifetime of the demands are not known in advance, and random processes may be utilized to model their arrival times and lifetimes [146].

3.4 Routing and Wavelength Assignment problem

RWA is the process of optimizing the number of optical connections by assigning routes and wavelengths to lightpath requests. The classic RWA problem is known to be NP-complete, and this means it is not possible to find its optimal solution in polynomial time [147], [148]. Since it may be difficult to find an exact solution for the RWA problem, RWA is ideally split into two sub-problems, and these are: *(1) routing sub-problem*, and (2) *wavelength assignment sub-problem*. It will be possible then to solve each sub-problem separately and each step can be further sub-divided into two parts, namely: (i) search and (ii) selection. In the first step, a set of candidate lightpaths is searched, subject to some established constraints. The second step deals with decision making on the available candidate lightpath set.

Previous studies have focused their attention on RWA problems and most of the proposals largely ignore the role played by physical-layer impairments in the degradation of signal quality [147]. Current studies have drawn some attention on the incorporation of physical-

layer impairments in RWA algorithms. The PLIs are either incorporated as constraints for RWA algorithms or the RWA algorithms decisions consider these impairments, the so-called physical-layer impairment aware routing and wavelength assignment (PLI-RWA).

3.4.1 Routing

Routing essentially refers to the process of selecting a path from one place to another on which an information packet can traverse. Algorithms are employed to select the desired path, and are generally spread amongst several routers in order to jointly share relevant information. Generally, routing comprises three essential elements, and these are:

- Routing algorithms, for paths determination.
- Routing protocols, for facilitation of information gathering and dissemination.
- Routing databases, for storage of information obtained by algorithms.

It is vital to bear in mind that the routing algorithms are designed to optimally facilitate data transfer, and thus should take into consideration criteria such as throughput, delay, reliability and flexibility in their decision making.

3.4.1.1 Fixed routing

Fixed routing is one of the widely employed techniques for addressing the routing sub-problem. In this approach, a single fixed predetermined route for each source/destination pair is always selected. For every connection request, the network will try to establish a lighpath along the predetermined route, otherwise a connection is blocked if there is no available wavelength on the fixed route. The shortest-path routing is one of the most popular and widely deployed techniques that is based on the fixed routing approach. To a very large extent, Dijkstra and Bellman-Ford algorithms are the most prevalent implementations based on the shortest-path routing approach [149]. Although fixed routing is simple to implement, its major drawback is the limitation that it imposes on routing options and thus it usually leads to unnecessarily high connection blocking rates. Figure 3.6 shows an example of possible routes between nodes 1 and 4, where R1 and R2 stand for the shortest routes in terms of hop count.

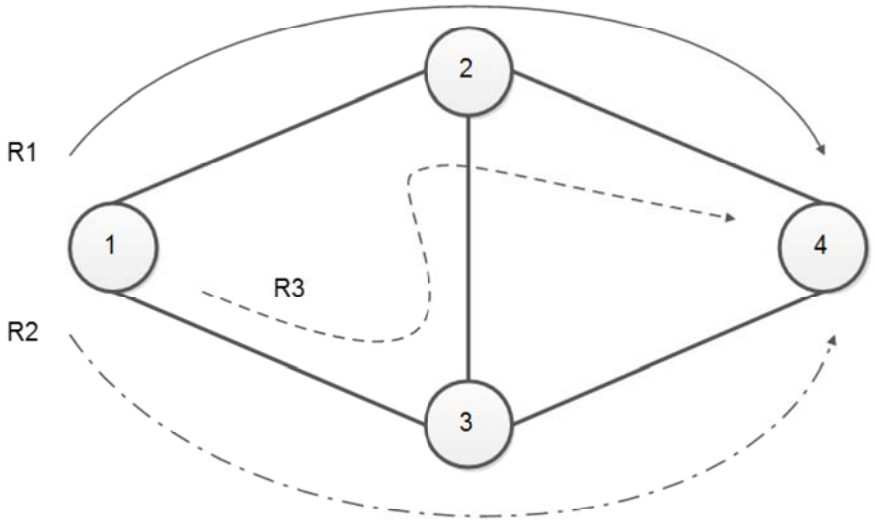

Figure 3.6: A schematic diagram of fixed routing

3.4.1.2 Fixed-alternate routing

In fixed-alternate routing, a definite number of fixed alternate routes is predetermined for each source/destination pair, and each node in the network stores and maintains a routing table that contains an ordered list of multiple fixed routes to each destination node [150]. For every connection request, the source node tries to establish a connection sequentially on each of the routes retrieved from the routing table that resides at the node. If all the alternate routes are unavailable to accommodate the connection request, the request is blocked and subsequently lost. The *k*-shortest path algorithm is one of the popular widely implemented technique based on the fixed-alternate routing approach. In a typical *k*-shortest path algorithm, candidate paths (*k*) are arranged according to their respective link costs such as number of hops, link length or link energy consumption.

Besides significantly lowering the connection blocking probabilities as compared to fixed routing, fixed-alternate routing also provides healthy possibilities of some fault tolerances to link or node failures [151].

3.4.1.3 Adaptive routing

In contrast with fixed and fixed-alternate routing, adaptive routing establishes routing tables dynamically at each node according the prevailing link-state information. It can therefore safely be inferred that adaptive routing increases the chances of establishing a connection compared to fixed and fixed-alternate routing [147].

Since the routing table at each node requires to be updated on a call-to-call basis, adaptive routing's computational complexity is significantly high. In addition, adaptive routing continuously require extensive support from management and control protocols. Authors in [152] present the least-congested-path (LCP) routing, which is one of the most important examples of the adaptive routing approach. Figure 3.7 shows an example of adaptive routing whereby costs are assigned to links with regards to the availability of a link. Accordingly, the cost of a link with available resources is 1, whereas a busy link cost is equal to ∞. Suppose a connection request arrives for lightpath establishment between nodes 1 and 4, the minimum-cost based adaptive routing would facilitate the provisioning of request R3.

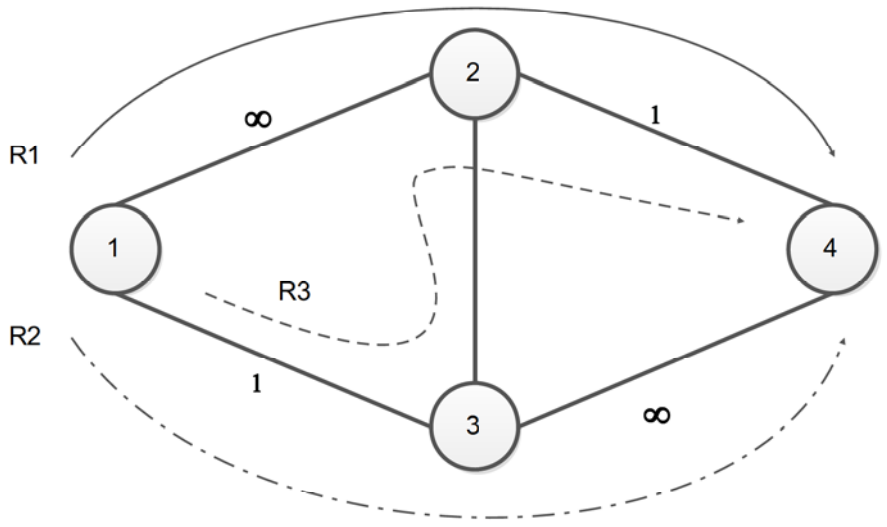

Figure 3.7: Schematic diagram of adaptive routing

3.4.2 Wavelength Assignment

A number of heuristic algorithms have been proposed to solve the wavelength assignment sub-problem in both static and dynamic lightpath establishment environments [153]. A brief description of the most prevalent wavelength assignment strategies is provided below.

3.4.2.1 Random

In this approach, the space of wavelengths is searched first to obtain a set of all available wavelengths on the desired route. One wavelength, ideally with uniform probability, is then randomly selected from the set [154].

3.4.2.2 First-fit

In the first-fit scheme, all wavelengths are initially numbered and then subsequently searched in sequence from the least to the highest numbered wavelength. The first free available wavelength is then chosen for lightpath establishment. Since this scheme does not require the searching of the entire wavelength space, its computational complexity is lower than that of random wavelength assignment [155]. In addition, the fairness and blocking rates of the first-fit approach are superior to those of the random scheme. It is mainly due to the above-stated attributes that the first-fit approach is favoured over the random wavelength assignment scheme.

3.4.2.3 Least-Used

This scheme chooses the least used wavelength in the network so as to balance the load amongst all wavelengths. In terms of performance and computational costs, this approach does not fare well compared with both random and first-fit approaches [147]. Due to the above-mentioned short-comings, the least-used approach is generally not preferred in practice.

3.4.2.4 Most-Used

In this approach, the most used wavelength in the network is selected. This approach performs better than the least-used and the first-fit approaches in some network topologies [154]. However, its main undoing is its introduction of communication overhead and extra storage requirements.

3.5 Impairment-aware routing and wavelength assignment (IA-RWA) approaches

One of the main objectives of a RWA algorithm is to minimize the number of network resources required to facilitate the connection of a set of candidate lightpaths for a specified topology. Previous studies have proposed the application of heuristic and meta-heuristic algorithms to solve the routing and/or wavelength assignment sub-problems in order to achieve the aforesaid objective. The heuristic and meta-heuristic algorithms normally yield a sub-optimal solution that may be obtained without the aid of complex computations [156].

A sufficiently large number of IA-RWA algorithms presented in literature are mainly anchored on simple heuristics. It is therefore important to consider fairly complex algorithms that incorporate most of the key physical-layer impairments in optical networks. Considering the routing sub-problem, literature provides us with various heuristic algorithms, and most of them are based on the shortest path (SP) algorithm. These algorithms can be further sub-divided into; (i) single-path routing algorithms and (ii) multipath routing algorithms (also known as *k*-shortest path routing algorithms).
In SP algorithms, a cost parameter that has additive properties is assigned to each network link, and the cost is utilized by the algorithm to select a path with minimum overall cost.

3.5.1 Heuristics

In as far as single-path routing is concerned, several IA-RWA proposals have been made that utilize the minimum hop SP technique as stated in [157], [158], [159] and [160].

Alternatively, some IA-RWA algorithms employ link costs that are functions of four wave mixing (FWM), crosstalk (XT), noise variance and the Q-factor [161], [162], [163].

IA-RWA algorithms hinged on multi-path routing algorithms work on a cluster of pre-computed different paths. Considering that these paths are commonly the shortest paths, such group of multi-path algorithms are also known as *k*-Shortest Path (*k*-SP) algorithms. In certain instances the group of prospective paths is confined to disjoint paths.
Multi-path IA-RWA routing algorithms usually use a set of pre-defined alternate paths that are normally the shortest paths. Thus, these algorithms are commonly referred to as *k*-Shortest Path (*k*-SP) algorithms. As the case with single-path routing, the link cost in multi-path routing may be a function of hop distance as reported in [164], [165] and [166] or can be PLI-aware as in [167]. A considerable number of proposals also employ the Q-factor as a link cost. The Q-factor can be measured from network devices or can be analytically deduced by incorporating the PLIs [168], [169].

Some more elaborate link cost approaches bring together several key metrics such as the number of available wavelengths and hop length [170]. Generally, when prospective paths are located, the allocation of a suitable path is done either in sequence or in parallel. Sequential selection of a path occurs via a series of re-attempts until the first available path that meets the required performance criteria is found. [171], [172]

In parallel selection, the most appropriate path is selected, subject to some laid down relevant criteria [173], [174]. The wavelength assignment (WA) task works on a set of candidate wavelengths that are provided on a formerly chosen routing path/s. The set of candidate wavelength may either be ordered or unordered. The ordering of the wavelengths may be done in line with some clearly defined rules, such as frequency separation magnitude of candidate wavelengths [159].

As with the routing sub-problem, wavelength assignment can be performed either sequentially or in parallel. The sequential approach assigns the first available wavelength that meets all the imposed network and physical layers constraints. This is commonly known as the first-fit (FF) selection technique, and has been extensively explored in several IA-RWA

proposals [146], [157], [165], [174], [175], [176]. On the other hand, some IA-RWA algorithms attempt to scan through all the candidate wavelengths in order to select the most appropriate one (known as the Best-Fit). For instance, this can be realized by finding the least utilized wavelength in the network based on the available data furnished by the source nodes [158], [177], [178].

Lastly, random selection may be done by randomly selecting a wavelength from the available wavelengths. This technique tends to limit the effects of crosstalk, but unfortunately, generally leads to relatively high blocking probabilities compared with the FF algorithms [147], [179]. There are some proposed algorithms that solely make decisions based on PLI, the algorithm presented in [162] attempts to minimize the crosstalk effect. The algorithms in [180] focus on the selection of lightpaths with the highest Q-factors.

3.5.2 Metaheuristics

Metaheuristic algorithms are steadily evolving in becoming a crucial cog in the optimization of optical networks. The term metaheuristic was first coined by Fred Glover and can be explained as a key strategy that guides and modifies other heuristics to yield solutions that are normally obtained in a quest for local optimality [181].

Essentially, all metaheuristic algorithms employ a tradeoff of randomization and local search, and possible solutions to complex optimization problems can be obtained in a fairly acceptable amount of time. However, the arrival at optimal solutions is not a given, and it is normally desired that the algorithms function most of the time, but not all the time [182].

A number of metaheuristics have been proposed to solve IA-RWA algorithms in optical networks, and the most prevalent ones include: (i) Tabu-Search metaheuristic, (ii) Ant Colony Optimization (ACO), (iii) Predictive Algorithm, and (iv) Genetic Algorithm (GA).

The Tabu-Search (TS) metaheuristic attempts to elude local minimum solutions by choosing worse solutions through the use of the solutions' search history. For the proposed solution, the TS metaheuristic works on a set of k-SP, where the k is constantly changing. This uniqueness property of the TS algorithm generally enhances the efficiency of the technique [170].

The Ant Colony Optimization (ACO) is one of the most important metaheuristics employed to solve the IA-RWA problem [183], [184], [185]. Ant colony optimization (ACO) is a population-based metaheuristic that can be employed to realize general answers to complex optimization cases. In ACO, a group of mobile agents referred to as *artificial ants* hunt for sound solutions to a presented optimization scenario. In order to employ ACO, the optimization scenario is changed into the issue of obtaining the best path on a weighted graph. The ants iteratively assemble solutions by being mobile on the graph. The solution development exercise is stochastic and is determined by a set of parameters associated with graph components, called pheromones, whose values are modified at runtime by the ants [186]. The proposed IA-RWA in [186] use the ACO algorithm in calculating the path via network hops, and subsequent hops are calculated based on pheromone values of the nodes. The algorithm calculations incorporates constraints that are as a result of ASE noise and optical power budget.

Authors in [179] propose a Predictive Algorithm (PA) for the IA-RWA problem. The PA primarily selects the routes for the lightpaths based on the topology of the network, with or without consideration of the physical layer, but learns from history of previous connection requests. One of the main advantages of this algorithm is that it has a fairly modest computational runtime since it does not require any update messages in computing potential lightpaths [187].

The IA-RWA in [188] uses a Genetic Algorithm (GA) in its decision-making process.
Genetic Algorithms (GAs) are search algorithms anchored on the evolutionary concepts of natural selection and genetics. They constitute a powerful and smart utilization of a random search utilized to unravel optimization problems. GAs exploit historical data to focus the search into the area of favourable execution within the search space. The key procedures of the GAs are patterned to imitate natural processes essential for evolution, in particular, those that follow Charles Darwin's "survival of the fittest" principles. This emanates from the fact

that, competition among individuals for scanty resources results in the fittest individuals dominating over the weaker ones [189], [190]. The proposed algorithm tries to calculate a lightpath by taking into consideration the effects of both ASE and PMD.

3.6 IA-RWA Classes

Transparent optical networks have been viewed as the ultimate solution for ultrahigh speed and bandwidth-hungry applications such as video streaming and high-definition television (HDTV). The main drawback of these networks is their lack of signal regenerators, and this normally leads to serious degradation of the transmitted signal due to physical layer impairments accumulated along the optical path. There is therefore, a need to solve the so called IA-RWA problem so as to guarantee an acceptable quality of transmission (QoT) in these all-optical networks.

Three main ways have been proposed in literature that cater for transmission impairments in network design and subsequent operation [185], [191], [192]. These are: (i) the route and the wavelength are computed by the use of traditional RWA algorithms, and finally, the signal quality is verified by considering the effects of physical layer impairments.; (ii) The effects of PLIs are considered during the routing and/ or wavelength assignment processes, and (iii) The effects of the PLIs are considered during the routing and/or wavelength assignment processes and finally, the signal quality of the candidate lightpath is verified (figure 3.8).

Authors in [193] present a shortest-path based RWA whose objective is to find candidate paths for the primary and protection paths subject to a wavelength-continuity constraint. The Q-factor of each candidate path is then computed, and the route with the greatest Q-factor is chosen to establish a connection request.

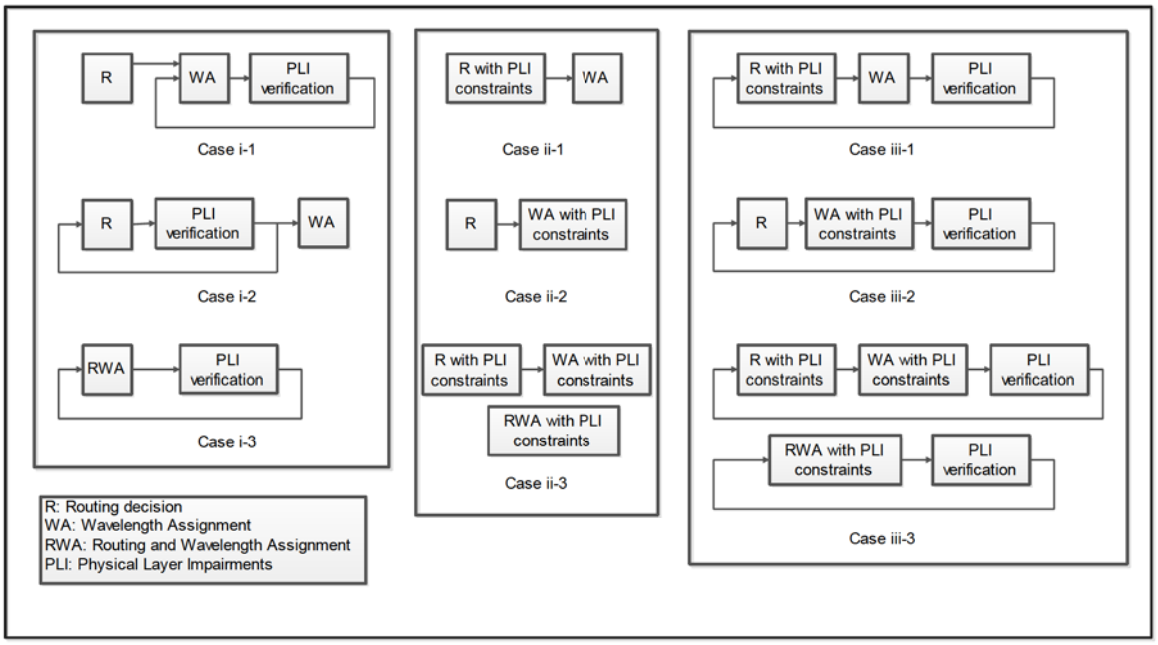

Figure 3.8: PLIA-RWA algorithms

In [194], the authors propose IA-RWA algorithms that are based on the *k*-SP and cater for the most dominant impairments such as ASE, GVD and PMD. The Q-factor penalties are utilized to compute the edge weights, instead of the actual lengths. Comparison is then made between off-line and on-line routing IA-RWA algorithms, and the on-line routing algorithms require more computational time compared to their off-line counterparts. However, the on-line IA-RWA algorithms have a significantly lower blocking probability compared to the off-line algorithms. The main disadvantage of the proposed algorithms is that they do not consider all the key impairments and thus the algorithms may not be applicable for use in high speed networks such as those that operate at 100 Gb/s and above.

An ILP formulation and heuristic approaches in which route computation is done via calculation of link costs derived from impairment effects of ASE and PMD is proposed in [170]. In [195], crosstalk is considered in the wavelength assignment decision making. Authors in [196] propose an adaptive routing algorithm that is based on dynamic computation of Q-factor values obtained from network devices.

The work in [167] presents algorithms that calculate the *k*-SP by employing Q penalties as link costs. A threshold Q-factor is eventually compared with the overall Q value to make a decision on the establishment of a connection request. In [164], the algorithm proposes the selection of a route by verification of the extent of signal degradation due to impairments at each and every node in the network.

3.7 Summary

Efficient utilization of energy is discussed and specific focus is on improving the energy efficiency of backbone optical networks. Distributed power generation is touted as a possible solution to the challenges currently faced in as far as the use of "green" energy sources for optical networks is concerned. Several RWA and energy-efficient RWAs are also presented, and their performances are compared and contrasted. Lastly, pertinent PLI-RWAs are discussed and their applicability in various network scenarios are analyzed.

4 Physical Layer Impairment-Aware Algorithms

4.1 Introduction

This chapter presents proposed models and their subsequent evaluation. A Q-factor tool that incorporates most of the pertinent physical layer impairments is presented. The tool is evaluated via simulations to gauge its usefulness and effectiveness. An analytical model to compute the blocking probabilities for RWA with physical impairments in transparent networks is also presented. The main advantage of using an analytical model in this instance is its lucrative efficiency in terms of time taken to attain results, and it also aids in getting a deeper understanding of the dynamics of designing RWA algorithms that are subject to impairment constraints. Numerical examples are also provided to show the performance of the proposed model, and it is validated through the use of simulations.

4.2 Physical-layer impairments model

There are two general models that have been proposed in literature that makes it possible to cater for physical layer impairments effects in RWA algorithms [185]. The proposed models are: (i) analytical models, and (ii) hybrid models. In analytical models, the physical impairments are computed by making use of closed-form formulae, and in hybrid models, analytical models accompanied by simulation techniques are normally employed to evaluate the performance of the physical layer.

Among a host of available optical performance measuring attributes, the Q-factor is preferred as the most suitable metric to use for the routing algorithms because it has a strong correlation with the BER [197], [198], [199].

The relationship between BER and the Q-factor is shown in the following equation:

$$BER = \frac{1}{2} erfc\left(\frac{Q}{\sqrt{2}}\right) \tag{4.1}$$

Where, $Q = \left(\frac{\langle I_1\rangle - \langle I_0\rangle}{\sigma_1 + \sigma_2}\right)$

$\langle I_1\rangle$ and $\langle I_0\rangle$ are the mean photocurrent values of high and low signal levels respectively.

σ_1 and σ_0 are the standard deviations of high and low signal noise levels respectively.

Authors in [200] report the use of the quality of transmission (QoT) parameter in evaluating the signal health in impairment aware optical networks.
In our contributions, we extend the work in [1] to incorporate the effects of crosstalk (XT) and filter concatenation (FC). We quantify the physical layer impairments effects by employing analytical models presented in [201], [202] and [203].
The model developed includes the effects of the following physical impairments: ASE, CD, XT, PMD, FC, SPM, XPM and FWM. The proposed expression is given in the following equation:

$$Q_d = (Eye\ Penalty) \times (Noise\ Penalty) \times Q_s \tag{4.2}$$

Where:

Q_d is the connection destination Q-factor value, Q_s is the connection source Q-factor value.

$$Eye\ Penalty = \left(\frac{\langle I_1\rangle_d - \langle I_0\rangle_d}{\langle I_1\rangle_s - \langle I_0\rangle_s}\right) \tag{4.3}$$

$\langle I_1\rangle_d$ and $\langle I_0\rangle_d$ are the mean photocurrent values of high and low signal levels at the connection destination respectively.

$\langle I_1\rangle_s$ and $\langle I_0\rangle_s$ are the mean photocurrent values of high and low signal levels at the connection source respectively.

$$Noise\ Penalty = \left(\frac{\sigma_{1,s} + \sigma_{0,s}}{\sigma_{1,d} + \sigma_{0,d}}\right) \tag{4.4}$$

$\sigma_{1,s}$ and $\sigma_{0,s}$ are the standard deviations of high and low signal noise levels at the connection source respectively.

$\sigma_{1,d}$ and $\sigma_{0,d}$ are the standard deviations of high and low signal noise levels at the connection destination respectively.

The eye-related penalty is due to the impairment effects of CD, PMD and FC, whereas the noise-related penalty is due to the impairment effects of XT, ASE, SPM, XPM and FWM. It is important to note that the variances of XT, ASE, SPM, XPM and FWM of a lightpath may be computed as the summation of the constituent electrical variances of links making up the entire lightpath.

The proposed model is comprised of three key stages. In the first phase, all the information concerned with the traffic requests and network characteristics is gathered. This information includes optical channel characteristics, network topology and capacity. The traffic characteristics incorporate data about the bit-rate, lightpath demands, amongst others. Link costs are then evaluated that are based on the obtained information and characteristics. These link costs will be taken into consideration during the path selection process. The second phase is responsible for the assignments of paths and wavelengths. The shortest-widest path (SWP) and first-fit with ordering (FFwO) schemes are proposed in this model. A set of *k*-shortest paths for each connection request is identified and an ILP optimization problem is solved that minimizes network costs. The final stage validates the lightpaths generated in the second stage. The analytically modeled Q-factor that incorporates the effects of physical layer impairments is employed as the link-cost metric. If a candidate lightpath meets the pre-set signal quality requirements and incorporates all the stated impairments, then a connection is established. If the proposed lightpath signal quality does not satisfy the given requirements and /or does not take into account the effects of physical impairments, the connection is blocked.

The Pan-European Network is used in this model to verify its applicability and accuracy. The network topology has 16 nodes and 23 bidirectional fibre links. We assume that the connection requests follow a Poisson distribution and the nodes do not have wavelength conversion capabilities. Furthermore, no protection or regeneration is taken into consideration.

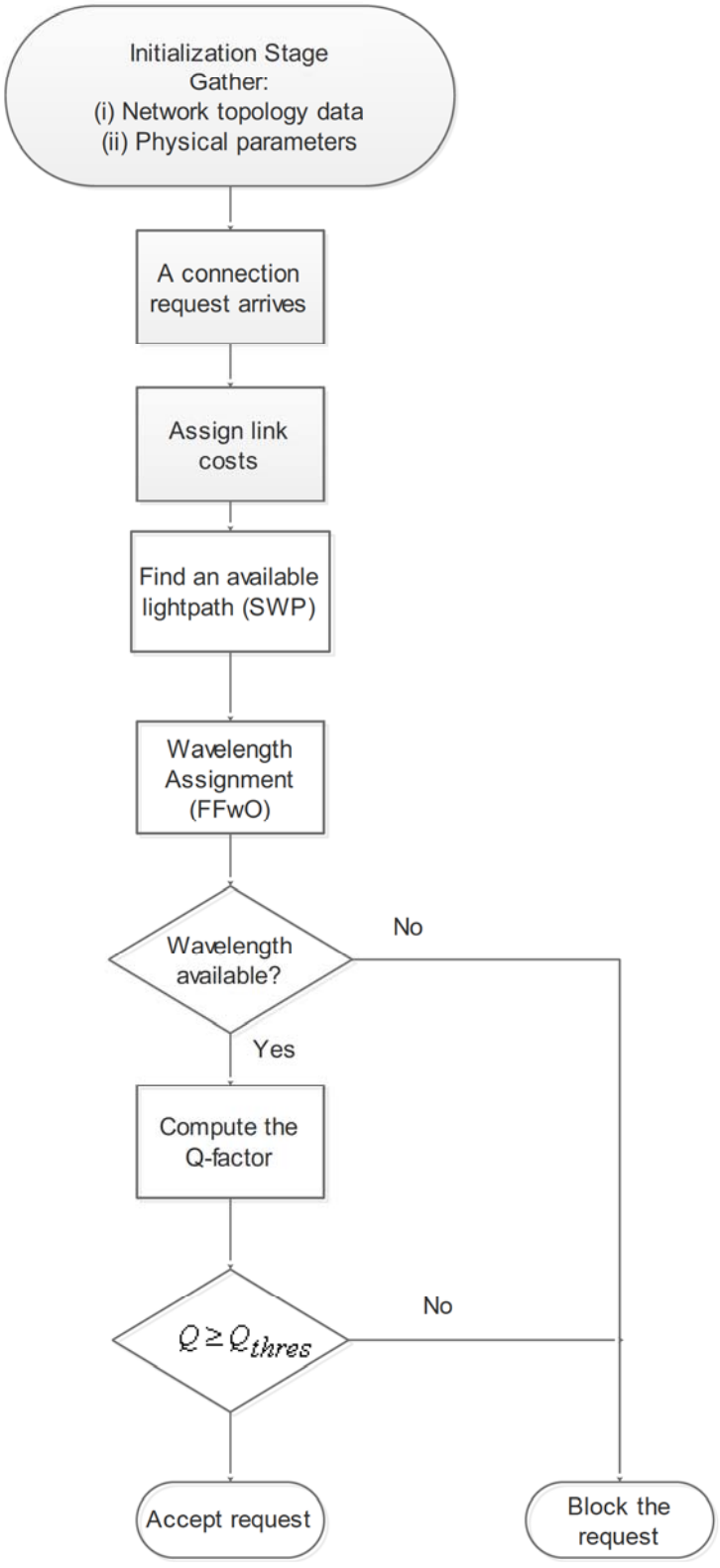

Figure 4.1: Flowchart of the proposed algorithm

The shortest-widest path (SWP) algorithm is employed to solve the routing sub-problem and the First-fit with Ordering (FFwO) algorithm is used to solve the wavelength assignment sub-problem.

When a connection request is received, the engine looks for the shortest-path that is least congested and process them in their order. The FFwO algorithm is then applied to choose an available wavelength from the available wavelengths (Figure 4.1).

Each candidate path's Q-factor is calculated and those paths that have a Q-factor that is lower than a pre-set threshold (Q_{thres}) are blocked.

We selected the whole network to comprise of SSMF with a dispersion, D = *12 ps/nm/km*, an attenuation constant of $\alpha = 0.25$ *dB/km* and a nonlinearity constant of $\gamma = 1.5$ $(W{\cdot}km)^{-1}$. We also assume a communication channel plan a maximum of *40 wavelengths per link* spaced at *50 GHz*. The threshold q-factor is configurable and overall noise figure is set at *5 dB.W*

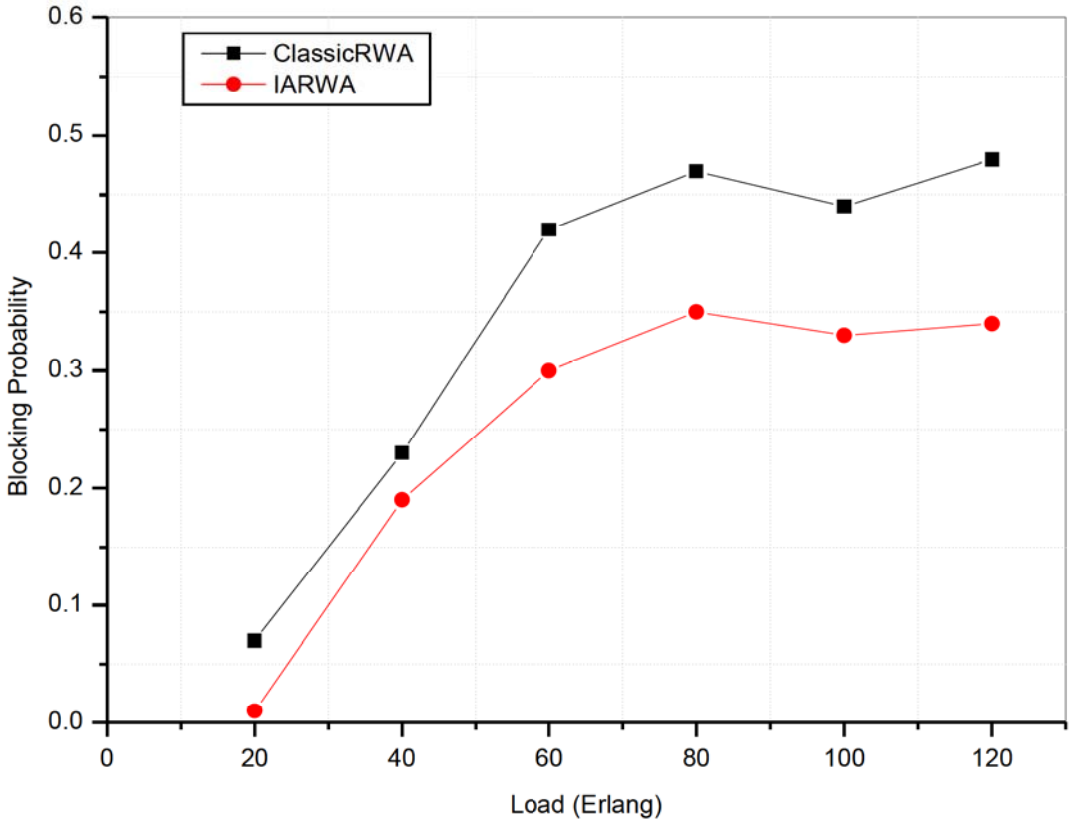

Figure 4.2: The relationship between blocking probability and network load for the Pan-European Network

Figure 4.2 compares the blocking probability of the classic RWA algorithm with our proposed IA-RWA algorithm in the Pan-European Network topology.

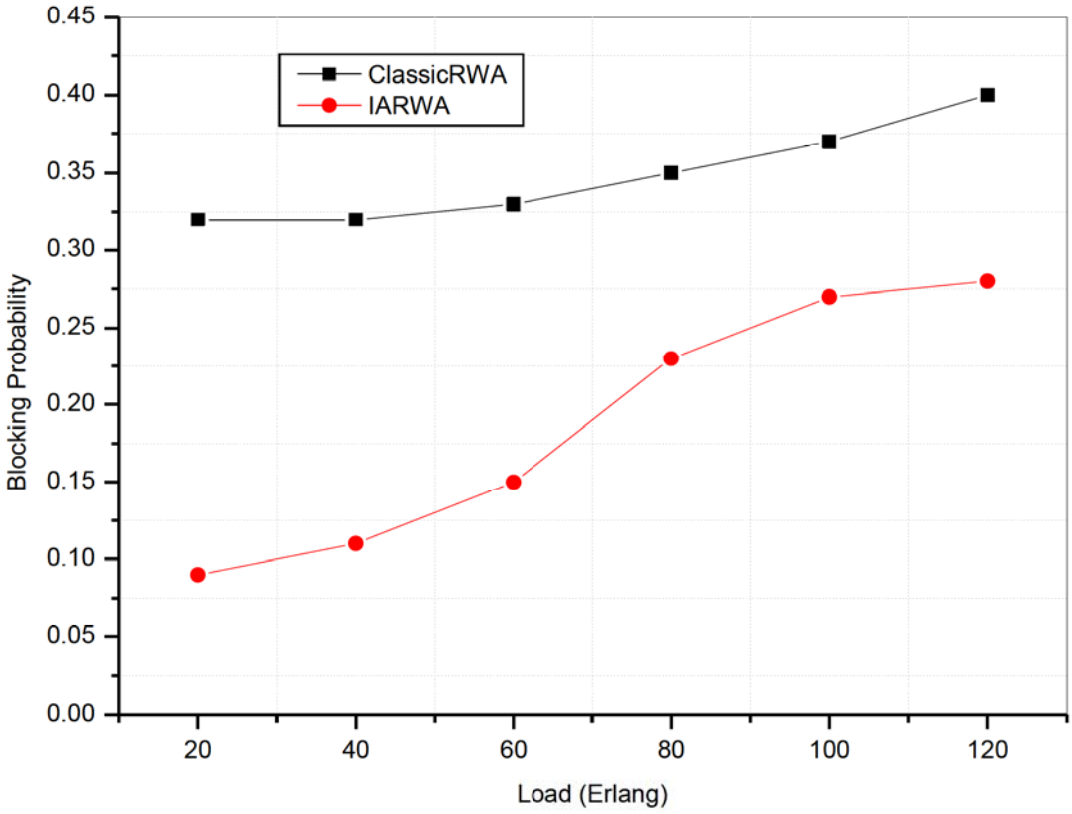

Figure 4.3: The relationship between blocking probability and network load for the MESHNET topology.

Figure 4.3 compares the blocking probabilities of the classic RWA algorithm with that of our proposed IA-RWA for different traffic loads in the MESHNET topology. The MESHNET topology consists of 16 mesh toroid nodes that have identical link lengths of 100 km. We can clearly observe that, at low network loads, the performances of the two algorithms is almost similar in the Pan-European Network, however, there is clear distinction of their performances at high loads. We further note that in the MESHNET topology, there is a significant reduction in the blocking probability for our proposed model compared with the Pan-European Network. This implies that the performance of the MESHNET topology is appreciably improved by our model. Furthermore, this shows that the model can certainly

improve the performance of regular networks and fairly large irregular networks at high loads. In a nutshell, our proposed algorithm evidently outshines the classic one, and it thus helps improve the network performance.

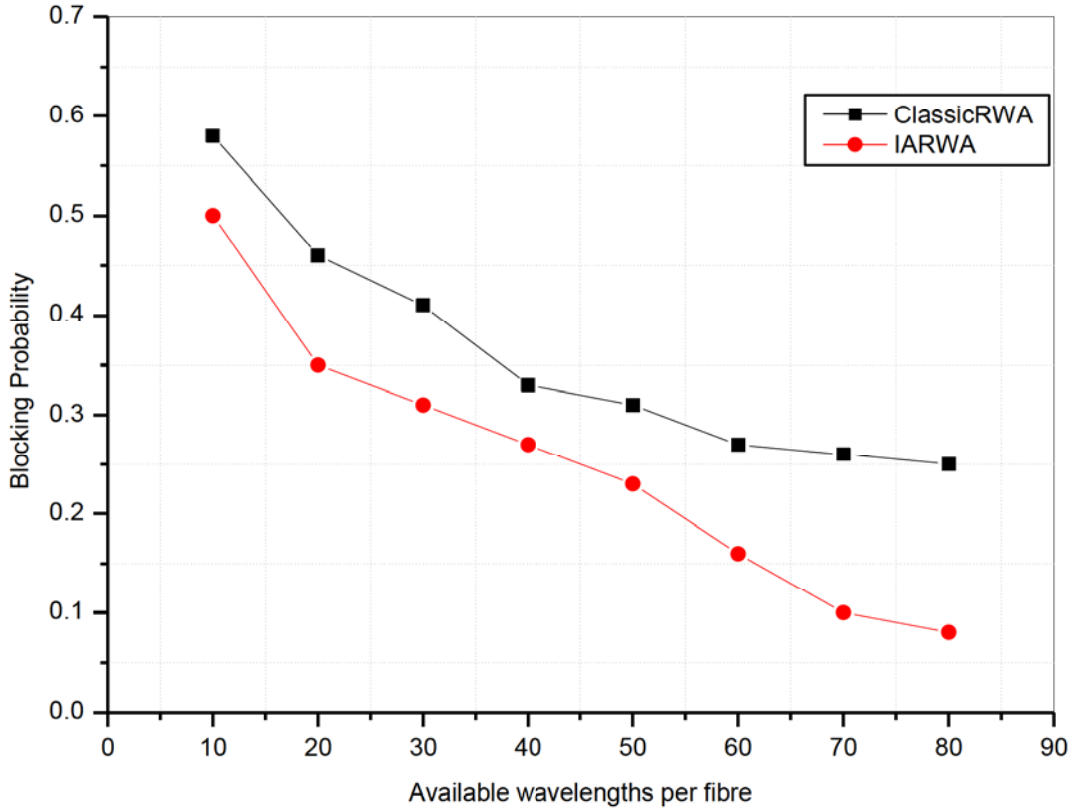

Figure 4.4: Relationship between blocking probability and number of wavelengths per fibre

The simulation results of the classic RWA and our IA-RWA algorithms showing the variation of blocking probability and the number of available wavelengths per fibre are shown in Figure 4.4. The proposed model offers lower blocking rates, especially when the number of wavelengths is limited. When the number of wavelengths reaches a certain threshold ($\approx$ 60), the blocking probability becomes fairly steady, implying that physical impairments become the key determinants of the network blocking rates performance.

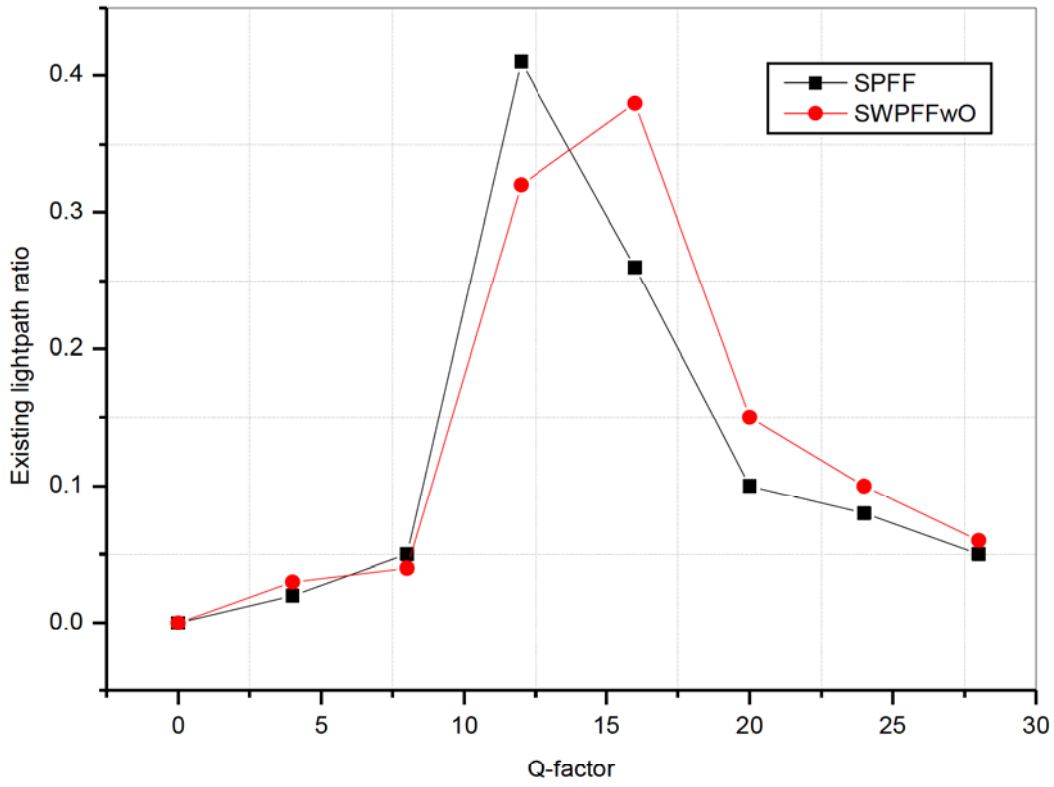

Figure 4.5: Relationship between existing lightpaths and Q-factors

Figure 4.5 shows the relationship between the Q-factors and the ratio of existing lighpaths for the shortest path (SP) combined with first fit (FF) algorithm, as well as that of the SWP with FFwO algorithm. The traffic load is set at 10 Erlangs, and it can be seen that a significant ratio of the lightpaths have a Q-factor of less than 14 for the SP with FF algorithm. This is in contrast with that of the SWP, FFwO algorithm, were a substantial ratio of existing lighpaths have a Q-factor that is above 14. It is clear that SWP, FFwO algorithm leads to better utilization of network resources and satisfactory physical performance.

Figure 4.6 shows that the average computation time of the proposed IA-RWA algorithm is longer than that of the pure RWA algorithm. This may be due to the fact that our IA-RWA algorithm incorporates the effects of impairments in its decision-making process. In our algorithm, the set up collects information on impairment effects experienced by the signal during transmission in the selection of a route and wavelength assignment and then calculates the effects' value before finally evaluating the signal quality against a preset threshold value.

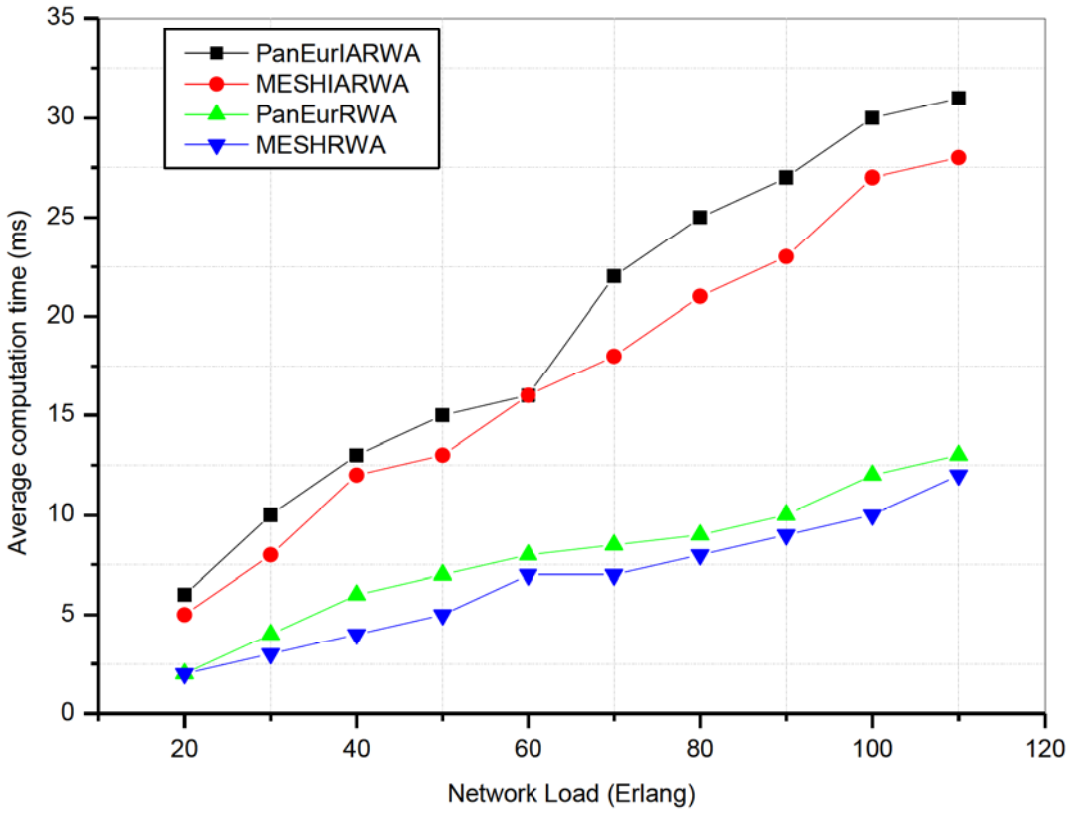

Figure 4.6: Variation of average computation time with network load

This process certainly leads to an increase in computation time. It implies that a trade-off should be struck between attaining high QoT and computational time. In addition, it is also shown that classic RWA computational time is more or less the same regardless of the network topology, especially at low network loads.

4.3 QoT-Constrained RWA Analytical Model

We extend the approach presented in [204] and decompose the RWA with physical impairments by wavelengths as a stratified system. A RWA with Λ wavelengths in each link is decomposed to Λ stratified networks, where each has the same network topology but is only capable of carrying one wavelength per link.

The prevailing network traffic initially goes into layer 1, then the overflow traffic goes down to layer 2 and the pattern is repeated for the next available layers. At network layer Λ, the overflow traffic turns out to be the overall blocked network traffic and the blocking probability can be calculated. The wavelength continuity constraint, which ensures that a request remains on the same wavelength along the route, is instinctively implemented in this perspective. The independence of wavelength is also presumed to be in place, which implies that each wavelength is appraised individually and the probability is only subject to the arrival speeds.

Since the proposed model handles each wavelength independently and the overflow of traffic from one wavelength with a big index to the next wavelength with a little index, it is logical to employ this technique to analyse the effectiveness of the first-fit wavelength assignment (FF WA) [204]. Firstly, all the essential assumptions relating to the proposed model are presented, and the analysis of the model follows thereafter. It is assumed that each link between nodes in unidirectional and consists of only one optical fibre; fixed routing is implemented and the FF WA is utilized in WA. The set of all source-destination pairs (s-d) in the networks is taken as Z. Generally, a path from a source node to a destination node is represented by $r(s,d)$ or $r(z)$ for $z \in Z$, where $r(z)$ is determined by shortest path (SP) algorithm. A segment $r(i,j)$ is defined as a subset of route path $r(s,d)$. It is important to bear in mind that $r(i,j) \cap r(l,m) = \emptyset$, implying that there are no links shared between $r(i,j)$ and $r(l,m)$. The Poisson arrival rate for a s-d pair is denoted by $\Phi_{s,d}$, and it is also assumed that the duration of requests follow an exponential distribution with an average value of $E(X)$, and if there is no loss of generality, $E(X) = 1$. We also represent the equivalent Poisson offered load to wavelength λ for $r(z)$ to be A_z^{λ}.

Generally, a route from a source node to a destination node is represented by $r(s,d)$ or $r(z)$ for $z \in Z$, where $r(z)$ is determined by shortest path (SP) algorithm. A segment $r(i,j)$ is defined as a subset of route path $r(s,d)$. It is important to bear in mind that $r(i,j) \cap r(l,m) = \emptyset$, implying that there are no links shared between $r(i,j)$ and $r(l,m)$. The Poisson arrival rate for a s-d pair is denoted by $\Phi_{s,d}$, and it is also assumed that the duration of requests follow an exponential distribution with an average value of $E(X)$, and if there is no loss of generality, $E(X) = 1$. We also represent the equivalent Poisson offered load to wavelength λ for $r(z)$ to be A_z^{λ}.

Therefore, it is clear that $A_{s,d}^{1} = \Phi_{s,d}$, and $a_{i,j}^{\lambda}$ represents the total Poisson offered load to wavelength λ from node i to node j. It is crucial to bear in mind that $A_{i,j}^{\lambda}$ denotes the traffic that originates at node i and terminates at node j, $a_{i,j}^{\lambda}$ represents the overall traffic that passes through the segment of $r(i,j)$. We also take $\beta_{i,j}^{\lambda} \in \{0,1\}$ to represent the current number of active calls in $r(i,j)$ at wavelength λ. $\Lambda_{s,d}$ is taken as the capacity of the path for $r(s,d)$, and we assume that each link possesses an equal number of wavelengths. It therefore implies that $\Lambda_{s,d}$ may be represented by Λ for all $(s,d) \in Z$. The following parameter, $P_{s,d}^{\lambda}$ is taken as the wavelength blocking probability and $\rho_{s,d}^{\lambda}$ denotes the quality of transmission (QoT) blocking probability for $r(s,d)$ on wavelength λ. In a similar fashion, we take $\hat{P}$ to stand for the total network wavelength blocking probability and $\hat{P}_{s,d}$ denotes the overall wavelength blocking probability of the path. The overall network blocking probability is represented by $\bar{P}$, and the overall blocking probability of the path is denoted by $\bar{P}_{s,d}$.

We consider the model in [204] and extend it to factor in QoT in its decision-making procedure, and Figure 4.7 depicts the proposed layered network model that relies on QoT-Aware RWA algorithms (QARWA).

In this proposed model, each stratum is split into two layers, and the prevailing traffic is initially checked for the acceptability of the QoT for each candidate path on which the requests may be assigned in the QoT blocking sublayer. The offered traffic then enters a second layer where the availability of the path and wavelength is checked. The resulting overall blocked traffic from these two sublayers then overflows down to the next stratum. The QoT blocking, which relies on the use of other layers, is calculated by utilizing the static states probabilities in other layers and iterations are employed in the process until a steady-state is reached. In the traditional RWA that strictly guarantee the QoT, the part of the traffic

that is blocked due to an unacceptable QoT automatically flows out of the system, and thus if a request finds an inactive path with an insufficient QoT, the request is summarily blocked and there is no provision to attempt to utilise other wavelengths. We assume that the chance that an inactive path exists for a s-d pair in the wavelength-blocking sublayer is close to the idle s-d pair likelihood in the QoT blocking sublayer, and thus a portion of the traffic is directly blocked in each layer and taken out of the system so that it does not move to the next layer. By employing this model, it will be possible to evaluate the FFwO wavelength assignment algorithm. It is important to note that the layer and wavelength indices are not the same in the FFwO approach, thus we need to select different statum state probabilities to attain the QoT blocking, subject to the ordering of wavelengths in the sublayer. We also assume that the computation for wavelength blocking is the same as with that of the FF WA.

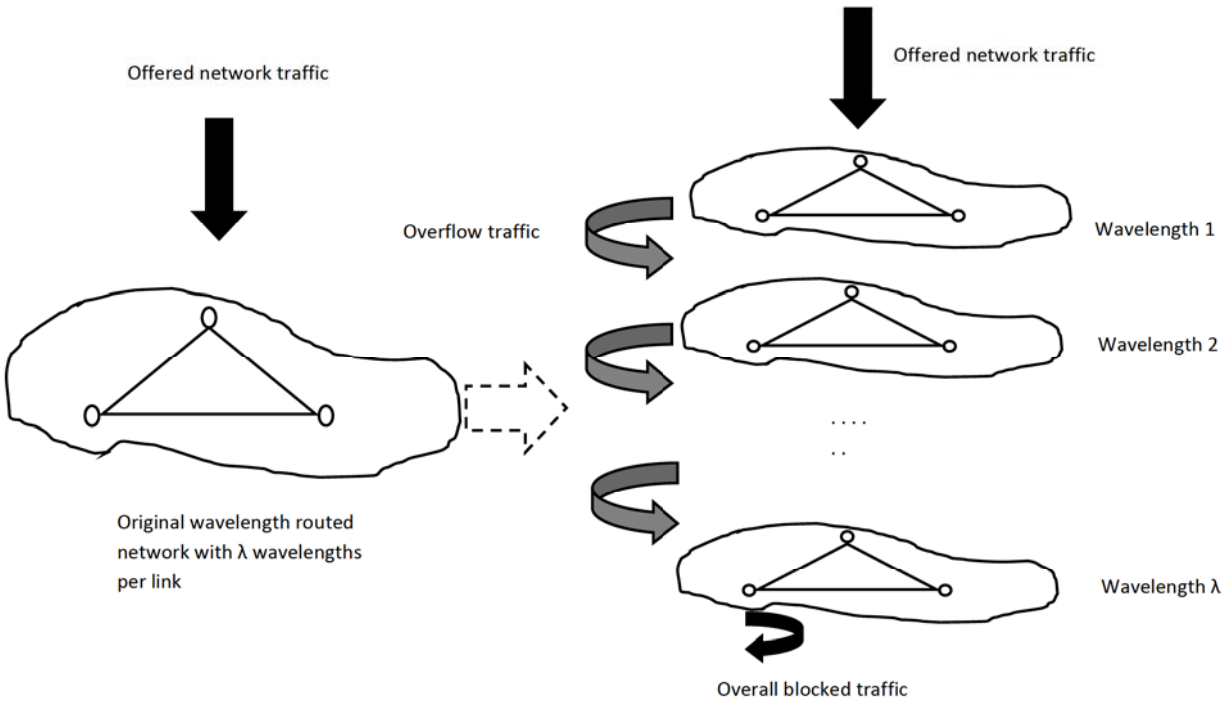

Figure 4.7: Layered network model

4.3.1 Strategy for Computing Wavelength Blocking Probabilities in Transparent Networks

In this section, we describe and explain the process of computing wavelength blocking probability in the wavelength sublayer. We believe that this technique may also be easily applied to other models to compute the wavelength blocking probabilities.

4.3.1.1 Blocking Probability for a Single Wavelength

If we consider an n hop path, the wavelength state (λ) at time t may be expressed by the following $\frac{n(n+1)}{2}$ process:

$$\left(\beta_{0,1}^{\lambda}(t), \beta_{0,2}^{\lambda}(t), \dots, \beta_{n-1,n}^{\lambda}(t)\right), \tag{4.5}$$

Where

$$\beta_{i,j}^{\lambda} + \beta_{l,m}^{\lambda} \leq 1, \quad \forall r(i,j) \cap r(l,m) \neq \emptyset, \;\; 0 \leq l < m \leq n$$

The procedure presented above depicts a time-reversible Markov process whose static probability vector π^{λ} is given by:

$$\pi^{\lambda}\left(\beta_{0,1}^{\lambda}.\beta_{0,2}^{\lambda}, \dots, \beta_{n-1,n}^{\lambda}\right) = \frac{1}{G_r^{\lambda}(0,n)}\left[\left(\left(a_{0,1}^{\lambda}\right)^{\beta_{0,1}^{\lambda}}.\left(a_{0,2}^{\lambda}\right)^{\beta_{0,2}^{\lambda}}, \dots, \left(a_{n-1,n}^{\lambda}\right)^{\beta_{n-1,n}^{\lambda}}\right)\right], \tag{4.6}$$

Where $G_r^{\lambda}(0,n)$ represents the recursively computed normalization constants [34].

$$G_r^{\lambda}(0,n) = G_r^{\lambda}(0,n-1) + \sum_{i=0}^{n-1} G_r^{\lambda}(0,i)a_{i,n}^{\lambda}, \;\; \lambda = 1, \dots, \Lambda \tag{4.7}$$

When $G_r^{\lambda}(0,0) = 1$, $a_{i,j}^{\lambda}$ denotes the total of all equivalent Poisson network traffic from all s-d pairs on segment $r(i,j)$ at wavelength λ, and may be expressed as follows:

$$a_{i,j}^{\lambda} = \sum_{\substack{r(i,j)\subseteq r(s,d) \\ r(i,j)\Leftarrow A_{s,d}^{\lambda}, then\ r(m,l)\Leftarrow A_{s,d}^{\lambda} \\ \forall r(l,m)\subseteq r(0,n)}} \frac{A_{s,d}^{\lambda}\cdot(1-P_{s,d}^{\lambda})}{1-P_{i,j}^{\lambda}}, \tag{4.8}$$

Where, the following expression: "$r(i,j) \Leftarrow A_{s,d}^{\lambda}, then\ r(m,l) \Leftarrow A_{s,d}^{\lambda}, \forall r(l,m) \subseteq r(0,n)$" states that the traffic that belongs to segment $r(i,j)$ is eccentric. The blocking probability of the wavelength for $r(0,n)$ at wavelength λ is calculated as follows:

$$P_{0,n}^{\lambda} = 1 - \pi^{\lambda}(0,0,\ldots,0) = 1 - \frac{1}{G_r^{\lambda}(0,n)} \tag{4.9}$$

4.3.1.2 Computation of the Overall Wavelength Blocking Probability

The overflow model is utilized to compute the overall wavelength blocking probability in this section. We recall our earlier assumption that, the traffic blocked at wavelength λ is capable of flowing down to the next wavelength. It is observed that the overflow traffic is not Poisson distributed and its variance is greater than its mean, and thus the traffic is taken as bursty [205]. From the studies presented in [205], the overflow traffic model is proposed for implementation in various conventional switching networks, and the average overflow traffic to the next layer is given by:

$$\bar{A}_{s,d}^{\lambda+1} = A_{s,d}^{\lambda}.P_{s,d}^{\lambda} \tag{4.10}$$

The Riordan's formula is used to compute the overflow traffic variance, $\bar{V}_{s,d}^{\lambda+1}$, as shown below [56].

$$\bar{V}_{s,d}^{\lambda+1} = \bar{A}_{s,d}^{\lambda+1}\left(1 - \bar{A}_{s,d}^{\lambda+1} + \frac{\Phi_{s,d}}{\bar{\Omega}_{s,d}^{\lambda}+1+\bar{A}_{s,d}^{\lambda+1}-\Phi_{s,d}}\right), \tag{4.11}$$

Where $\bar{\Omega}_{s,d}^{\lambda}$ represents the capacity of an alternate single link system for layer 1 to λ, and it can be established from:

$$\Phi_{s,d}.Er\left(\Phi_{s,d},\bar{\Omega}_{s,d}^{\lambda}\right)=\bar{A}_{s,d}^{\lambda+1} \tag{4.12}$$

Where, $Er\left(\Phi_{s,d},\bar{\Omega}_{s,d}^{\lambda}\right)$ is the Erlang-B generalized formula for non-integral capacity and is given by [206]:

$$Er(x,y)=\frac{x^{y}e^{-x}}{\Gamma(y+1)[1-\Gamma(x,y+1)]} \tag{4.13}$$

Where $\Gamma(x,y+1)$ is known as the incomplete Gamma function.

The ratio between the variance and the mean value is referred to as the burstiness of a system, and is given by:

$$\bar{Z}_{s,d}^{\lambda+1}=\frac{\bar{V}_{s,d}^{\lambda+1}}{\bar{A}_{s,d}^{\lambda+1}} \tag{4.14}$$

The non-Poisson distribution nature of the overflow traffic is accounted for by using the Fredericks and Hayward's approximation techniques as provided in [205] as follows:

$$A_{s,d}^{\lambda+1}.P_{s,d}^{\lambda+1}\approx\bar{A}_{s,d}^{\lambda+1}.Er\left(\frac{\bar{A}_{s,d}^{\lambda+1}}{\bar{Z}_{s,d}^{\lambda+1}},\frac{\Omega_{s,d}^{\lambda+1}}{\bar{Z}_{s,d}^{\lambda+1}}\right) \tag{4.14}$$

Where, $\Omega_{s,d}^{\lambda+1}$ is computed by using the following relationship:

$$P_{s,d}^{\lambda+1}=Er\left(A_{s,d}^{\lambda+1},\Omega_{s,d}^{\lambda+1}\right) \tag{4.15}$$

In addition, the value of $\Omega_{s,d}^{\lambda+1}$ may be taken as the capacity of another equivalent single-link system only for layer $\lambda+1$ that has an average arrival rate of $A_{s,d}^{\lambda+1}$.

By utilizing the equations presented in this section, the wavelength blocking probability and the path arrival rate for each layer may be approximated, and the wavelength blocking probability of the overall path is computed as follows:

$$\hat{P}_{s,d} = \frac{A_{s,d}^{\Lambda} \cdot P_{s,d}^{\Lambda}}{\Phi_{s,d}} = \frac{\bar{A}_{s,d}^{\Lambda+1}}{\Phi_{\mathrm{s,d}}} \tag{4.16}$$

Therefore, the overall network wavelength blocking probability for a given network is computed as follows:

$$\hat{P} = \frac{\sum_{(s,d)\epsilon Z} \bar{A}_{s,d}^{\Lambda+1}}{\sum_{(s,d)\epsilon Z} \Phi_{\mathrm{s,d}}} \tag{4.17}$$

Algorithm 4.1 presents the algorithm that is used to calculate the overall network and path wavelength blocking probabilities for the FF WA under the following conditions:

$\lambda_0 = 1, \quad \bar{A}_{s,d}^{1} = \Phi_{\mathrm{s,d}}, \ \bar{V}_{s,d}^{1} = \Phi_{\mathrm{s,d}} \ , \ \bar{Z}_{s,d}^{1} = 1$ for all $(s,d) \in Z$.

It is assumed that if the relative difference of the blocking probabilities between two consecutive iterations differs by a figure less than ϵ per path, then the present layer may be viewed as stable and iterations for the next layer will be initiated.

4.3.2 Analytical Model for QARWA

In this section, an analytical model for the proposed QoT-Aware RWA (QARWA) algorithm is presented. The QoT blocking takes into account the effects of ASE noise, thermal noise, shot noise, and XT. The proposed approach may be infused with other algorithms that attempt to calculate wavelength blocking per path and also per available layer.

Algorithm 4.1: Algorithm for computation of the wavelength blocking from $\boldsymbol{\lambda = \lambda_0}$ *to* $\boldsymbol{\Lambda}$

1. Assume initial values of $\boldsymbol{A^{\lambda}_{s,d} = \overline{A}^{\lambda}_{s,d}}$, and the initial wavelength blocking probability of the path as $\boldsymbol{\overline{P}'_{s,d} = 0\ \forall\ (s,d) \in Z}$
2. Compute $\boldsymbol{P^{\lambda}_{s,d}}$
3. Obtain $\boldsymbol{\Omega^{\lambda}_{s,d}\ \forall\ (s,d) \in Z}$
4. Compute the corresponding Poisson traffic $\boldsymbol{A^{\lambda}_{s,d}}$ for stratum $\boldsymbol{\lambda\ \forall\ (s,d) \in Z}$
5. **if** $\boldsymbol{\frac{\left|P^{\lambda}_{s,d} - \overline{P}'_{s,d}\right|}{\overline{P}'_{s,d}} > \epsilon, \forall (s,d) \in Z}$ **then**
6. $\boldsymbol{\overline{P}'_{s,d} = P^{\lambda}_{s,d}}$
7. go to step 2
8. **else**
9. $\boldsymbol{\lambda = \lambda + 1}$
10. Calculate $\boldsymbol{\overline{A}^{\lambda}_{s,d}}$, $\boldsymbol{\overline{V}^{\lambda}_{s,d}}$, and $\boldsymbol{\overline{Z}^{\lambda}_{s,d}}$
11. **if** $\boldsymbol{\lambda \leq \Lambda}$, **then**
12. go to step 1
13. **else**
14. Compute the net path and network wavelength blocking probabilities
15. **return** $\boldsymbol{\widehat{P}}$ and $\boldsymbol{\widehat{P}_{s,d}\ \forall\ (s,d) \in Z}$
16. **end if**
17. **end if**

4.3.2.1 QoT Blocking Events

In order to calculate the blocking due to QoT, it is necessary to count all possibilities that may lead to the occurrence of a QoT act when a call z reaches wavelength λ, where z refers to a call for a s-d pair. For a given network topology, the ASE noise and the other above-stated impairments may be determined by the route $r(z), \forall z \in Z$. We assume that the effects of thermal and shot noises are low enough that they do not severely compromise the value of QoT, therefore, the QoT will effectively depend on the strengths of XT. This in turn implies that the number of XT terms $N^{ad}(z)$ is essentially determined by the state of the network,

and $N_{max}^{ad}(z)$ denotes the utmost number of XT terms that are permissible in $r(z)$ prior to the violation of the QoT constraint.

All the possible paths in Z can be listed as $z_1, \dots, z_{|z|}$, and we define a $1 \times |Z|$ vector $\Im^{\lambda} = \left[I_{z_1}^{\lambda}, \dots, I_{z_{|z|}}^{\lambda}\right]$ for wavelength λ, where $I_z^{\lambda} = 1$ if $r(z)$ is operational at wavelength λ and $I_z^{\lambda} = 0$ if the converse is true. The term $\Im^{\lambda}$ denotes the extent of usage of the path at layer λ , and $\Im^{\lambda}(z') = \left[I_{z_1}^{\lambda}, \dots, I_{z'}^{\lambda} = 1, \dots, I_{z_{|z|}}^{\lambda}\right]$ represents all the states such that path $r(z')$ is considered to be utilized at wavelength λ. A subset of Z (referred to as $\mathcal{Z}_u^{\lambda}$) is formed that represents all the utilized paths at wavelength λ, and is expressed as follows: $\mathcal{Z}_u^{\lambda} = \{z: I_z^{\lambda} = 1\}$. From this expression, it can be observed that it is impossible to simultaneously use two paths if they reside in the same layer and share a link. It is important to bear in mind that XT occurs when two different paths share at least two successive hops on adjacent wavelengths, and that a single unit of XT is added to each call per set of two successive hops. By taking use of a routing table, it is possible to count the number of units of XT, for instance, suppose $X_{z'}^{Z} \in \mathbb{Z}$, are actuated by $z, \forall z \in Z$ to a selected z'. If we state a $|Z| \times 1$ vector $\mathcal{X}_{z'} = \left[X_{z'}^{z_1}, \dots, X_{z'}^{z_{|z|}}\right]^T$. Where, $\mathcal{X}_{z'}$ represents the potential interference due to XT at a selected z' from other s-d pairs.

Since we only focus on XT from the closest adjacent wavelengths, the lightpaths in the following wavelengths are capable of producing XT to $r(z), \forall z \in Z$ in layer $w_0 = \lambda$:

$w_{-1} = \lambda - 1$, and $w_{+1} = \lambda + 1$.

A QoT blocking episode arises at wavelength λ if the present network scenario at w_{-1} and w_{+1} meets the following condition:

$$(\Im^{w_{-1}} + \Im^{w_{+1}}).\mathcal{X}_{z_c} > N_{max}^{ad}(z_c) \tag{4.18}$$

We further assume that the new path allocated at wavelength λ does not cause the QoT of variant prevailing lightpaths to drop below the acceptable QoT threshold. Therefore, we should consider wavelengths w_i for $i = -2, -1, 0, 1, 2$, and thus, $\lambda - 2, \lambda - 1, \lambda, \lambda + 1, \lambda + 2$.

As a consequence of these conditions, an arriving call z_c should be barred if either equation 4.18 holds, or:

$\exists z_e \in \mathcal{Z}_u^{w+1}$, such that $(\Im^{w_0}(z') + \Im^{w+2}).\mathcal{X}_{z_e} > N_{max}^{ad}(z_e);$ (4.19)

or

$\exists z_e \in \mathcal{Z}_u^{w-1}$, such that $(\Im^{w_0}(z') + \Im^{w-2}).\mathcal{X}_{z_e} > N_{max}^{ad}(z_e);$ (4.20)

A $5 \times |Z|$ vector, $\mathbb{I}^{\lambda}$, is defined that depicts the states in five strata w_i for $i = -2, -1, 0, 1, 2$ whose centre is at stratum $w_0 = \lambda$.

$$\mathbb{I}^{\lambda} = [\Im^{w-2}; \Im^{w-1}; \Im^{w_0}; \Im^{w-1}; \Im^{w-2}] \quad (4.21)$$

It is possible to capture all the probable modes that the QoT blocking can adopt through the utilization of the above vector for a given arrival request z'.

If we assume that a set $\mathbb{I}^{\lambda}(z')$ comprises all probable QoT blocking episodes, we may let $= \mathbb{I}^{\lambda}(z')$, and if each QoT blocking episode is represented by $\xi_k^{\lambda,z'}, k = 1, \ldots, K, \xi_k^{\lambda,z'} \in \mathbb{I}^{\lambda}(z')$.

We obtain:

$$\xi_k^{\lambda,z'} = \left[\Im_k^{w-2}(z'); \Im_k^{w-1}(z'); \Im_k^{w_0}(z'); \Im_k^{w-1}(z'); \Im_k^{w-2}(z')\right] \quad (4.22)$$

It should be noted that the above equations are valid only for $\lambda > 2$ and $\lambda < \Lambda - 2$, for $\lambda - 1, 2, \Lambda - 1, \Lambda$.

To illustrate the operations of the above equations and conditions, we make use of a 4-node unidirectional network presented in figure 4.8.

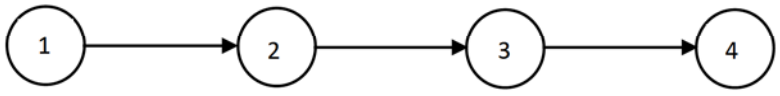

Figure 4.8: A four-node tandem network topology

We propose that every node is connected to an input EDFA that has a gain of 20 dB and an output EDFA that has a gain of 15 dB, and that there are no additional EDFAs between the stated nodes. Furthermore, we take each link to consist of five wavelengths; $X_{ad} = -20\ dB$, and a routing table that includes N_{max}^{ad} is shown in Table 4.1. It is also assumed that XT does not affect single-hop traffic in our model.

Table 4.1: Routing table for a 4-node tandem topology

Z	z_1	z_2	z_3	z_4	z_5	z_6
$s-d$ pair	(1,2)	(1,3)	(1,4)	(2,3)	(2,4)	(3,4)
$r(s,d)$	$1 \rightarrow 2$	$1 \rightarrow 2 \rightarrow 3$	$1 \rightarrow 2 \rightarrow 3 \rightarrow 4$	$2 \rightarrow 3$	$2 \rightarrow 3 \rightarrow 4$	$3 \rightarrow 4$
N_{max}^{ad}	2	1	1	2	1	2

The counting of the QoT blocking events is now illustrated by using the two-hop path z_2 at wavelength 1 via the utilization of FF WA. Suppose $w_0 = \lambda = 1, w_{+1} = 2$, and $w_{+2} = 3$, the QoT blocking events $\xi_k^{w_0,z_2}$, $k = 1, \dots, 10$ are given as:

$$\xi_1^{w_0,z_2} = \begin{bmatrix} - & - & - & - & - & - \\ - & - & - & - & - & - \\ * & * & * & * & * & * \\ 0 & 1 & 0 & 0 & 0 & 0 \\ 0 & 1 & 0 & 0 & 0 & 0 \end{bmatrix} \begin{matrix} w_{-2} \\ w_{-1} \\ w_0 \\ w_{+1} \\ w_{+2} \end{matrix}, \quad \xi_2^{w_0,z_2} = \begin{bmatrix} - & - & - & - & - & - \\ - & - & - & - & - & - \\ * & * & * & * & * & * \\ 0 & 1 & 0 & 0 & 0 & 0 \\ 0 & 1 & 0 & 0 & 0 & 1 \end{bmatrix},$$

$$\xi_3^{w_0,z_2} = \begin{bmatrix} - & - & - & - & - & - \\ - & - & - & - & - & - \\ * & * & * & * & * & * \\ 0 & 1 & 0 & 0 & 0 & 1 \\ 0 & 1 & 0 & 0 & 0 & 0 \end{bmatrix}, \quad \xi_4^{w_0,z_2} = \begin{bmatrix} - & - & - & - & - & - \\ - & - & - & - & - & - \\ * & * & * & * & * & * \\ 0 & 1 & 0 & 0 & 0 & 1 \\ 0 & 1 & 0 & 0 & 0 & 1 \end{bmatrix},$$

$$\xi_5^{w_0,z_2} = \begin{bmatrix} - & - & - & - & - & - \\ - & - & - & - & - & - \\ * & * & * & * & * & * \\ 0 & 0 & 1 & 0 & 0 & 0 \\ 0 & 1 & 0 & 0 & 0 & 0 \end{bmatrix}, \quad \xi_6^{w_0,z_2} = \begin{bmatrix} - & - & - & - & - & - \\ - & - & - & - & - & - \\ * & * & * & * & * & * \\ 0 & 0 & 1 & 0 & 0 & 0 \\ 0 & 1 & 0 & 0 & 0 & 1 \end{bmatrix},$$

$$\xi_7^{w_0,z_2} = \begin{bmatrix} - & - & - & - & - & - \\ - & - & - & - & - & - \\ * & * & * & * & * & * \\ 0 & 0 & 1 & 0 & 0 & 0 \\ 0 & 0 & 0 & 0 & 1 & 0 \end{bmatrix}, \quad \xi_8^{w_0,z_2} = \begin{bmatrix} - & - & - & - & - & - \\ - & - & - & - & - & - \\ * & * & * & * & * & * \\ 0 & 0 & 1 & 0 & 0 & 0 \\ 1 & 0 & 0 & 0 & 1 & 0 \end{bmatrix},$$

$$\xi_9^{w_0,z_2} = \begin{bmatrix} - & - & - & - & - & - \\ - & - & - & - & - & - \\ * & * & * & * & * & * \\ 0 & 1 & 0 & 0 & 0 & 0 \\ 0 & 0 & 1 & 0 & 0 & 0 \end{bmatrix}, \quad \xi_{10}^{w_0,z_2} = \begin{bmatrix} - & - & - & - & - & - \\ - & - & - & - & - & - \\ * & * & * & * & * & * \\ 0 & 1 & 0 & 0 & 0 & 1 \\ 0 & 0 & 1 & 0 & 0 & 0 \end{bmatrix},$$

Where the sign " $-$ " means not applicable because there are no wavelengths $< w_0 = \lambda = 1$, " $*$ " means not known and can be either 1 or 0. It can be noted that w_0 is not assigned to any arrival request because it is only present for it to be evaluated for compliance of the QoT. Since we earlier on stated the assumption that the wavelengths are independent, it is therefore possible to directly compute the probability of each event. A typical computation example is presented below for $\xi_1^{w_0,z_2}$:

$$Pr\left(\xi_1^{w_0,z'}\right) = \left(1 - \rho_{z_2}^{w+1}\right)\pi^{w+1}(0,1,0,0\ 0,0).\left(1 - \rho_{z_2}^{w+2}\right)\pi^{w+2}(0,1,0,0\ 0,0) \tag{4.23}$$

Where π^{λ} represents the static probability and $\beta_{s,d}^{\lambda}$ is set to the value of I_z^{λ} for each z. The probability of $\xi_i^{w_0,z'}$ can be more generally computed as follows:

$$Pr\left(\xi_i^{w_0,z'}\right) = \prod_{j=-2}^{-1}\left[\prod_{z_e \in \{z: I_z^{wj}=1\}}\left(1 - \rho_{z_e}^{w_j}\right)\frac{\pi^{\lambda j}\left(\Im_i^{\lambda_j}(z')\right)}{1 - Pr\left(r(z') \text{ is idle in } \lambda_j\right)}\right] \cdot \prod_{j=0}^{2}\left[\prod_{z_e \in \{z: I_z^{wj}=1\}}\left(1 - \rho_{z_e}^{w_j}\right)\pi^{\lambda j}\left(\Im_i^{\lambda_j}(z')\right)\right], \quad 2 < w_0 < \Lambda - 1. \tag{4.24}$$

It should be noted that for strata greater than λ ($j = 0, 1, \text{and } 2$), the network may be in any mode, yet for layers less thanλ ($j = -1 \text{ and } -2$), $r(z')$ may not be inactive since z'would have proceeded down to λ from an upper stratum.

Hence, the QoT blocking may be viewed as the sum of all the K blocking events probabilities and may be presented as follows:

$$\rho_{s,d}^{\lambda} = \sum_{i=1}^{K} Pr\left(\xi_i^{\lambda,z'}\right) \tag{4.25}$$

The complexity of the computation of the proposed algorithm may be lowered by grouping states together so that they may be treated as more generic blocking episodes, thus the QoT blocking may be easily computed as the probability of the union of the presented episodes.

4.3.2.2 The blocking probability for QARWA

The sophistication of calculating the QoT events is fairly reasonable for small to medium networks, but becomes a living nightmare if it is extended to cover large networks such as optical backbone networks. It therefore calls for the incorporation of techniques that give a good approximation of the solution via less complex computing processes. In this section, we propose an estimation that approximates the QoT blocking for backbone networks. In this approximation technique, the network is viewed to be made up of several small tandem networks that comprise 5 or fewer layers that are independently related.

The overall path and network blocking probabilities for QARWA are calculated by making use of the equations presented in the previous section, where $\bar{A}_{s,d}^{\lambda+1}$ now incorporates the blocking traffic QoT. Algorithm 4.2 outlines the pertinent steps of the proposed approach, where, $\bar{A}_{s,d}^{1} = \Phi_{s,d}$, $\bar{V}_{s,d}^{1} = \Phi_{s,d}$, and $\bar{Z}_{s,d}^{1} = 1 \ \forall \ (s,d) \in Z$. The rates of arrival and state probabilities without the consideration of physical impairments are obtained in step 2, and these parameters are in turn used as the initial QoT estimation values. The flow of traffic next moves to the QoT blocking sublayer, thereafter traffic of flow rate $\bar{A}_{s,d}^{\lambda} = A_{s,d}^{\lambda}.\left(1 - \rho_{s,d}^{\lambda}\right)$ reaches the wavelength blocking sublayer. The Poisson arrival rate and the blocking probability are obtained for the respective sublayer in step 4. Step 5 computes layer 2 overflow traffic, which is equal to the sum of the overflow due to wavelength blocked and

QoT blocked requests. Thereafter, the probabilities and arrival rates for layers 2 to Λ are updated without taking into account the QoT, and they are utilized as the initial figures for the ensuing layer. After processing requests for the last layer, the results are returned if the overall blocking probability converges, otherwise, the procedure goes back to the initial step and iterations commence again from layer 1.

4.3.3 Blocking probability of the QoT-Guaranteed RWA

The main distinction between QARWA and the QoT-Guaranteed RWA (QGRWA) algorithms is that for the later algorithm, a portion of the traffic is blocked out of the flow per every layer, and the rate of the traffic that exits the flow is estimated by the following expression:

$$\mathbb{A}_{s,d}^{\lambda} = A_{s,d}\rho_{s,d}^{\lambda}\left(1 - P_{s,d}^{\lambda}\right) \tag{4.26}$$

Therefore, the total path blocking probability ($\bar{P}_{s,d}$) may be calculated using the following:

$$\bar{P}_{s,d} = \frac{\bar{A}_{s,d}^{\Lambda+1} + \sum_{\lambda=1}^{\Lambda} \mathbb{A}_{s,d}^{\lambda}}{\Phi_{s,d}} \tag{4.27}$$

The effective blocking probability for the entire network is given by:

$$\bar{P} = \frac{\sum_{(s,d)\in Z} \Phi_{s,d}\bar{P}_{s,d}}{\sum_{(s,d)\in Z} \Phi_{s,d}} \tag{4.28}$$

Algorithm 4.2: Algorithm to calculate the total blocking for QARWA from $\boldsymbol{\lambda = 1\ to\ \Lambda}$

1. Set $\boldsymbol{\lambda = 1}$.
2. Use the previous algorithm to calculate the wavelength blocking probabilities $\boldsymbol{P_{s,d}^{\lambda}}$ and rates of arrival $\boldsymbol{A_{s,d}^{\lambda}}$ for every path from $\boldsymbol{\lambda\ to\ \Lambda}$. Set $\boldsymbol{\overline{P}'_{s,d} = \widehat{P}_{s,d}}$
3. Calculate the QoT blocking probability $\boldsymbol{\rho_{s,d}^{\lambda}}$, $\boldsymbol{\forall z = (s,d) \in Z}$.
4. Re-compute the rate of arrival for the wavelength sublayer as $\boldsymbol{\overline{A}_{s,d}^{\lambda} = A_{s,d}^{\lambda}.(1 - \rho_{s,d}^{\lambda})}$ for every path. Obtain $\boldsymbol{\overline{V}_{s,d}^{\lambda}}$, and $\boldsymbol{\overline{Z}_{s,d}^{\lambda}}$ $\forall$ $\boldsymbol{(s,d) \in Z}$. Re-compute the wavelength blocking probability $\boldsymbol{\rho_{s,d}^{\lambda}}$, to get the sublayer corresponding Poisson traffic estimate for all paths.
5. Compute the traffic overflow rate $\boldsymbol{\overline{A}_{s,d}^{\lambda+1} = A_{s,d}^{\lambda}.(1 - \rho_{s,d}^{\lambda}) + \widehat{A}_{s,d}^{\lambda} P_{s,d}^{\lambda}}$ for every s-d pair and revise $\boldsymbol{\overline{V}_{s,d}^{\lambda+1}}$, and $\boldsymbol{\overline{Z}_{s,d}^{\lambda+1}}$ for all $\boldsymbol{(s,d) \in Z}$. Set $\boldsymbol{\lambda = \lambda + 1}$
6. **if** $\boldsymbol{\lambda \leq \Lambda}$, **then**
7. go to step 2
8. **else**
9. Compute the overall path blocking probabilities $\boldsymbol{\overline{P}_{s,d}}$.
10. **if** $\boldsymbol{\frac{|\overline{P}_{s,d} - \overline{P}'_{s,d}|}{\overline{P}'_{s,d}} > \epsilon, \forall (s,d) \in Z}$ **then**
11. return to step 1
12. **else**
13. Compute the total path blocking probabilities $\boldsymbol{\overline{P}}$.
14. **return** $\boldsymbol{\overline{P}}$and $\boldsymbol{\overline{P}_{s,d}}$ $\forall$ $\boldsymbol{(s,d) \in Z}$
15. **end if**
16. **end if**

Algorithm 4.3 is implemented to calculate the total blocking probability for QGRWA, where, $\bar{A}_{s,d}^{1} = \Phi_{s,d}$, $\bar{V}_{s,d}^{1} = \Phi_{s,d}$, and $\bar{Z}_{s,d}^{1} = 1$ for all $(s,d) \in Z$. It is clearly evident that this algorithm is similar to that of the QARWA except on step 5, where the traffic rate of overflow is calculated by using $\bar{A}_{s,d}^{\lambda+1} = A_{s,d}^{\lambda}.(1 - \rho_{s,d}^{\lambda}) P_{s,d}^{\lambda} + \hat{A}_{s,d}^{\lambda} P_{s,d}^{\lambda}$ and $\mathbb{A}_{s,d}^{\lambda}$ should be subtracted from the overflow load to the adjacent following stratum.

Algorithm 4.3: Algorithm to calculate the total blocking for QGRWA from $\boldsymbol{\lambda = 1\ to\ \Lambda}$

1. Set $\boldsymbol{\lambda = 1}$.
2. Use the previous algorithm to calculate the wavelength blocking probabilities $\boldsymbol{P^{\lambda}_{s,d}}$ and rates of arrival $\boldsymbol{A^{\lambda}_{s,d}}$ for every path from $\boldsymbol{\lambda\ to\ \Lambda}$. Then, set $\overline{\boldsymbol{P}}'_{s,d} = \widehat{\boldsymbol{P}}_{s,d}$
3. Calculate the QoT blocking probability $\boldsymbol{\rho^{\lambda}_{s,d}}$, $\forall\ \boldsymbol{z = (s,d) \in Z}$.
4. Re-compute the rate of arrival for the wavelength sublayer as $\overline{\boldsymbol{A}}^{\lambda}_{s,d} = \boldsymbol{A^{\lambda}_{s,d}}.\left(\boldsymbol{1 - \rho^{\lambda}_{s,d}}\right)$ for every path. Get $\overline{\boldsymbol{V}}^{\lambda}_{s,d}$, and $\overline{\boldsymbol{Z}}^{\lambda}_{s,d}$ $\forall\ \boldsymbol{(s,d) \in Z}$. Re-compute the wavelength blocking probability $\boldsymbol{\rho^{\lambda}_{s,d}}$, to get the sublayer corresponding Poisson traffic estimate for all paths.
5. Compute the traffic overflow rate $\overline{\boldsymbol{A}}^{\boldsymbol{\lambda+1}}_{s,d} = \boldsymbol{A^{\lambda}_{s,d}}.\left(\boldsymbol{1 - \rho^{\lambda}_{s,d}}\right)\boldsymbol{P^{\lambda}_{s,d}} + \widehat{\boldsymbol{A}}^{\lambda}_{s,d}\boldsymbol{P^{\lambda}_{s,d}}$ for every s-d pair and revise $\overline{\boldsymbol{V}}^{\boldsymbol{\lambda+1}}_{s,d}$, and $\overline{\boldsymbol{Z}}^{\boldsymbol{\lambda+1}}_{s,d}$ for all $\boldsymbol{(s,d) \in Z}$. Set $\boldsymbol{\lambda = \lambda + 1}$
6. **if** $\boldsymbol{\lambda \leq \Lambda}$, **then**
7. go to step 2
8. **else**
9. Compute the overall path blocking probabilities $\overline{\boldsymbol{P}}_{\boldsymbol{s,d}}$.
10. **if** $\frac{|\overline{P}_{s,d} - \overline{P}'_{s,d}|}{\overline{P}'_{s,d}} > \boldsymbol{\epsilon}, \forall \boldsymbol{(s,d) \in Z}$ **then**
11. return to step 1
12. **else**
13. Compute the total path blocking probabilities $\overline{\boldsymbol{P}}$.
14. **return** $\overline{\boldsymbol{P}}$and $\overline{\boldsymbol{P}}_{\boldsymbol{s,d}}$ $\forall\ \boldsymbol{(s,d) \in Z}$
15. **end if**
16. **end if**

The blocking probability of the FFwO WA can be computed with ease and in a similar manner to that for the FF WA by employing the technique called static ordering where a wavelength-channel index mapping table is developed. For a given channel index, a corresponding wavelength index λ for the channel can be found, and XT in this scenario is induced by adjacent wavelengths. Through the use of the mapping table, the channel index for adjacent wavelengths can be correctly found. By making use of the proposed analytical model, the FFwO WA can be solved in a similar way to that of the FF WA except that the mapping changes as follows: $\lambda \longrightarrow w_i$.

4.4 Validation by Simulations

In this section, we validate our proposals with simulations and we also make comparisons of the results. Firstly, a comparison of the results of the analytical model and the approximation technique for the 4-node network topology depicted in figure 4.8 is made.

Secondly, an evaluation is carried out using the approximate technique for the NSFNET topology and the network topology shown in figure 4.9.

Table 4.2 shows the physical parameters used for simulation purposes, and the simulation results are obtained after running at least 10^6 calls. We assume that, $\epsilon = 10^{-2}$, XT has no effect on the switching fabric, and the network load is uniform. Since our proposed wavelength blocking model is presumed to be accurate for the first few network layers, our analysis involves the use of a small number of wavelengths for the topologies used in the validation process.

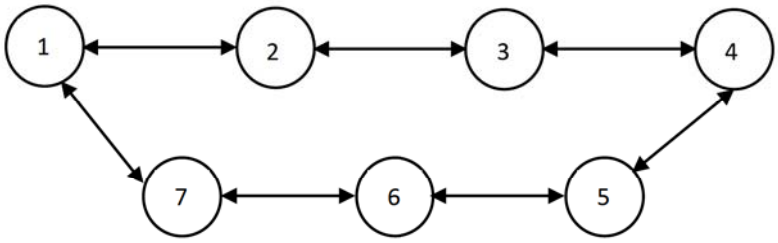

Figure 4.9: A 7-node network topology

Table 4.2: The physical parameters used for simulations

Parameter	value
Wavelength spacing	50 GHz
Data rate per channel	10 Gbps
ASE factor	1.5
Laser source power	0 dBm
Receiver responsivity	0.95 A/W
BER threshold	10^{-12}
Q-factor threshold	7
Optical bandwidth	= wavelength spacing
Input EDFA gain	22 dB
Output EDFA gain	16 dB
Centre wavelength	1550 nm

Since the 4-node network topology used in the simulation and validation process is symmetric, we treat its behaviour as that of a bidirectional link.

4.4.1 FF and FFwO WA

Algorithms 4.2 and 4.3 are used to get the estimate values of the blocking probabilities of the QoT-Aware FF WA and QoT-guaranteed FF WA as shown in figure 4.10.

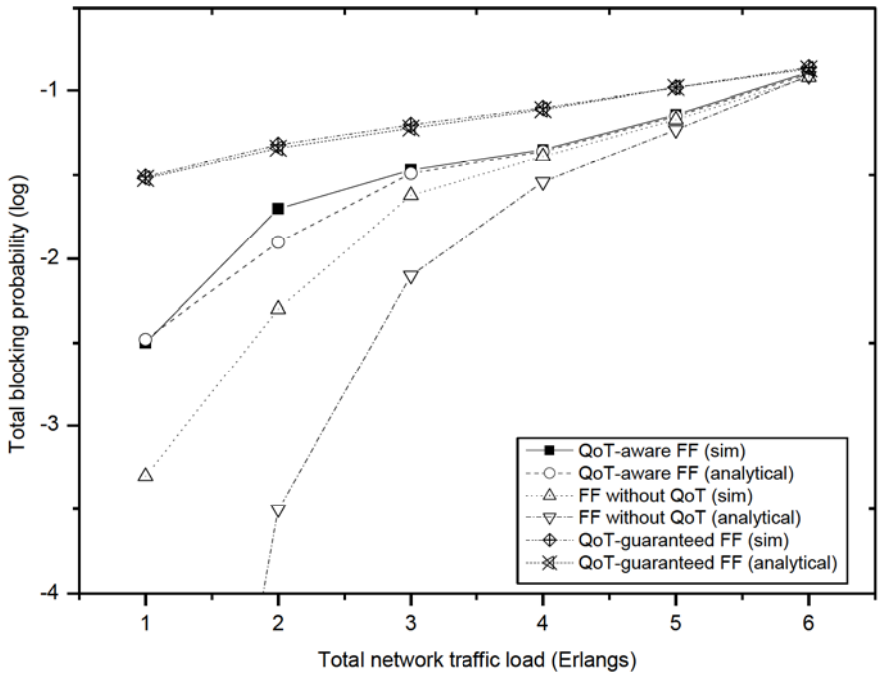

Figure 4.10: FF WA blocking probabilities calculated using the analytical technique and simulations for the 4-node network

From the figure 4.10, we can observe that the analytical results for the QoT-aware FF WA and QoT-guaranteed FF WA very closely resemble the simulation results for medium and large traffic scenarios. At low traffic loads, the model presented in [204] becomes inaccurate, and this may be due to the inadequacies of the Fredericks and Hayward's approximation technique that is applied to estimate the non-Poisson overflow traffic. Our proposed algorithm maintains its accuracy mainly because the proposed computation of QoT blocking is fairly accurate since the QoT constraints are used to initially block the flows. Since the QoT blocking dominates in low traffic situations, the traffic flow rate will thus be still close to the actual traffic present. As expected, more requests are blocked in the QoT-guaranteed cases compared to the QoT-aware cases, thus ample proof that our proposal is accurate and valid. This implies that the analytical model accurately provides the enhancement from QoT-guaranteed to QoT-aware WA and gives an acceptable approximation to the network performance by factoring in QoT and wavelength blocking.

In the case of FFwO WA, the technique of static ordering proposed in this work is employed, and we assume the following ordering table for five wavelengths: {1,5,2,4,3}. Figure 4.11 shows the performance of the proposed technique. It can be observed that the analytical model accurately captures the gains attained by implementing the FFwO approach instead of the traditional FF in QoT-guaranteed cases. In addition, the model clearly shows that QoT-aware FF method outperforms the QoT-aware FFwO when XT is dorminant at certain traffic loads. This could be due to the idea that the QoT-aware FFwO approach initially utilizes all channels with low XT and leaves only low quality channels for forthcoming requests, whereas QoT-aware FF simply selects channels based on the wavelength index. Since QoT-guaranteed techniques do not sift through all available wavelengths, this opens a good opportunity for the exploitation of the ordering technique. We can firmly assume that if other physical impairments are factored-in, the FFwO will definitely outshine the FF due to the added complexities of the scenario. Once again, it can be seen that the analytical results are very close to the results from simulations for different traffic conditions and algorithms, thus further upholding the accuracy and validity of our model.

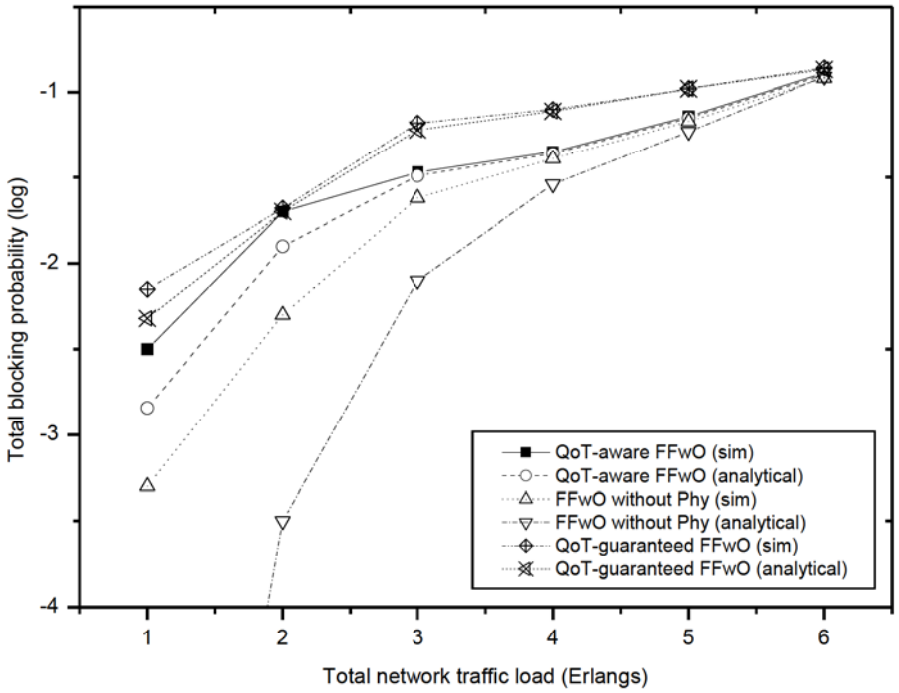

Figure 4.11: FFwO WA blocking probabilities calculated using the analytical technique and simulations for the 4-node network

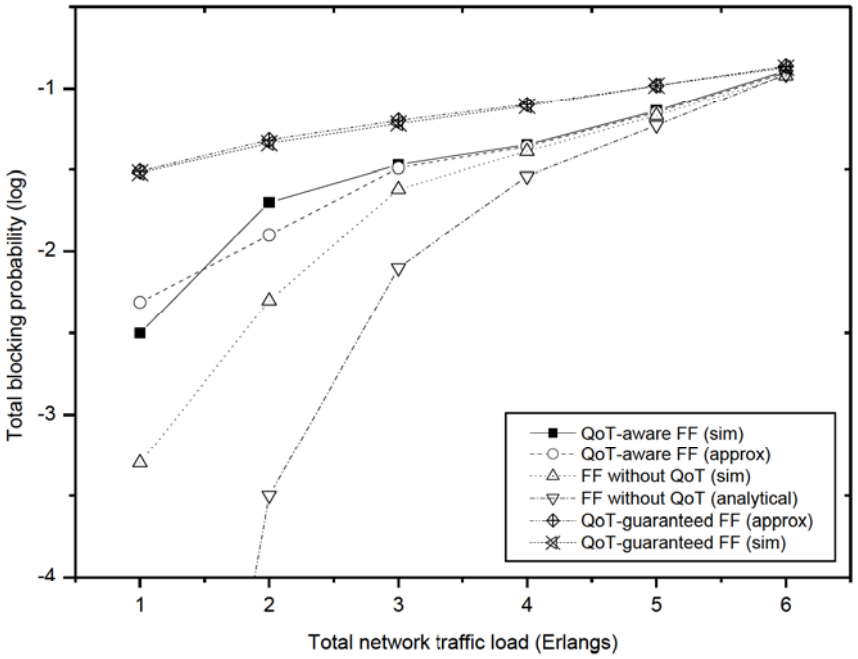

Figure 4.12: FF WA blocking probabilities calculated using the approximation method and simulations for the 4-node network

4.4.2 Approximation Method Results

Due to the rigorous task of counting QoT blocking events, we proposed an approximation technique for the estimation of the QoT that is fast and less complex. Although the approximation underestimates the actual blocking because it only considers QoT blocking occasions that occur in the fibres that the selected route takes, it nonetheless gives an accurate approximation of the overall blocking probabilities. Figures 4.12 and 4.13 show the results of the approximation technique and the respective simulations equivalents. From the graphs presented, it can be seen that the approximation technique provides a good estimation of the actual blocking probabilities and thus gives a great opportunity to analyse the performance of backbone optical networks. In brief, our approximations and estimations of the impact of QoT-aware and QoT-guaranteed WA are accurate and may be extended to assist in the analysis of complex networks where it is practically impossible to employ analytical techniques.

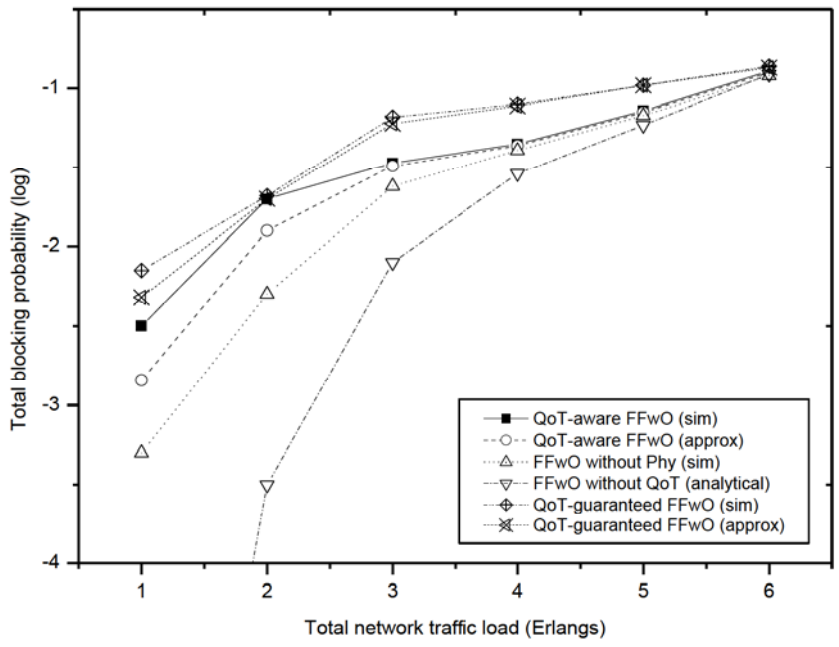

Figure 4.13: FFwO WA blocking probabilities computed using the approximation method and simulations for the 4-node network

4.4.3 Validation in other Networks

In this section, we validate our proposals by simulations conducted in two different network topology environments. We make use of the 7-node ring network where we assume the presence of five wavelengths per link and two bidirectional fibre links. The NSFNET topology is also utilized where we assume the presence of six wavelengths per fibre link and that are the links are also bidirectional. We divide each link into several spans, and each span is equipped with an EDFA amplifier to counter the effects of signal attenuation. The length of the lightpaths is limited to 3 hops in the NSFNET topology so as to reduce the effects of noise. Other key physical parameters remain the same as those used in the 4-node tandem topology. Figures 4.14 and 4.15 show the results for the 7-node ring network where FF WA and FFwO WA approaches are used respectively. The NSFNET network is used to obtain results for the FF WA and FFwO WA as shown in figures 4.16 and 4.17 respectively.

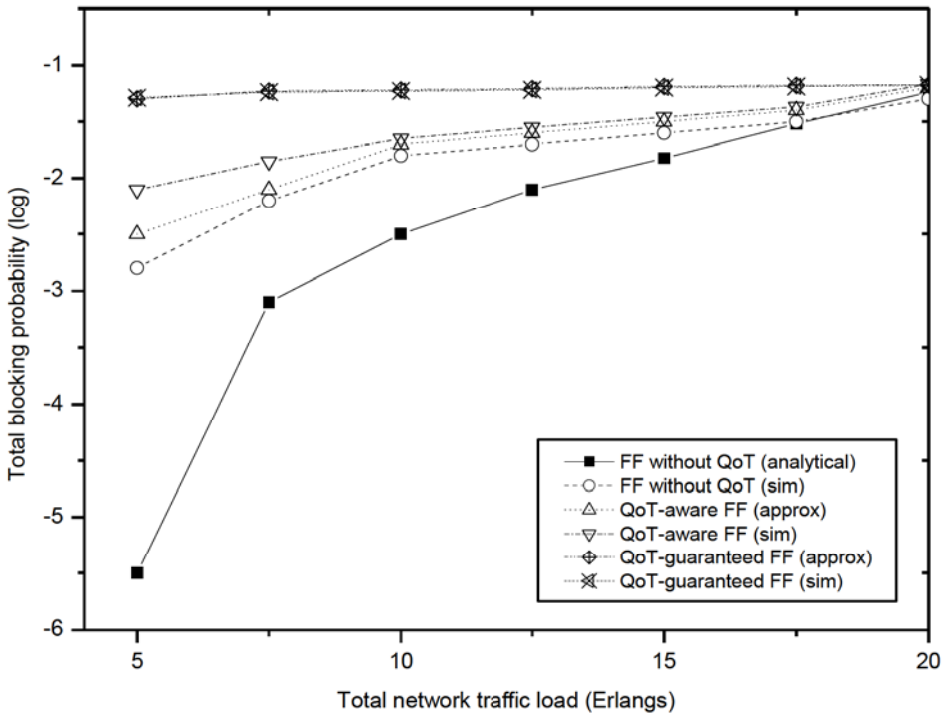

Figure 4.14: FF WA blocking probabilities computed using the approximation method and simulations for the 7-node network

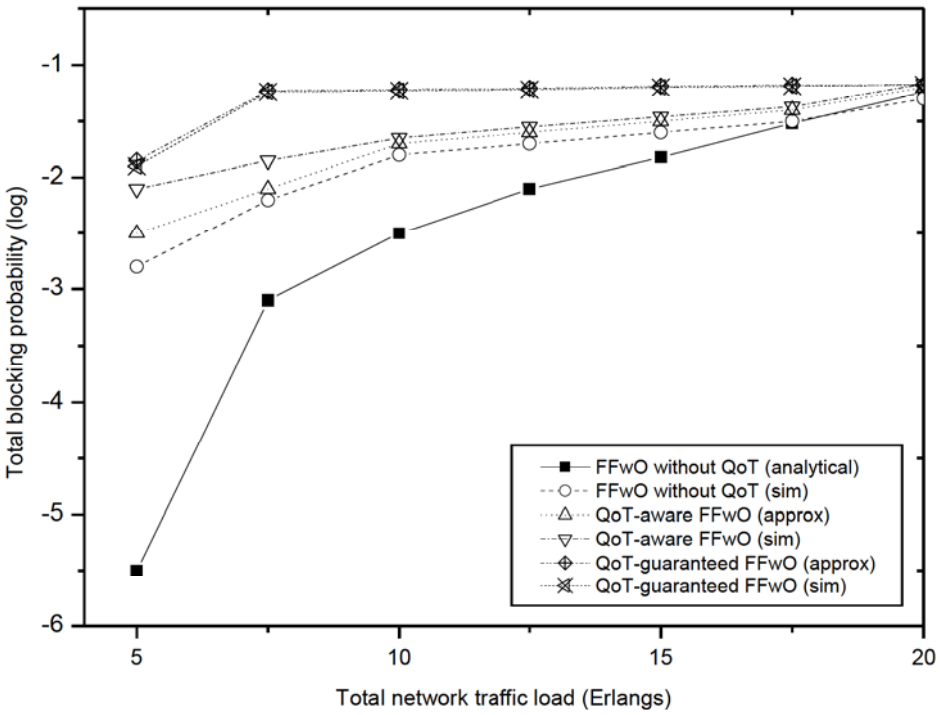

Figure 4.15: FFwO WA blocking probabilities computed using the approximation method and simulations for the 7-node network

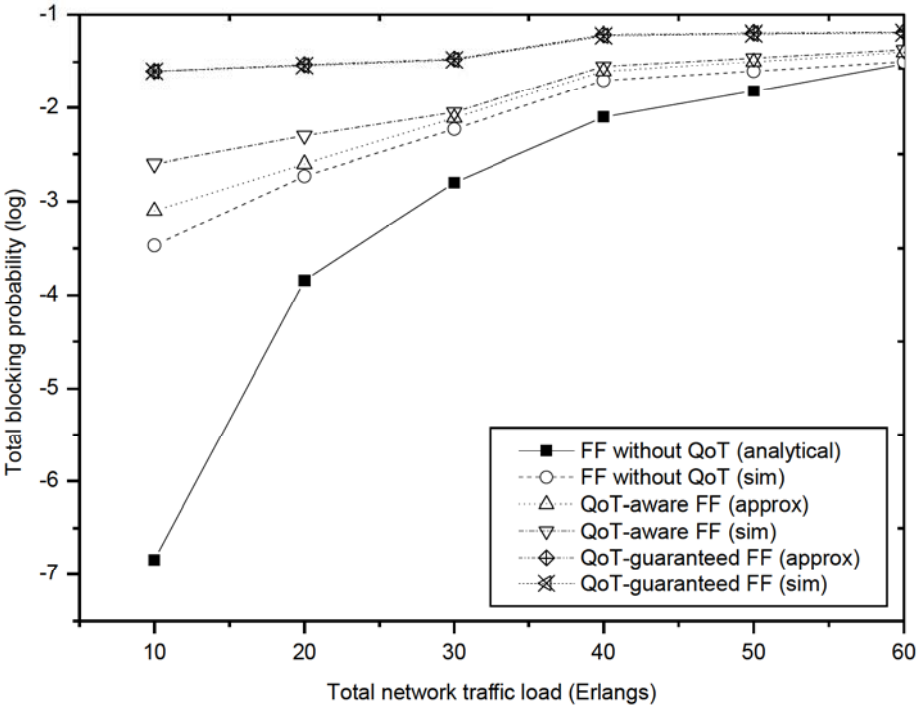

Figure 4.16: FF WA blocking probabilities computed using the approximation method and simulations for the NSFNET network

From the results, we can observe that at low traffic loads, the blocking probability of the analytical technique is lower than that obtained from the simulations. This is caused by the underestimation of the wavelength blocking probability that exists in real networks which is not appropriately captured in the analytical method. On the other hand, in the medium to high traffic conditions, the results obtained by the two approaches are almost the same. We can conclude that our proposed analytical method accurately forecasts the behaviour of QoT-aware and QoT-guaranteed algorithms in both the traditional FF WA and FFwO WA.

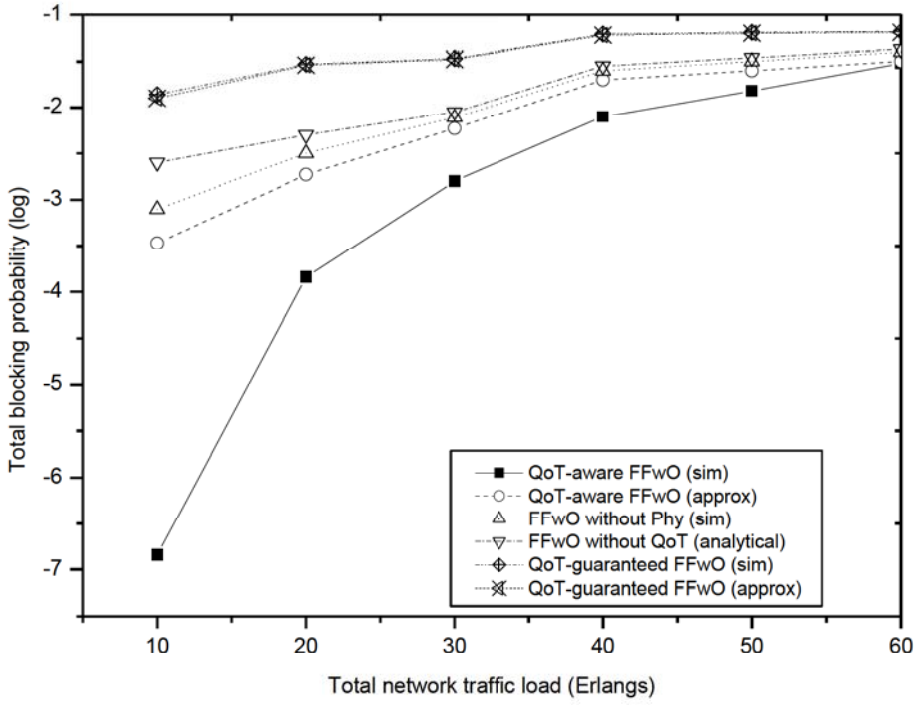

Figure 4.17: FFwO WA blocking probabilities computed using the approximation method and simulations for the NSFNET network

4.5 Summary

In this chapter, a Q-factor tool that incorporates most of the pertinent physical layer impairments is proposed. The tool is evaluated through simulations, and a comparison of its performance with those of traditional approaches is made. The proposed Q-factor tool outperforms the ones that are traditionally employed. An analytical technique to compute the blocking probabilities for RWA with physical impairments in transparent networks is also proposed. Numerical examples are also provided to show the performance of the proposed model, and it is validated through the use of simulations. QoT-aware and QoT-guaranteed WA approaches are implemented in various networks to evaluate the performance of the model, and its validation is done through simulations. It is clearly observed that the proposed model provides reasonably accurate results in all given network scenarios.

5 Energy-efficient Impairment-Aware Algorithms

5.1 Introduction

This chapter presents energy-efficient algorithms that take into effect various parameters in their decision-making processes. Although the ultimate goal of the deployment of energy-efficient strategies and algorithms is to lower the overall energy consumption of the networks, care must also be taken to ensure that the amassed energy gains do not compromise the integrity of the transmitted signals. Thus, in our work, we also take the impact of physical impairments into consideration in the formulation of energy-efficient algorithms and strategies. The proposed algorithms are compared with the traditional algorithms that do not take cognisance of energy consumption in their computations.

5.2 Energy-efficient Architecture

In this section, we propose an energy efficient architecture that is cluster-based. In the proposal, the nodes of the core network are divided into disjoint sets, and each subsequent set is composed of more than one node to make a unitary cluster. The clusters may be configured to conform to a *sleep* mode initiated by the control plane. The *sleep* mode is an energy conserving, stand-by mode, that "rests" some network resources and may be quickly triggered to switch back to a normal operating mode [207]. There are unprecedented huge energy conserving benefits of implementing the *sleep* mode functionality in modern high-speed optical networks.

Authors in [208], [209] propose an *Anycasting* communication paradigm in order to reduce the blocking probability that may be increased due to a decrease in network connectivity owing to the use of the *sleep* mode functionality.

Anycasting is a communication paradigm in which the user has the freedom to choose a potential destination from a group of possible destinations. Since *anycasting* is highly flexible, if a destination cannot be reached due to some intermediate nodes being in the *sleep* mode, a next vacant destination can be chosen [210], [211].

We denote an anycast request by (s, D_s) where s is the source node and $D_s$is a set of probable destination candidates. Since a selected destination using the anycasting paradigm may be longer than other possible destinations, the signal quality may be compromised and the propagation delay may also increase. It is therefore prudent and necessary to formulate algorithms that are aware of these important parameters and the algorithms should incorporate their respective effects in the eventual lightpath establishment process. We propose a network element vector (NEV) that contains information about the BER and propagation delay of a link, and is shown by the following,

$$NEV_i = [BER_i, \tau_i]^T \tag{5.1}$$

Where, BER_i is the bit-error rate and τ_i is the propagation delay for link i respectively. The transpose is shown by T.
The threshold expression for a given request is given by,

$$T^{(r)} = [BER_{thres}, \tau_{thres}] \tag{5.2}$$

For a given request r, the NEV is given by,

$$NEV^{(r)} = \left[BER^{(r)}, \tau^{(r)}\right]^T = \left[\prod_{\forall i} BER_i^{(r)}, \sum_{\forall i} \tau_i^{(r)}\right]^T \tag{5.3}$$

We assume that a lightpath can only be established provided the following constraints are observed,

$BER^{(r)} < BER_{max}$ and $\tau^{(r)} < \tau_{max}$.

Figure 5.1 shows the proposed energy efficient algorithm pseudo code.

Input: $NEV_{initial} = [10^{-12}, 0], (s, D_s), T^{(r)}$

1: $SORT.SWP(D_s)$.
2: $D_s' = \{d_1', d_2', \dots, d_z'\}$.
3: $PATH = \{s, d_i'\}$.
4: ***if*** $(n_k \forall k \in PATH = FREE) and (|D_s'| \neq 0)$ ***then***
5: $Compute\ NEV^{(r)} = \left[\prod_{\forall i} BER_i^{(r)}, \sum_{\forall i} \tau_i^{(r)}\right]^T$
6: ***if*** $NEV^{(r)} > T^{(r)}$, ***then***
7: Request r is discarded
8: exit
9: **else**
10: $PATH = \{s, \dots n_k, \dots, d_1'\}$.
11: ***if*** $(n_i \in C_{OFF})\ and\ (|D_s'| \neq 0)$ ***then***
12: $MODF\_CALLREQUEST = (s, d_j'), i \neq j$
13: $UPDATE(D_s') = D_s' \backslash d_i'$
14: **else**
15: $CONFIG\_LP \equiv (s, d_i')$
16: $CALCULATE\_ENERGY(s, d_i')$
17: **end if**
18: **end if**
19: **else**
20: $UPDATE(D_s') = D_s' \backslash d_i'$
21: **end if**

Figure 5.1: The pseudo code for the proposed algorithm

The proposed algorithm assumes an *anycast* request that follows the Poisson distribution for the source and destination pairs (s, D_s). A bit-error rate (BER) of 10^{-12} and a zero (0) propagation delay are assigned to initialize the network element vector (NEV).

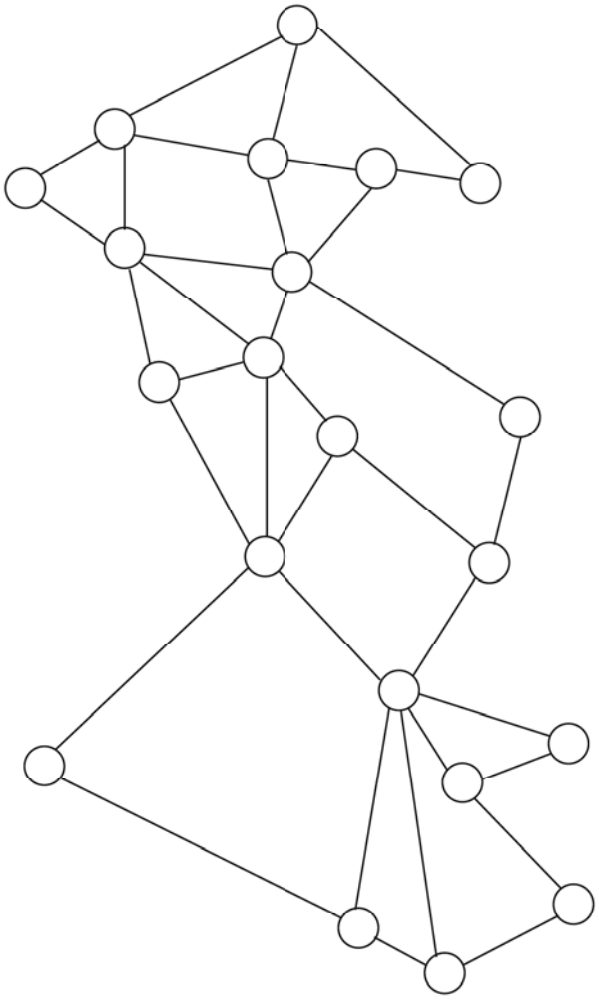

Figure 5.2: The Italian Mesh Network topology

The destination set (D_s) is arranged according to the shortest widest-path (SWP). The shortest destination is selected from the set and a route is computed. The NEV for the route is computed if all intermediate nodes are available. If the BER and the propagation delay are above the set threshold, the request is dropped to guarantee an acceptable QoS. If one or more of the intermediate nodes belongs to a cluster that is in the OFF state, a new destination is chosen. The selection is repeated with a modified destination set ($D_s^{'} \backslash d_i^{'}$) until a suitable destination is found. If any destination cannot be accessed, i.e. ($|D_s'| = 0$), then the request is discarded.

The proposed algorithm is validated by the aid of simulations. Figure 5.2 shows the topology of the Italian Mesh Network (IMnet) that is considered for simulation in our study. The IMnet topology consists of 36 bidirectional links and 21 nodes.

We consider a bit rate of 10 Gbit/s and assume that there are no wavelength converters and regenerators in the network. Connection requests follow a Poisson process and we consider the incorporation of EDFAs placed at 70 km intervals.

In our study, we partition the IMnet topology into four disjoint clusters. The proposed disjoint clusters are, C_A={1,2,3,4,5}, C_B={6,7,8,11,14,12,10}, C_C={9,13,15,19,20,16}, C_D={17,18,21,20}. A discrete-event model is used for our simulations, and 10^5 requests are considered for a given network load.

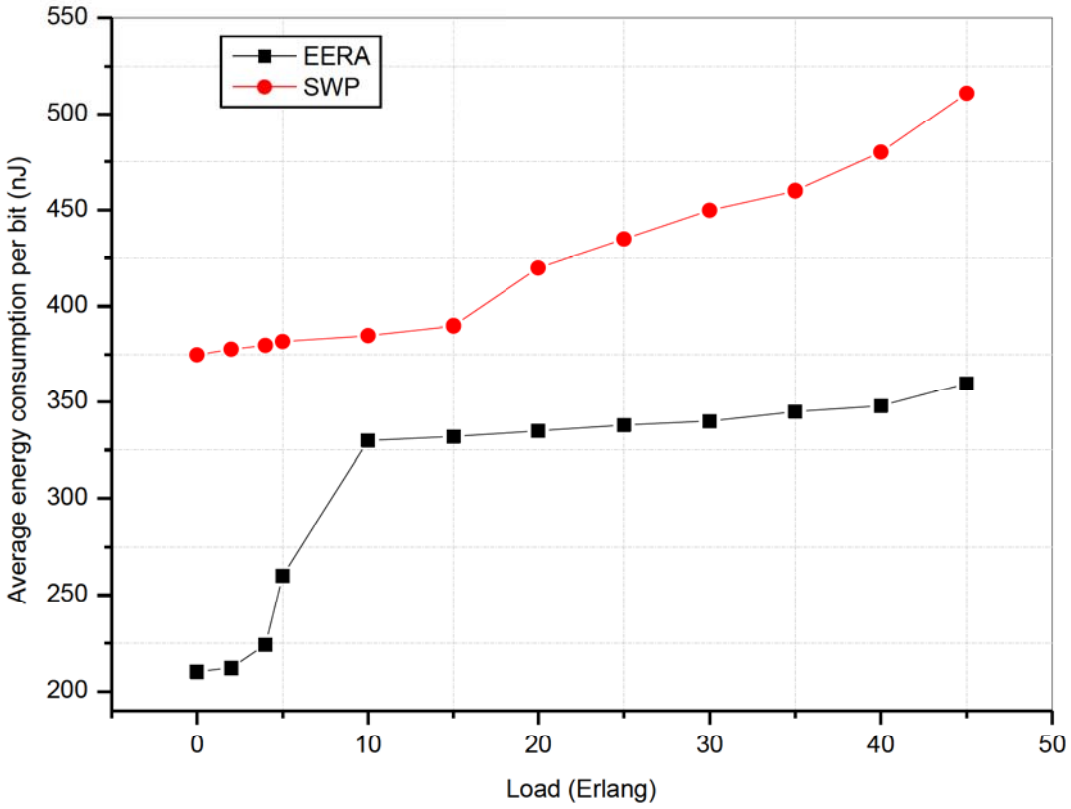

Figure 5.3: Relationship between average energy consumption per bit with network load for different clusters

Figure 5.3 shows the average power consumed per each request for various network loads under different cluster modes. The average power consumed for each given request is found

by obtaining the product of the average energy consumed per request and the bit rate. If all clusters are ON, it is observed that the energy consumption is considerably high. This scenario arises when the network does not incorporate sleep modes in its operations. Furthermore, we note that the average power consumed for a particular network load significantly declines when the clusters are in the sleep mode. Nonetheless, the reduction in energy consumption is at the expense of increasing the blocking probability that may lead to unacceptable Q-factor levels (shown in Figure 5.4). In order to address this challenge, careful consideration of all the pertinent parameters is important so as to strike a balance between the QoS and energy consumption in the networks.

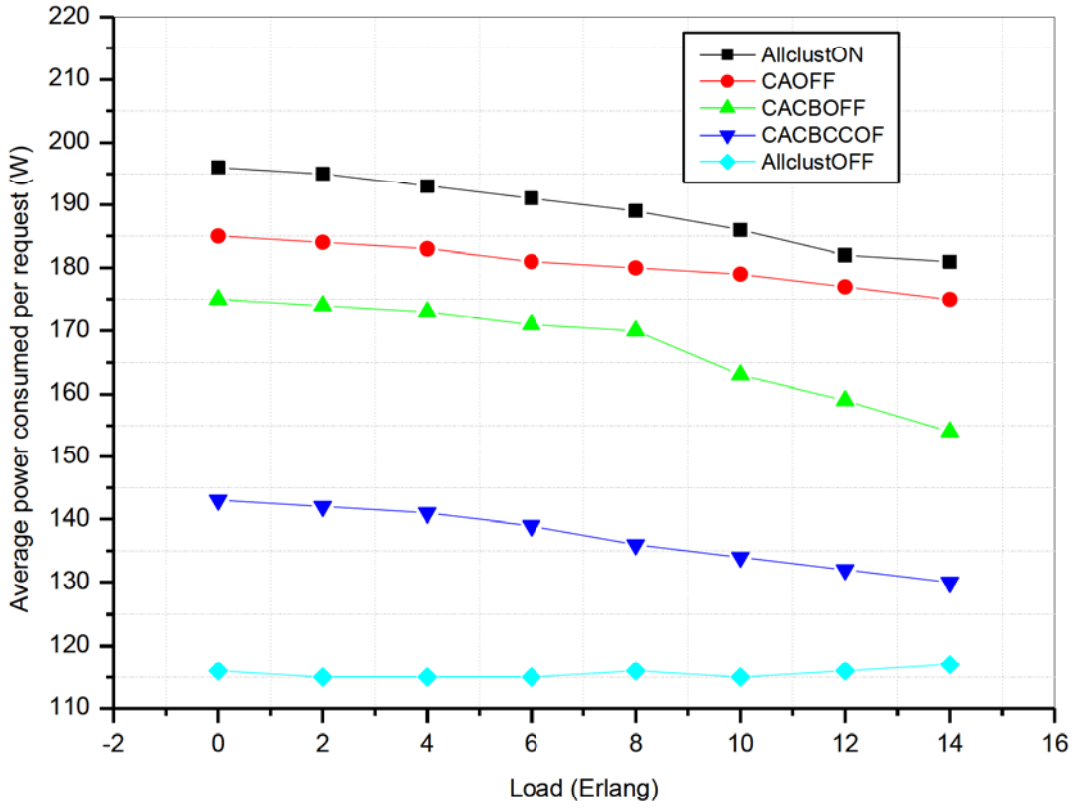

Figure 5.4: Average power consumed per request versus network load for various clusters

In Figure 5.5, the relationship between the average blocking probability and network load for various clusters under different modes is presented. A request may be blocked or lost when either, a wavelength is unavailable or because the network resources are in the sleep mode. It

is observed that the average blocking probability is low when all the clusters are in the ON state. This may be attributed to the fact that, the blocked requests arise only due to the unavailability of vacant wavelengths. When the entire network is in the sleep mode, the blocking probability is unacceptably high. This occurs because the majority of the requests have intermediate nodes that belong to clusters that are in the OFF state. A few calls that exist in the network are due to single hop requests.

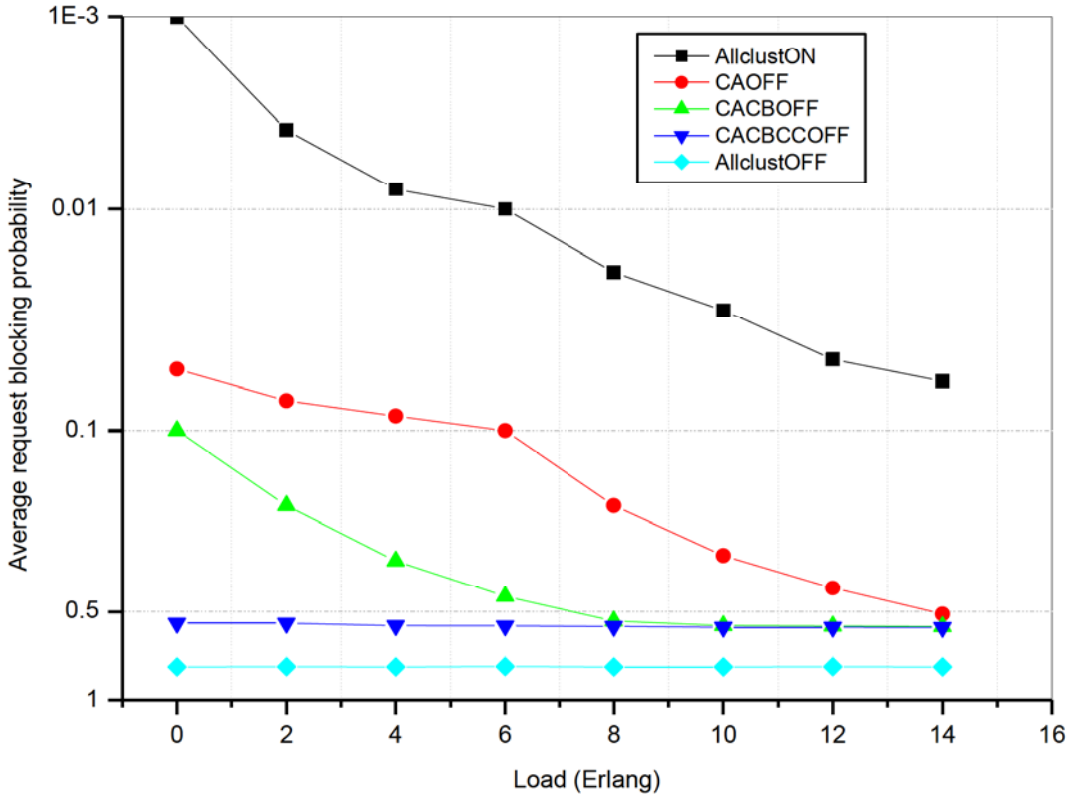

Figure 5.5: Variation of blocking probability for different cluster states with network load

5.3 Energy efficient dynamic sleep cycles

We propose a dynamic sleep cycle algorithm in which the network nodes switch between the ON and OFF states according to the volume of traffic traversing the network. A delicate balance is sought between network energy consumption and QoS provisioning. We argue and predict that in our proposal, a substantial amount of energy may be saved, while guaranteeing accepatable QoS within the network.

This will in turn lead to lower GHG emissions and thus a reduction in the overall carbon footprint of backbone optical networks. We assume that when the nodes enter into the *sleep mode,* they will still be capable of receiving and transmitting signals, but lack routing capabilities. In addition, the nodes should be able to monitor any traffic flowing through them, regardless of their mode. A threshold Q-factor value is set such that if the effective Q-factor of the network is above the set threshold, some of the nodes are triggered to enter the sleep mode, subject to their location and traffic flow. Furthermore, a mode that has only one adjacent node may not enter the sleep mode. If the Q-factor falls below the set threshold, the last node to enter the sleep mode wakes up to maintain an acceptable QoS (figure 5.6).

5.3.1 Simulation setup

An anycasting routing paradigm that enables the flow of traffic in the least number of hops is considered in the simulations. We consider simulations based on the IMNet topology and all nodes are assumed to be connected. The network is presumed to run at 10 Gb/s, and additionally, 64 payload channels and 2 control channels are considered.

We also assume that the traffic follows a Poisson distribution and traffic generation at the nodes is considered asymmetric. A Q-factor threshold of 7 is considered and the traffic monitoring period is taken to be 0.2 seconds.

5.3.2 Algorithm performance evaluation

The proposed energy-efficient algorithm leads to substantial energy savings as clearly depicted in Figure 5.7. On the other hand, the classic algorithm does not offer any energy savings since all the network resources are always active, regardless of the prevailing network load scenario. At full network load, it can be observed that the energy-efficient algorithm offers no energy savings. This arises precisely due to the decline of the overall network Q-factor such that, its value falls below the preset threshold. If the Q-factor declines below the threshold, a very limited number of nodes may be triggered to enter the sleep mode, and resultantly, the energy consumption of the network resources increases.

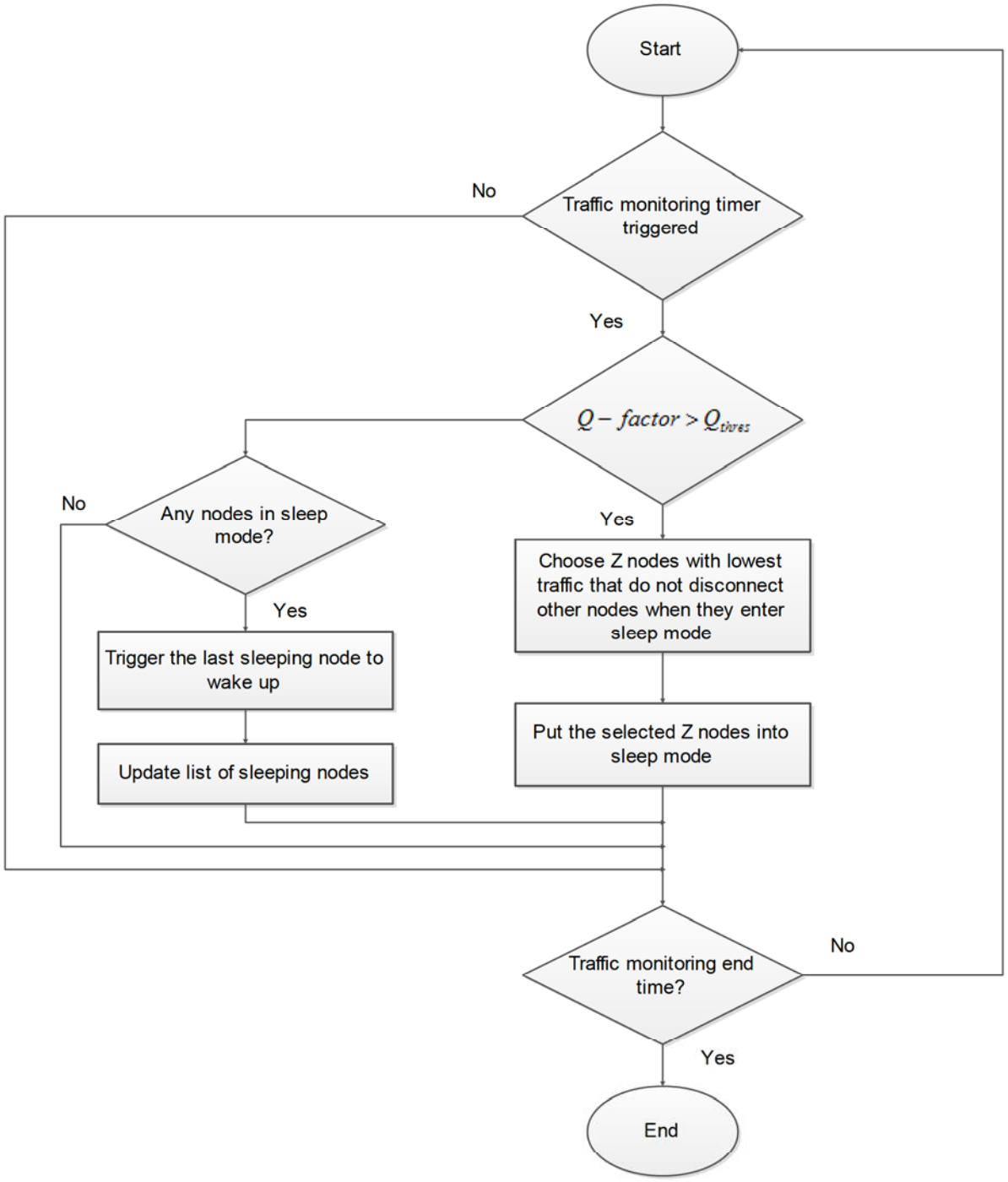

Figure 5.6: Flowchart for the energy efficient dynamic sleep cycles algorithm

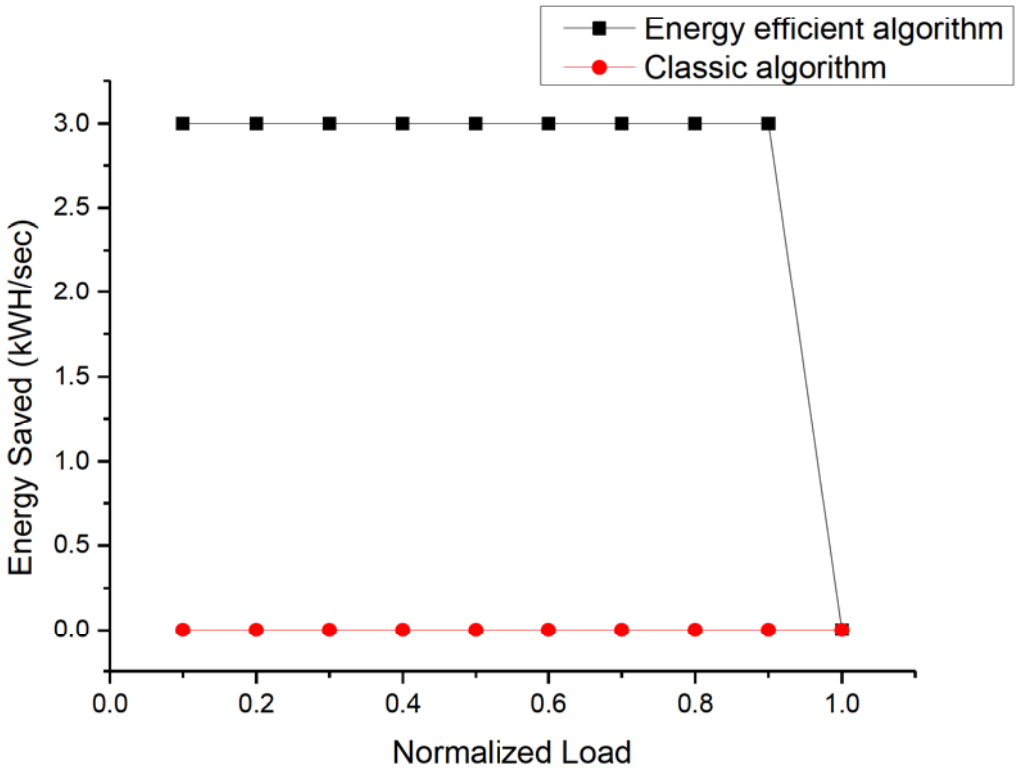

Figure 5.7: Relationship between energy saved and normalized load.

Figure 5.8 shows the blocking rates of both the classic algorithm and the proposed energy-efficient algorithm for various network loads. The blocking rates are almost the same for both algorithms at low and high network loads. Although some of the nodes enter the sleep mode at low network intensity in accordance with the proposed energy-efficient algorithm, the blocking probability is not seriously compromised due to sufficiently low congestion that characterises such network loads. At sufficiently high network loads (>0.95), the blocking rate is almost the same in both algorithms because the Q-factor falls below the set threshold and thus all nodes will be triggered to enter the "ON" state. The downside of the energy-efficient algorithm is clearly evident for network loads that fall in the range 0.25 to 0.9. This is attributed to the relatively high levels of congestion that arise due to the entrance of some of the nodes into the sleep mode, and thus the high blocking rates.

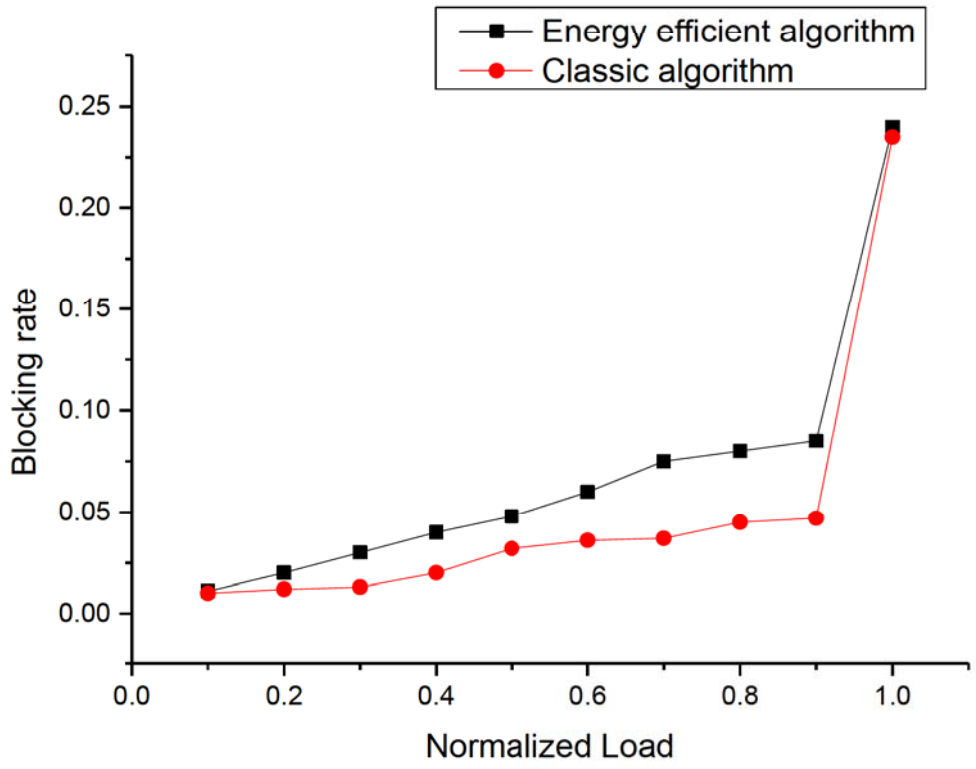

Figure 5.8: Blocking rate versus normalized load for different algorithms.

As shown in figure 5.9, it is revealed that the amount of energy saved is the same for various Q-factor threshold values at low network loads (0.3 and less). On the other hand, at high network loads (0.45 to 0.9), there is a significant reduction in energy savings as the Q-factor threshold values increase. This emanates from the fact that very few nodes will be triggered to enter the sleep mode at high Q-factor threshold values, and thus more energy is expended by the network resources.

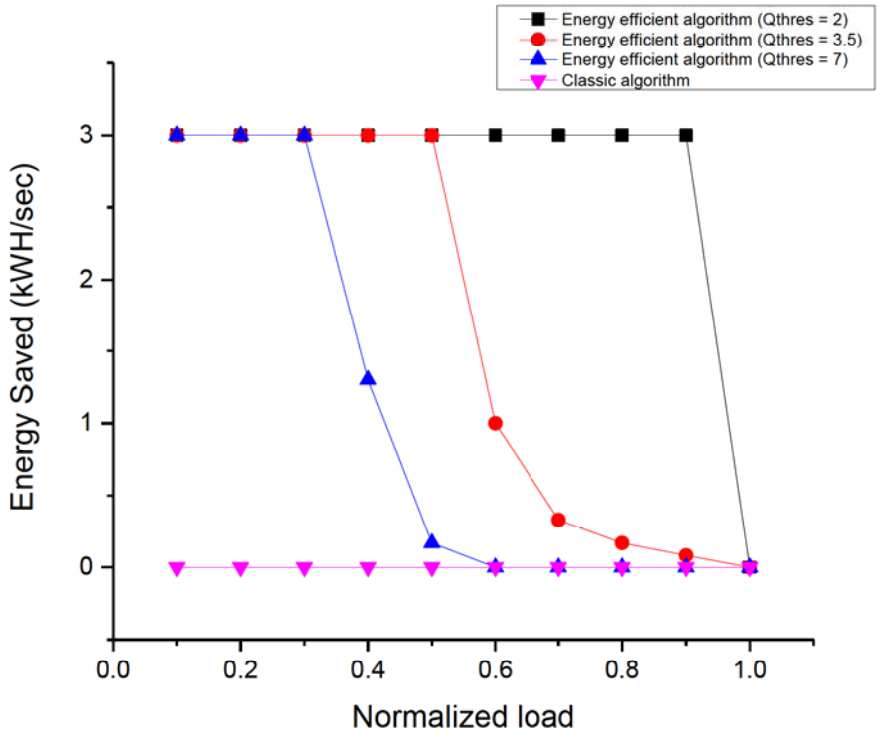

Figure 5.9: Relationship between energy saved and normalized load.

5.4 Optimized Energy-Aware Lightpath Routing Strategy (OEA-LR)

5.4.1 Introduction

A novel energy-aware routing approach is proposed that is utilized to study the effects of energy optimization on pertinent network performance metrics. In our proposal, we assume that a transparent WDM network is comprised of OXCs, EDFAs, transceivers, and various fibre link lengths. We further assume that connection requests from source to destination are entirely provisioned in the all-optical domain, thus OEOs are not present.

5.4.2 The OEA-LR Approach

The OEA-LR approach is premised on the assumption that the energy required to establish a connection request is equal to the summation of: the energy required for optical switching at

intermediate nodes, the energy consumed by the transceivers, and the EDFAs energy consumption along each fibre link. The net energy consumption of the network is therefore equivalent to the sum of the energy used by all presently provisioned connection requests at any specific moment. Furthermore, the OEA-LR is anchored on the modification of the $k-shortest$ path algorithm presented in [212].

Using the OEA-LR approach, up to $k-shortest$ paths are calculated when a connection request is received, and the algorithm takes into cognizance the link-state in its search for a candidate lightpath route. Thus, fibre links that do not possess available wavelengths at any given instance are deleted from the logical topology on a temporary basis. During the computation of each candidate lightpath, each link (l) is assigned a cost (C_l) that is calculated as follows:

$$C_l = \begin{cases} \gamma . E_l, & when\ fibre\ link\ is\ in\ use \\ E_l, & when\ fibre\ link\ is\ not\ in\ use \end{cases} \tag{5.4}$$

Where, E_l is the total energy consumption required to operate all amplifiers on the fibre link l, and γ is a weighting factor whose values lie between 0 and 1, and it indicates the extent of energy savings in the OEA-LR. If the value of γ is equal to 0, the OEA-LR behaves like a pure energy saving approach, whereas for the values of γ equal to or close to 1, the OEA-LR appears to provision connection requests according to shorter routes. Since EDFAs are deployed after every 80 km, it may be assumed that their numbers are proportional to the length of the route under study. By varying the values of γ between 0 and 1, both energy usage and resource utilization are optimized. If a candidate path is found, the FFwO approach is utilized to search for an available wavelength along the path. If a free wavelength is not found among the k-paths, or there is no existence of a candidate path, blocking of the connection request occurs.

5.4.3 Evaluation of the OEA-LR Approach

The proposed OEA-LR approach is evaluated via simulations of the Pan-European and the NSFNET network topologies. The considered Pan-European network comprises 11 nodes and 26 bidirectional fibre links, and the NSFNET topology is made up of 14 nodes and 21

bidirectional fibre links. It is further assumed that each fibre link is capable of carrying a maximum of 16 wavelengths, and that there is no wavelength conversion in the network. Furthermore, the source-destination pairs of the connection requests are uniformly selected among the network nodes, and the connection request arrivals follow a Poisson distribution and the holding time per connection is distributed exponentially.

The following assumptions are made for the energy consumption of the network devices:

i. EDFAs, OXCs and transceivers can be instantly ordered to enter into sleep mode or switched-on depending on the traffic conditions. In addition, it also assumed that no additional energy is expended during the transitions from sleep mode to switched-on mode, and vice-versa.
ii. Each EDFA consumes 12 W of power and the distance between consecutive EDFAs is 80 km.
iii. Each transceiver uses 7 W of power at 10 Gbps.
iv. An OXC consumes 6.4 W of power.

Our results are obtained by further assuming that the weighting factor γ lies between 10^{-4} and 1, and a maximum of k is equal to 3 candidate paths are calculated for each connection request.

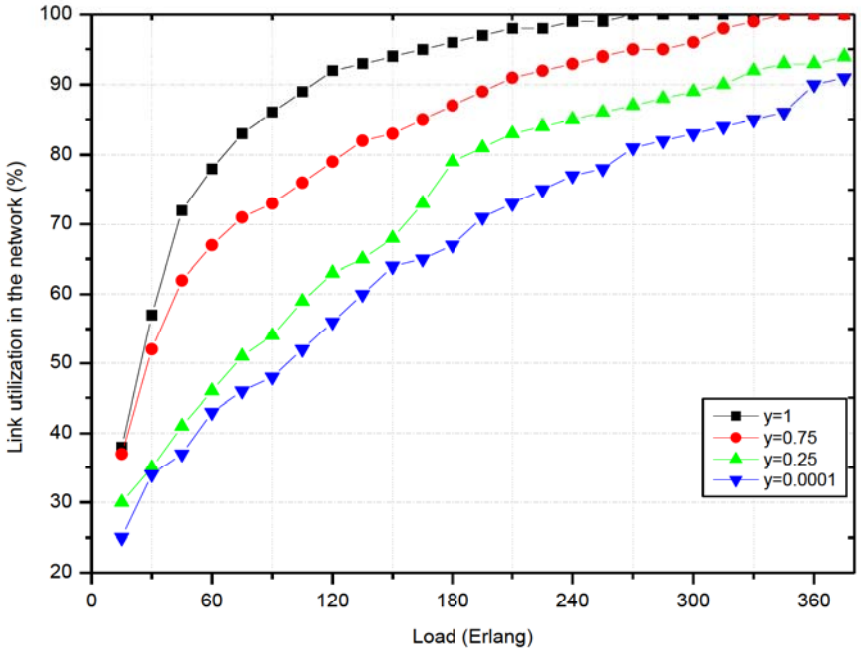

Figure 5.10: Relationship between link utilization and traffic load

Figure 5.10 shows the relationship between link utilization and traffic load for the Pan-European network. The results show that when the OEA-LR approach bases its decisions only on minimizing the lengths of provisioned lightpaths, the fibre links usage drastically increases with increasing traffic load. This behaviour is logically expected and acceptable since the routing strategy does not take into account the energy status of the network elements, but is solely based on ensuring the provisioning of connection requests of shortest available path at values of γ close to or equal to 1. On the other hand, when γ is close to 0, the OEA-LR strategy attempts to minimize the energy consumption in the network by limiting the number of devices to be energized. As a result, the fibre link utilization grows almost in a linear fashion as the load increases. This implies that a significant number of fibre links will remain unused, hence the presence of fewer energy-consuming elements in the network. Consequently, under these conditions, significant amount of energy will be saved in the network. Figure 5.11 shows the variation of potential energy savings and network traffic load. It can be observed that massive amounts of energy may be saved ($\approx 50\%$) at sufficiently low values of γ ($\gamma = 0.0001$). On the other hand, if γ is high (≥ 0.75), very little or no energy is saved in the network.

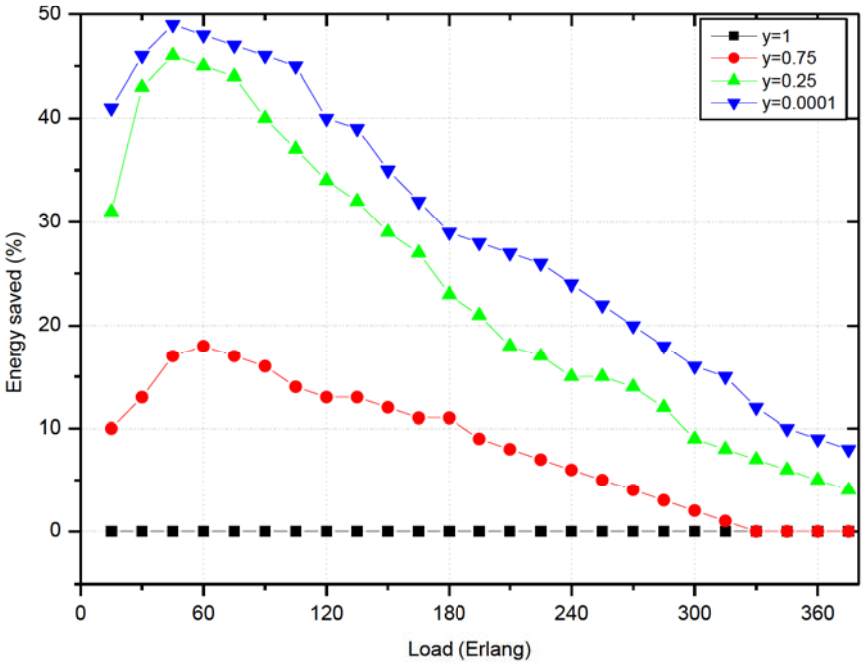

Figure 5.11: Relationship between saved energy and traffic load

Once again, this emphasizes the effectiveness of our proposed OEA-LR approach in realizing energy efficiency in optical networks.

Figures 5.12 and 5.13 present the relationship between average path length and traffic load for various values of γ for the NSFNET topology. In figure 5.12, the number of hops are presented as a function the network load, whereas in figure 5.13, the physical distance values are given as a function of the network load.

The results show that the use of the energy-aware routing strategy leads to higher average path lengths compared to the approach where energy awareness is not taken into account. These results confirm our expectation that, if path lengths are long, there is a likelihood that the network resources will be optimally utilized since traffic tend to traverse through already powered-on devices in the network. It can be clearly seen that the mean path length increase is capped at about 7% for γ values between 0.75 and 1, and thus a considerably acceptable increment in path length, bearing in mind the significant energy savings realized. However, there is need to trade-off the energy savings gains achieved through increased path lengths on one hand, and the transmitted signal quality on the other hand.

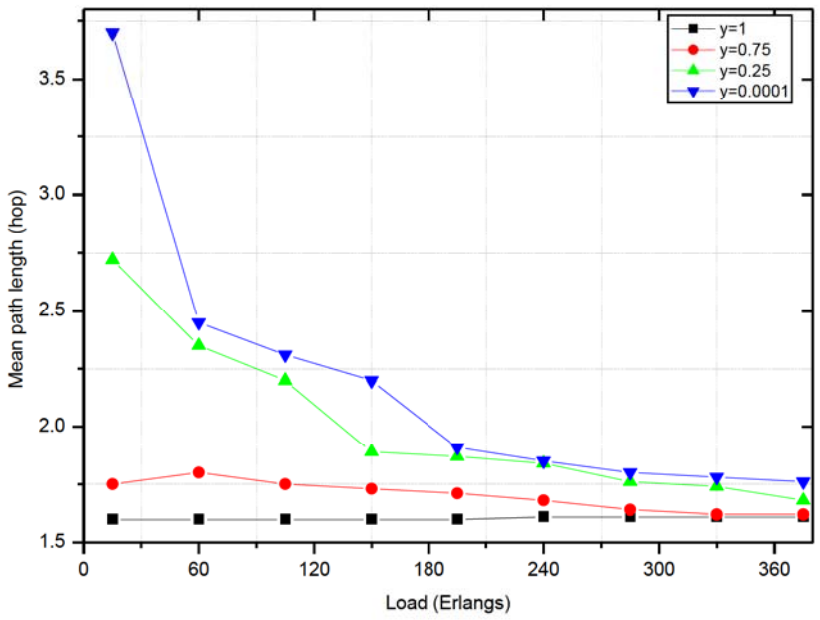

Figure 5.12: Relationship between mean path length (in hops) and traffic load

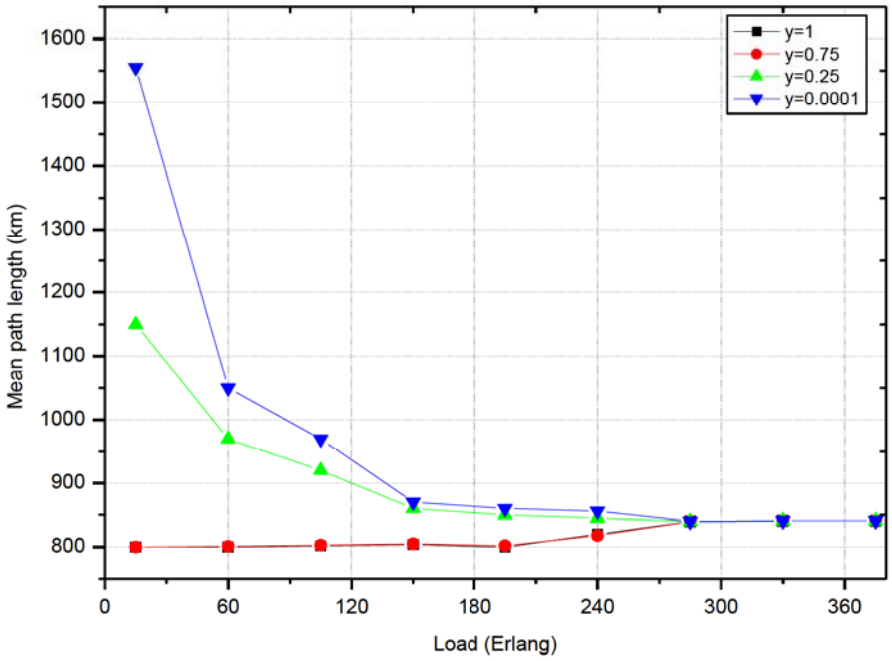

Figure 5.13: Relationship between mean path length (in km) and traffic load

In summary, a novel OEA-LR approach is presented that simultaneously considers both energy minimization and resource utilization as a unitary cost function. The results from the simulations confirm the competitive edge of the approach in terms of both energy and network utilization efficiencies. However, it is noted that care must be taken so as to strike a healthy balance between energy savings and signal quality.

5.5 Energy-efficient protection scheme subject to traffic variations

The 1+1 dedicated path protection scheme is still arguably the most widely deployed protection scheme in operational optical networks. This protection scheme is attractive mainly due to its unrivaled high availability and resilience. On the other hand, the 1+1 dedicated path protection scheme consumes substantial amounts of energy compared with networks where protection is not offered. In our work, we propose a protection scheme that takes cognisance of the traffic variations and thus attempt to reduce energy consumption of dedicated protection paths. Our proposed scheme focuses only on the protection path and traffic routing along the protection path is adapted to the prevailing bandwidth requirements.

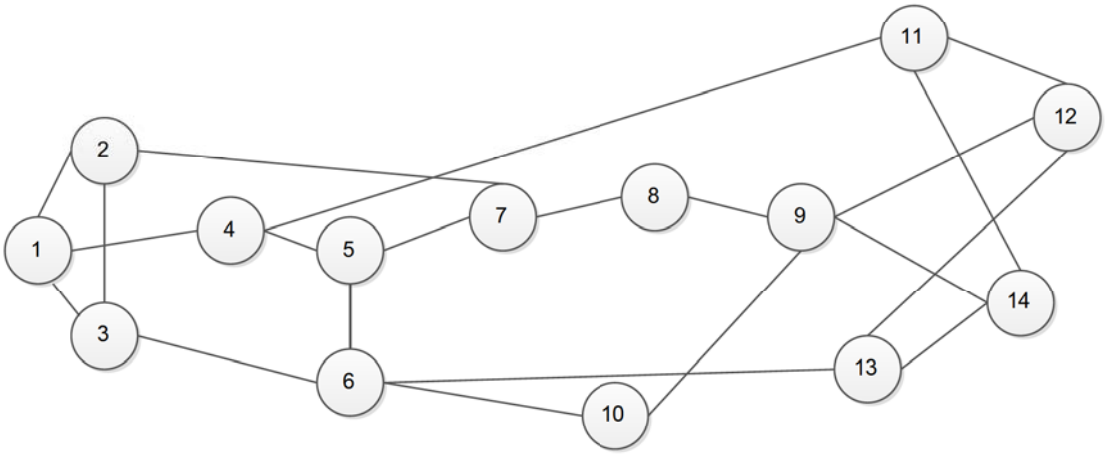

Figure 5.14: The NSFNET network topology

We consider the NSFNET network to evaluate the model (figure 5.14). The NSFNET network is comprised of 21 bidirectional links and 14 nodes. Since the NSFNET covers four different U.S. time zones, in our studies, we focused only on the Eastern Standard Time (EST), and Figure 5.15 shows the variation of normalized bandwidth with time on a typical day. We further assume that the traffic demand is random. Table 5.1 shows the input data for our simulations.

Table 5.1: Input simulation information

Parameter	**Unit**
Distance between adjacent EDFAs	80 km
Power consumed by an EDFA	8 W
Power consumed by a router port (40 Gb/s)	1 kW
Power consumed by a transponder (10 Gb/s)	45 W
Power consumed by a transponder (40 Gb/s)	73 W
Power consumed by a transponder (100 Gb/s)	135 W

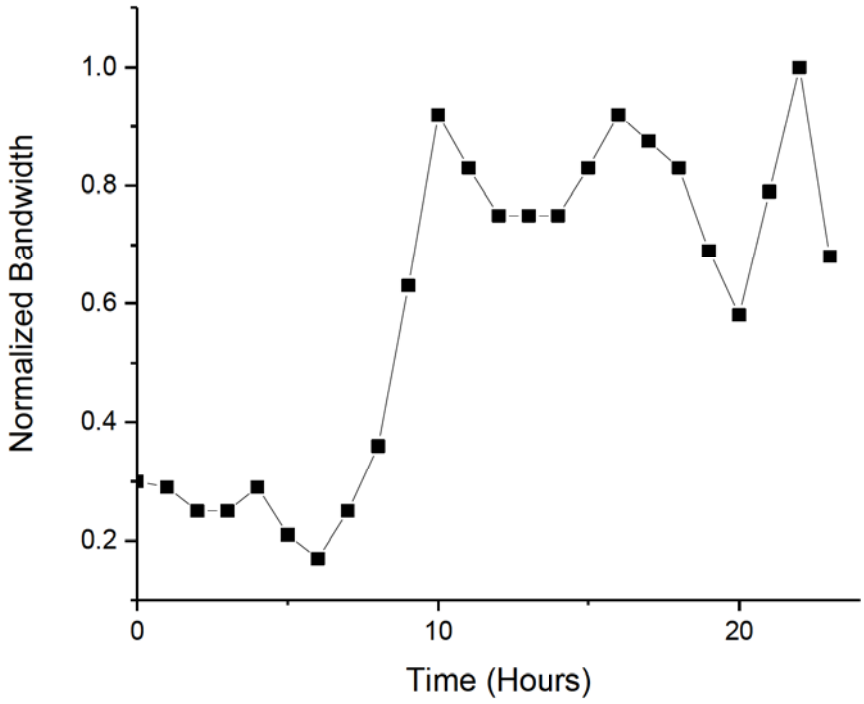

Figure 5.15: Bandwidth variation with time for the NSFNET EST time

5.5.1 Algorithm

We commence with the peak-rate traffic scenario where demands between source-destination pair nodes require continuously varying bandwidth throughout the day. The bandwidth demands are then fulfilled in a descending order and energy-aware scheme takes care of the routing and resource allocation in accordance with peak-rate traffic values.

Algorithm 5.1 shows that immediately after the working and protection paths have been chosen for all the traffic demands, the total peak power consumption will then be computed. It is assumed that the working path remains active and unaffected by the status of the backup path. As for the protection path, the status of transmission is adapted to the prevailing traffic situation, such that, some of the network resources may be deactivated during low traffic flow.

Algorithm 5.1: Energy-efficient protection scheme

STEP 1: Allocation of resources for 1+1 protection scheme:

Arrange the demands list (DL) in descending order of required bandwidth

While $DL \neq \emptyset$ **do**

Valuate resource allocation in working and protection path for each demand for its peak value;

end while

$Total\ peak\ power\ consumption = P_{Tx} + P_{EDFA} + P_{OXC} + P_{Rx}$

STEP 2: Adaption of protection path to hourly traffic demands

for all hourly traffic values during the day **do**

for all active demands **do**

Adapt protection path transponders rate to prevailing traffic demand;

Calculate energy savings compared to $Total\ peak\ power\ consumption$;

end for

end for

Figure 5.16 shows the energy saved (%) for the proposed energy-efficient dedicated path protection path 1+1 scheme in comparison with the classic 1+1 scheme for a typical day of the NSFNET topology at different traffic rates. It can be seen that at high data rates (100 Gb/s), significant amount of energy is saved, especially at off-peak periods where up to 29 % of savings are realized. This implies that the proposed algorithm is perfectly suited to be implemented in high speed long haul transparent optical networks. The implementation of the algorithm in such networks will undoubtedly reduce the amount of energy consumed, and thus lower the overall carbon footprint of telecommunication networks.

5.6 Energy efficiency through the utilization of solar energy sources

One novel way of realizing the dream of energy efficient and truly "green" optical networks is to utilize solar energy to power network devices. This will certainly reduce the carbon footprint of optical communication networks and thereby curtailing the overreliance on non-renewable energy sources. With the emergence of the concept of SGs, the use of renewable energy sources in telecommunication networks would be greatly enhanced.

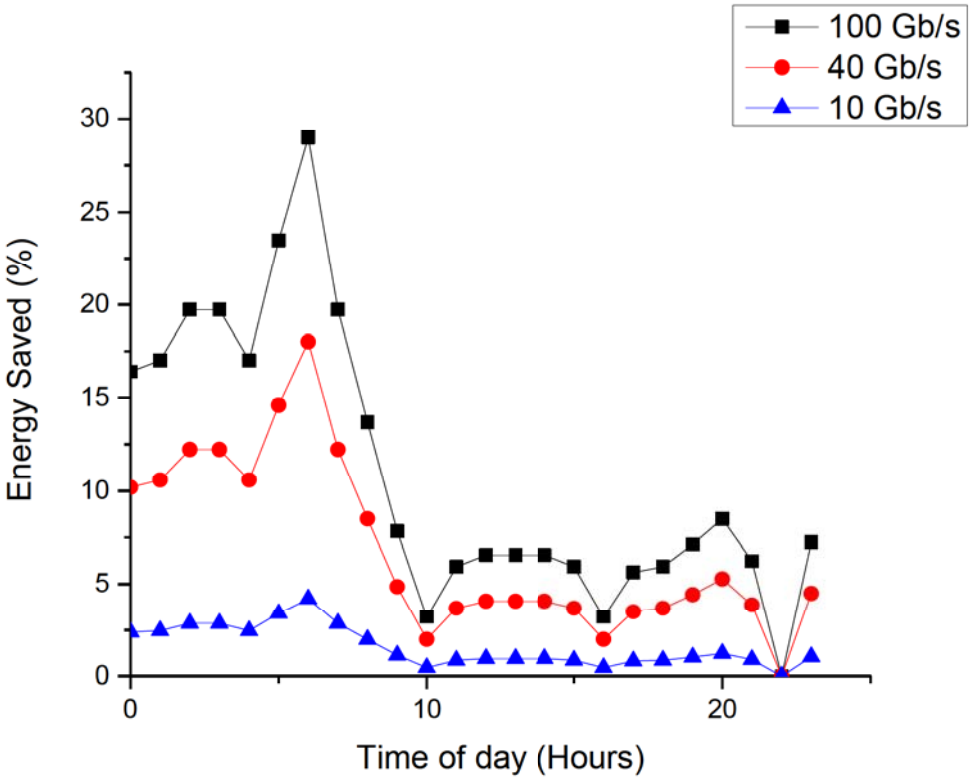

Figure 5.16: Energy saved (%) with respect to the classic 1+1 dedicated path protection scheme for different traffic rates.

5.6.1 The Energy Model

It is essential to come up with a model that estimates the non-renewable energy consumption of a given network so as to evaluate the impact of utilizing solar energy sources. We assume that there are two components of energy consumption for each network node. These components are respectively, (i) the static and (ii) dynamic energy consumptions. The static energy consumption arises due to the energy required to keep the network devices powered on, and it is independent of the network traffic. On the other hand, the dynamic energy consumption component depends on the volume of traffic through the node. We further propose that nodes that have access to solar energy sources should give precedence to the use of solar energy in connections set up and may only utilize non-renewable sources when the solar energy sources are either depleted or unavailable. Conversely, those nodes that are not connected to solar energy sources should use non-renewable sources for new connection set up. For a lightpath p, the consumption of non-renewable energy is given by:

$$C_p = \left[\sum_{n\epsilon p} e_n b_p \tau_n + \sum_{n\epsilon p} \frac{L_i}{k} r_n b_p \tau_n + \sum_{i\epsilon p} \frac{e_i L_i}{w_i \theta_{OA}}\right] t_p \quad (5.5)$$

with $\tau_n = 0$ $(solar\ energy\ source\ utilized\ for\ connection)$

$\tau_n = 1$ $(non - renewable\ energy\ source\ utilized\ for\ connection)$

Where, e_n is the energy consumption per Gbps for the traffic passing through node n, b_p is the path bandwidth measured in Gbps, τ_n is a constant that indicates the part of energy consumption to be either incorporated or not, L_i is the link length, k is the maximum allowed link length without signal regeneration, r_n is the energy consumption per Gbps during regeneration, e_i is the energy consumption of an optical amplifier on link i, w_i is the number of wavelengths used on link i, θ_{OA} is the maximum allowed link length without amplification, and t_p is the connection duration time.

It is important to note that the static component of the node energy consumption is not included in the formula for simplicity.

5.6.2 Model Implementation

OPNET event-driven simulator is implemented to the proposed networking environment. Our model takes use of the SWP in its routing decision-making process, and employs resource reservation protocol for signaling. The USNET network topology is used to evaluate the impact of deploying solar energy sources in the network (Figure 5.17). The network is assumed to comprise of OXCs as nodes and links with EDFAs placed at 80 km intervals. We further assume that 16 wavelengths are assigned to each link and the connection requests follow a Poisson distribution. The average traffic load per node is obtained from the duration of the connection and the inter-arrival rate and is varied from 2 to 12 Erlangs.

It is important to note that the solar energy availability is related to the geographic location of the nodes and it varies during the day in the USNET topology. The USNET network consists of four time zones, and these are, Eastern Standard Time (EST), Mountain Standard Time (MST), Central Standard Time (CST) and Pacific Standard Time (PST). Furthermore, the USNET network is made up of 24 nodes and 43 bidirectional links. In our studies, we utilize the EST as our reference time.

Figure 5.18 shows the variation of solar energy availability with EST time on a typical sunny day in June.

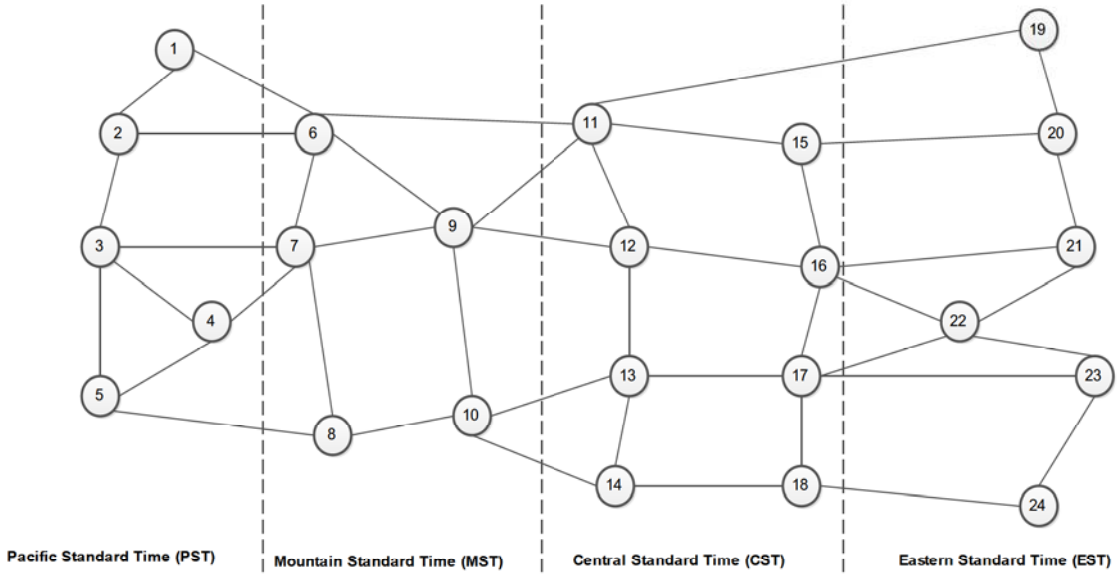

Figure 5.17: The USNET network topology

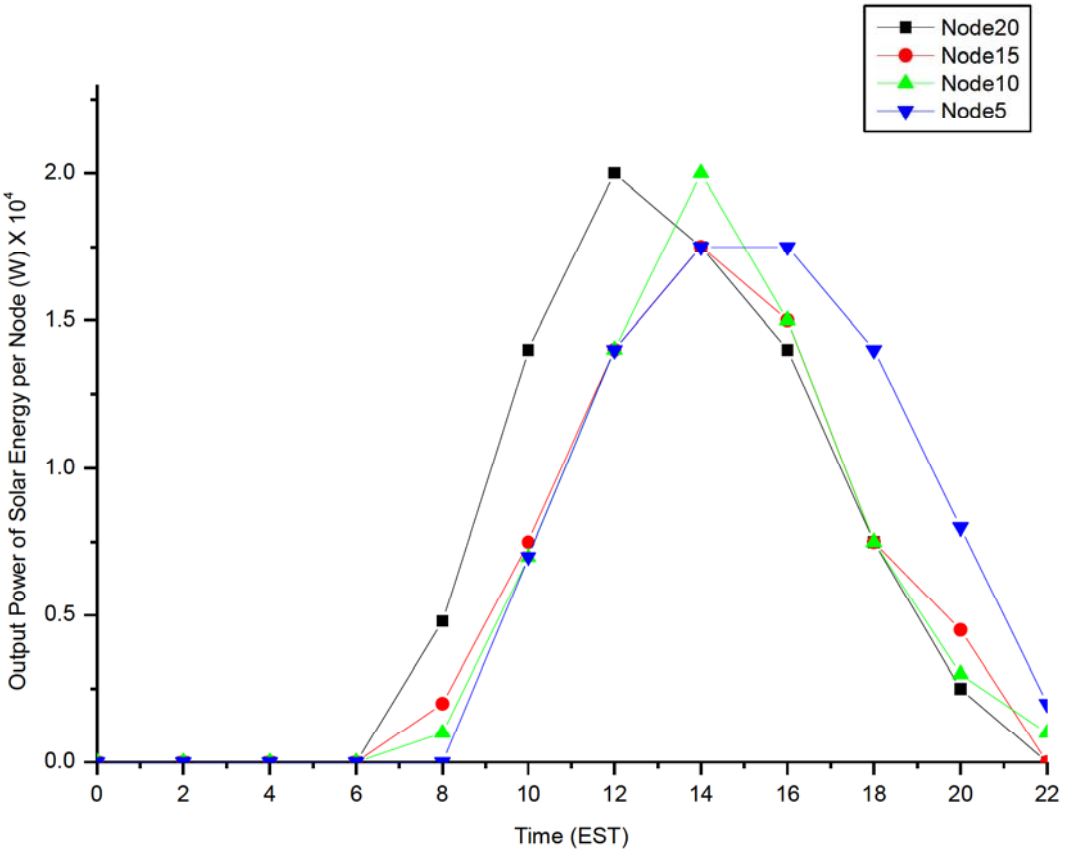

Figure 5.18: Availability of solar power against EST time

In our model, we take solar energy to be the alternative source to the traditional power source for powering the network, and assume a maximum solar energy output of 20 kW that requires a total solar cell area of approximately 100 m^2 (table 5.2) [213].

Table 5.2: Available solar power at each node in the USNET network

EST / Time / Node ID		0:00	2:00	4:00	6:00	8:00	10:00	12:00	14:00	16:00	18:00	20:00	22:00
		Power (kW)											
1	SR:5:12 SS: 21:09	0	0	0	0	0	6	13	18	18	13	8	4
2	SR:5:27 SS: 21:01	0	0	0	0	0	6	13	18	18	13	8	4
3	SR:5:44 SS: 20:10	0	0	0	0	0	6	13	18	18	13	8	2
4	SR:5:56 SS: 21:02	0	0	0	0	0	6	13	18	18	13	8	4
5	SR:5:42 SS: 20:08	0	0	0	0	0	6	13	18	18	13	8	2
6	SR:5:47 SS: 20:47	0	0	0	0	0.5	6	13	20	18	13	8	0.6
7	SR:5:57 SS: 21:01	0	0	0	0	0	6	13	20	18	13	8	3
8	SR:5:18 SS: 19:34	0	0	0	0	0.8	6	13	20	15	8	3	0
9	SR:5:32 SS: 20:31	0	0	0	0	0.5	6	13	20	15	8	3	0.8
10	SR:6:01 SS: 20:17	0	0	0	0	0	6	18	20	15	8	2	0.5
11	SR:5:55 SS: 21:02	0	0	0	0	0.5	8	13	18	15	8	5	0
12	SR:6:12 SS: 21:06	0	0	0	0	0.6	8	13	18	15	8	5	0
13	SR:6:13 SS: 20:46	0	0	0	0	0.5	8	13	18	15	8	4	0
14	SR:6:35 SS: 20:37	0	0	0	0	0.5	8	13	18	15	8	4	0
15	SR:5:27 SS: 20:33	0	0	0	0	1.5	8	13	18	15	8	4	0
16	SR:5:46 SS: 20:18	0	0	0	0	1.3	8	13	18	15	8	4	0
17	SR:5:54 SS: 20:11	0	0	0	0	1	7	13	18	15	8	4	0
18	SR:6:00 SS: 20:04	0	0	0	0	1	7	13	18	15	8	4	0
19	SR:5:08 SS: 20:41	0	0	0	1.8	5	15	20	18	13	8	2	0
20	SR:5:14 SS: 20:31	0	0	0	1.5	5	15	20	18	13	8	2	0
21	SR:5:25 SS: 20:32	0	0	0	1	4.5	13	20	18	13	8	2	0
22	SR:5:43 SS: 20:38	0	0	0	0.8	4.3	13	20	18	13	8	2	0
23	SR:5:54 SS: 20:28	0	0	0	0	4	13	20	18	13	8	2	0
24	SR:6:19 SS: 20:34	0	0	0	0	4	13	20	18	13	8	2	0

(SR: Sunrise, SS: Sunset)

(Adapted from: [213])

We assume that nodes 2, 5, 6, 8, 19, 21 and 22 are randomly chosen to deploy solar energy sources. The total non-renewable power consumption is shown in Figure 5.19, assuming that the maximum available solar power per node is 20 kW. It can be observed that during the period when there is appreciable amounts of solar energy (between 06H00 and 22H00), the network traffic is generally high, and the optimized heuristic outshines the one where the nodes are switched on and off. Consequently, significant non-renewable power savings can be realized that have a peak of about 3000 kW.

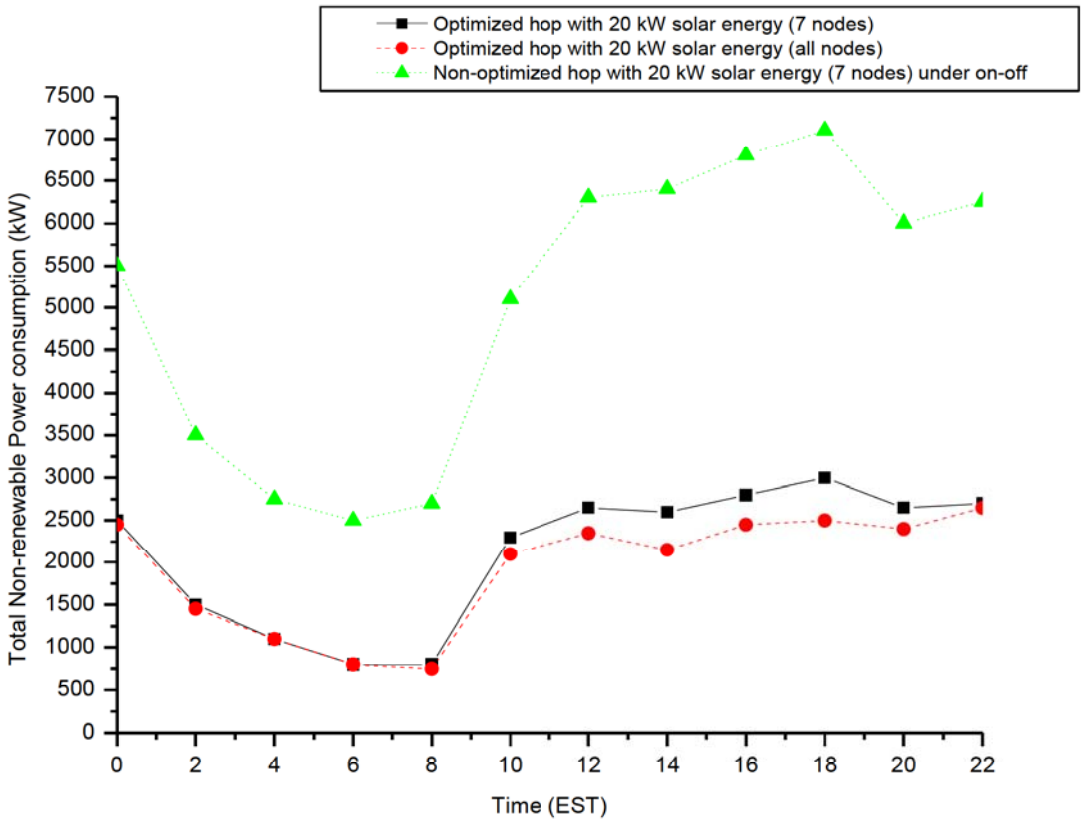

Figure 5.19: Relationship between consumption of non-renewable power with EST time

The effect of varying the maximum available solar power per node on the overall non-renewable energy consumption is captured in Figure 5.20. It is clearly evident that an increase in the maximum solar power output per node leads to an almost linear reduction in the total non-renewable energy consumed under different stated scenarios.

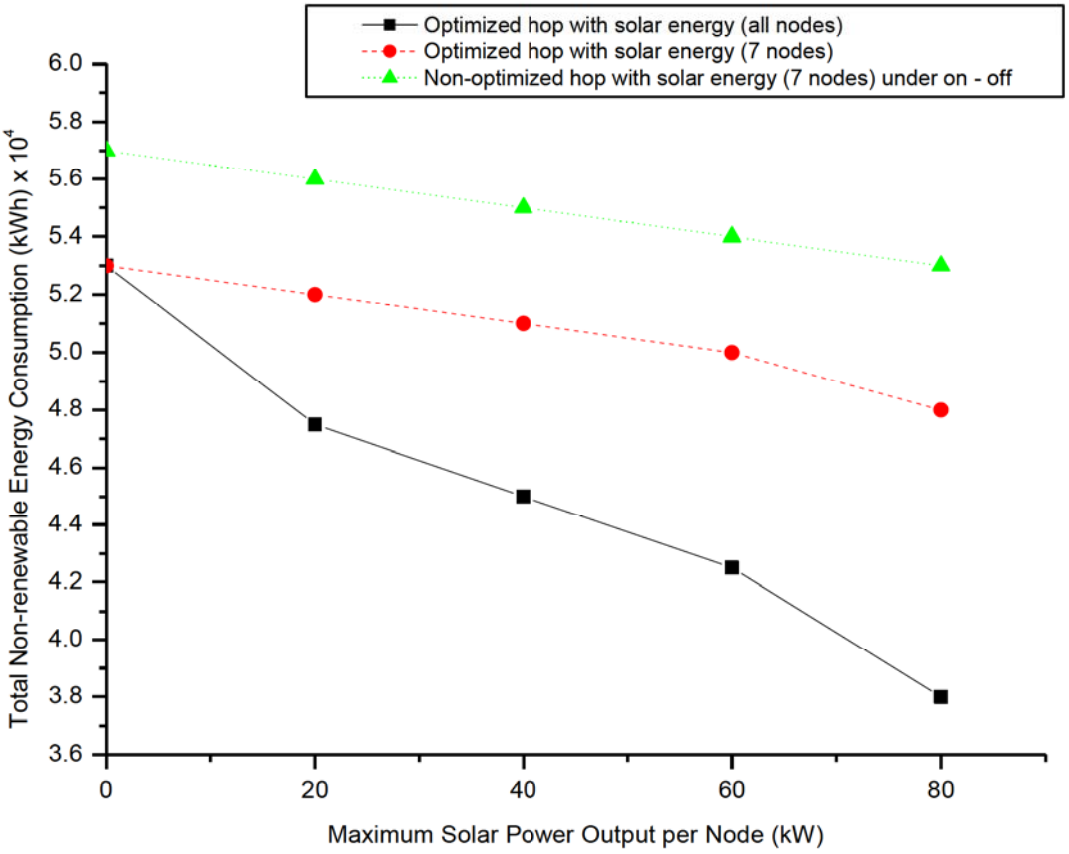

Figure 5.20: Variation of non-renewable energy consumption with solar power output

The deployment of nodes that are powered by both renewable and non-renewable energy sources appears to be very promising and will undoubtedly spearhead a revolutionary novel era in powering future high-speed telecommunication systems. It is clearly apparent that renewable energy sources will provide a platform for the realization of cheaper and cleaner next generation communication networks that will lower the overall GHG emission from telecommunication networks.

5.7 Mixed line rates (MLR) Networks

Since the traffic matrix of the core networks is now essentially heterogeneous, it therefore calls for the deployment of versatile techniques that are both responsive to the needs of the networks and energy-efficient as well. The rolling-out of MLR networks appear to be sensible choice since it will be possible to multiplex low data-rates connection requests onto high capacity wavelengths for high-speed requests through traffic grooming. In essence, the MLR network should be capable of handling different wavelengths on a link that transports different data rates such as 10 Gbps, 40 Gbps and 100 Gbps. In this work, we propose a transparent MLR network model that is energy-efficient, and we will compare its performance with that of existing translucent and opaque MLR networks.

5.7.1 Transparent Energy-efficient MLR Network Model

We present our problem of the design of a transparent energy-efficient MLR model. We propose that logical network connections will be mapped over physical links via multihoping in the networks. The following assumptions are made:

m and n represent the physical nodes in the network, and i and j represent the logical nodes in the virtual network topology, and s and d denote the source and destination nodes. We further propose the following input parameters:

1. $G(V, E)$ represents a physical topology with nodes set V and edges set E, and that each node router is connected to an OXC.
2. $T = [\Lambda_{sd}]$ indicates the traffic matrix forecast with demand Λ_{sd} between a source-destination pair.
3. $R = \phi_1, \phi_2, \ldots \phi_k$ represents the set of channel rates available.
4. W denotes the number of maximum wavelengths supported on a fibre, $\lambda \in \{1,2, \ldots W\}$.
5. E_{rk} is the energy cost of regenerator with rate ϕ_k.
6. E_{Rk} is the energy cost of a short reach transponder (SRT) with rate ϕ_k.
7. E_{amp} is the energy cost of an EDFA amplifier.
8. E_p is the energy cost of electronic processing.

To further describe our model, we introduce the following variables and parameters:

1. L_{mn} is the length of the fibre between nodes m and n.
2. A_{mn} is the number of amplifiers on a physical link (m and n).
3. P_{mn} is the set of lightpaths passing through the link (m and n).
4. F_{mn} is the variable that denotes the number of fibres on a link (m and n).
5. f_{ij}^{sd} denotes the volume of traffic from source to destination on lightpath (i, j).
6. Z_j is an integer that represents the amount of data that is transported by lightpaths that terminate at node j.

We also assume that there are no wavelength converters and that different line rates have different optical reaches. The model is further described by the use of the following parameters:

1. $l_{ijk\lambda}$ represents the lightpath between (i, j) node pair in the logical topology at rate ϕ_k over λ.
2. $\alpha_{ijk\lambda}$ stands for the feasibility of lightpath establishment for a given lightpath $l_{ijk\lambda}$ between $i\ and\ j$ nodes at rate ϕ_k for wavelength λ. The feasibility is based on the comparison with an acceptable preset threshold Q-factor.
3. $X_{ijk\lambda}$ is a variable that represents the number of lightpaths on link (i, j), and thus should be an integer.

Objective:

$$\text{Minimize}\quad 2\sum_{\lambda}\sum_{ij}\sum_{k} X_{ijk\lambda}.E_{rk} + \sum_{mn} A_{mn}.F_{mn}.E_a + \sum_{j} Z_j.E_p \qquad (5.6)$$

Subject to constraints presented below:

$$\sum_{\lambda}\sum_{k} \phi_k.X_{ijk\lambda}.\alpha_{ijk\lambda} \geq \sum_{sd} f_{ij}^{sd} \qquad \forall(i,j) \qquad (5.7)$$

$$\sum_{(i,j)\in P_{mn}} \sum_{k} X_{ijk\lambda} . \alpha_{ijk\lambda} \leq F_{mn} \qquad \forall (m,n), \ \forall \lambda \tag{5.8}$$

$$\sum_{i} f_{ij}^{sd} - \sum_{i} f_{ji}^{sd} = \begin{cases} \Lambda_{sd,} & if\ s = j \\ -\Lambda_{sd,} & if\ d = j \\ 0, & otherwise_{\forall j,\ \forall (s,d)} \end{cases} \tag{5.9}$$

$$Z_j = \sum_{sd} \sum_{i} f_{ij}^{sd} \qquad \forall_j \neq d \tag{5.10}$$

The above formulation apparently results in a mixed integer linear programming (MILP) set up. The objective function minimizes the usage of energy by the transparent MLR network. The first expression in equation (5.6) calculates the amount of overall energy consumption of WDM transponders, and the second term computes the energy consumption of all the EDFA amplifiers in the network. The parameter F_{mn} depicts the total number of required optical fibres to take care of the traffic requirements. The effective energy costs due to electronic components operations at intermediate nodes for all traffic volume is represented by the last term in equation (5.6).

We propose the SWP algorithm to determine the physical routes to be taken. The constraints due to capacity that hinder the traffic demands per logical link (i, j) are represented by equation (5.7). The wavelength-continuity constraint is represented by equation (5.8), whereby it is ensured that only one lightpath exists on a specific wavelength. Equation (5.9) ensures that there is a match between incoming and outgoing traffic in all nodes except for the source and destination ones. The aggregation of traffic flow that requires electronic processing at each node is represented by equation (5.10).

One key setback that arises due to the use of MLR in optical networks is the overall reduction of the optical reach, and it is therefore imperative to determine the maximum possible reach that can be achieved by our proposed model. Generally, SLR networks utilize the under-compensation of CD per fibre span by using pre- and post-compensation fibres at the transceivers to offset residual CD. The residual CD per span is known to be reliant on physical link distance, wavelength of the propagating signal, and the employed modulation

format [6]. The use of advanced modulation formats such as DPQSK in high-speed SLR networks appear to be attractive as the CD is effectively compensated for, implying that there will not be any requirements for the management of dispersion [20]. However, the next-generation networks that will be based on MLR techniques will certainly require some careful management of CD for them to guarantee acceptable QoS since their signal rates will be in excess of 100 Gbps. To compute the maximum reach achievable by MLR networks, we take into consideration three channels that are capable of optimally handling 10 G, 40 G and 100 G SLR on the legacy networks. We utilize a MATLAB code to come up with numerical values for simulations of the optical reach of the MLR networks. The following assumptions are made for our numerical simulations:

i. For a 10 G PSK signal, we assume an NRZ pulse with an average rise time of 20 ps.
ii. For 40 G DP-QPSK and 100 G DPSK signals, we assume 0.5 RZ pulse shapes.

We further assume that a SMF with a dispersion of $12\,ps/nm.km$, an effective area of 85 μm^2 and launch power of 0 dBm is utilized.

We also take the span of each fibre to be 80 km in a DCF and EDFAs are used as amplifiers. The split-step Fourier technique is used to compute the maximum optical reach of each wavelength per optical fibre. The optical reach of SLR 10 G, 40 G and 100 G are 1800, 2200 and 7000 km respectively [214]. For the MLR network optical reach, we assume that the network is dispersion optimized for 10 G links, and the numerical values obtained for the MLR 10 G, 40 G and 100 G are 1700, 1800 and 950 km respectively. These values are used to predetermine possible lightpaths in our model.

5.7.2 Numerical examples

The 11 node, 26 link Pan-European network topology is considered in our computations. Table 5.3 shows the traffic demand matrix used in our simulations [214]. We further assume that each fibre can accommodate 16 wavelengths and each link is considered to be bidirectional.

Table 5.3: Traffic demand matrix

Node	1	2	3	4	5	6	7	8	9	10	11
1	0	1	1	3	1	1	1	35	1	1	1
2	1	0	5	14	40	1	1	10	3	2	3
3	1	5	0	16	24	1	1	5	3	1	2
4	3	14	16	0	6	2	2	21	81	9	9
5	1	40	24	6	0	1	11	6	11	1	2
6	1	1	1	2	1	0	1	1	1	1	1
7	1	1	1	2	11	1	0	1	1	1	1
8	35	10	5	21	6	1	1	0	6	2	5
9	1	3	3	81	11	1	1	6	0	51	6
10	1	2	1	9	1	1	1	2	51	0	81
11	1	3	2	9	2	1	1	5	6	81	0

Table 5.4 presents the energy costs of the pertinent network components.

Table 5.4: Energy consumption of key network components

Component	Energy consumption (W)		
	10 G	40 G	100 G
Transponder	45	117	199.5
SRT	24.5	66.5	143.5
OXC	28	73.5	161
Regenerator	49	126	280
EDFA	35	35	35
Electronic Processing	17.5/ Gbps	17.5/ Gbps	17.5/ Gbps

Table 5.5 shows the total energy consumption of 10 G, 40 G, and 100 G SLR and MLR networks. The energy consumption values shown in Table 5.5 are normalized with respect to the10 G transponder energy consumption.

Table 5.5: Normalized energy consumption of MLR and SLR networks

Network	Traffic Load (Tbps)			
	1	5	10	20
10 G SLR	606.3	1832.5	3270.0	6241.1
40 G SLR	609.4	1344.4	2173.4	3632.4
100 G SLR	716.5	1480.9	2179.4	3498.2
MLR	536.2	1251.5	1944.7	3386.7

5.7.3 Transparent MLR Networks

From the tables above, we can infer that under various traffic loads, MLR networks are capable of saving energy costs of between 7 - 46 % as compared to 10 G SLR networks, 6 - 11 % as compared to 40 G SLR networks and 3 – 21 % as compared to 100 G SLR networks. We can clearly observe that 10 G SLR networks are the heaviest energy consumers and their energy consumption drastically increases at higher traffic loads.

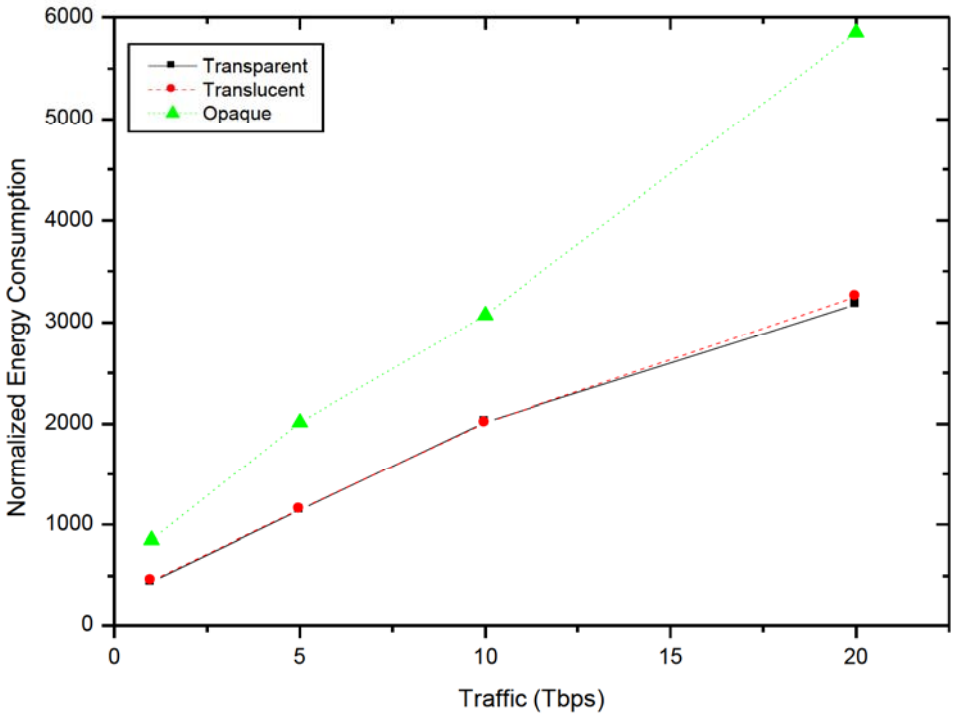

Figure 5.21: Normalized Energy Consumption for different types networks

This can be explained by noting that a significant number of network components will be required to meet the needs of 10 G SLR networks to support high traffic demands, whereas, the 100 G SLR networks consume the least energy primarily due to decreased deployment of high energy-consuming amplifiers.

Figure 5.21 shows and compares energy usage for different network types for the 11-node Pan-European Network. As can be observed from the graphs, opaque networks use up a lot of energy compared to their transparent and translucent counterparts. On the other hand, it is evident that translucent and transparent networks consume almost the same amounts of energy for the given network. This may be attributed to the fact that very few energy-hungry devices such as regenerators are sufficient to sustain the networks at these traffic loads.

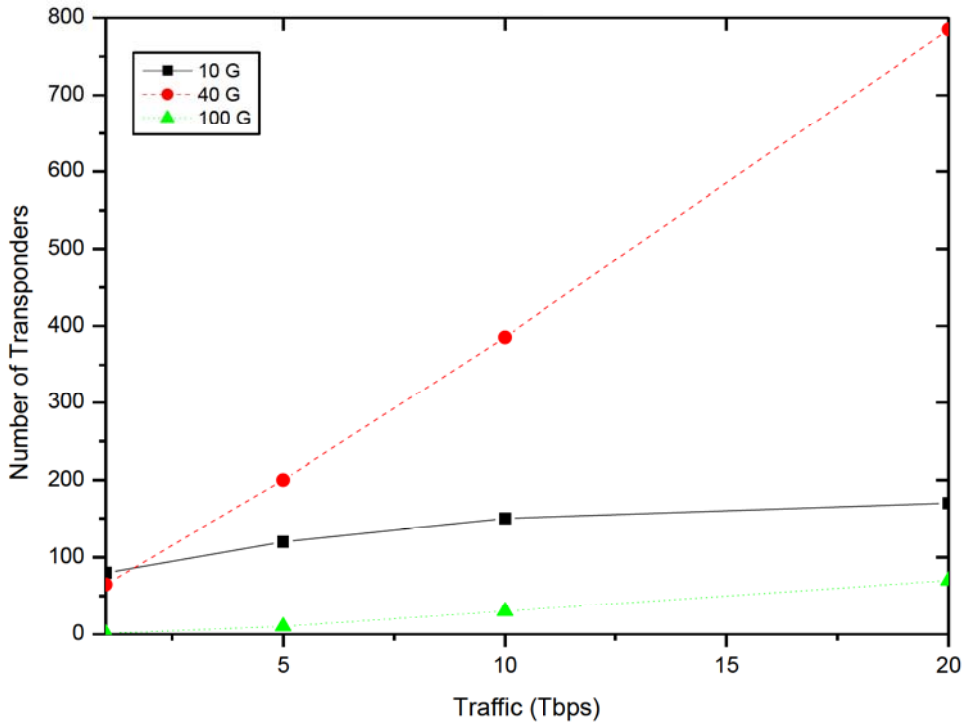

Figure 5.22: Relationship between number of transponders and traffic speed for SLR networks

The distribution of transponders at different loads in the MLR translucent network is shown in figure 5.22. It is observed that at the given traffic loads, 40 G transponders are mostly utilized compared to either 10 G or 100 G transponders.

This is mainly so due to the extensive use of 40 G transponders at high network loads and that 10 G transponders are fairly and effectively deployed to care of low traffic demands. However, we anticipate that at sufficiently high speeds (> 50 Tbps), the number of 100 G transponders required will surpass that of both 10 G and 40 G transponders.

In summary, it is crucial to note that MLR networks deployment leads to appreciable and important energy savings in heterogeneous networks that essentially constitute modern and future high-speed networks. Since there is a strong correlation between energy savings and reduced opex, it is therefore prudent to ensure that future backbone networks are designed in a way that will enable them to effectively and efficiently support MLR.

5.8 Summary

In this chapter, energy-efficient algorithms that take into account various parameters in their decision-making processes are proposed. An energy-efficient dynamic sleep cycle technique is proposed and its performance is evaluated against that of other algorithms found in literature. The technique gives satisfactory results and is found to be adaptable to different network designs and topologies. A novel OEA-LR is also presented and its performance is evaluated through simulations, and it provides fairly good energy savings potential. An energy-efficient protection scheme is also proposed and evaluated through simulations. In this scheme, during low traffic periods, some of the protection lines and devices are switched off, thereby conserving energy. The results from the simulations reveal massive potential energy savings if this scheme is implemented. Another proposal makes use of the solar energy to power the networks in order to augment the traditional energy sources. The results from the simulations indicate that the model provides a huge relief in as far as energy consumption from the non-renewable energy sources is concerned, thus lowering the carbon footprint of backbone networks. Lastly, an energy-efficient technique that employs MLR is proposed. This approach allows traffic that operates at different network speeds to coexist and traverse the same physical links. Simulations are once again used to check the efficiency and usefulness of the proposal, and it is observed that the approach promises to be a clear favourite of future green networks, mainly due to its elasticity and energy efficiency.

6 Conclusion and Future Work

6.1 Conclusion

The rapid increase in demand for high-bandwidth services and applications has certainly propelled the development of backbone transparent optical networks. These networks are highly attractive since they operate without the optical-electrical-optical (OEO) converters that essentially slow down traffic transmission speeds, and often very bulky. In addition, the elimination of these OEO converters lead to significantly lower energy consumption and thus the realization of environmentally friendly *green networks.* However, physical layer impairments become significantly important at high bit-rates, and may not be ignored in the design and operation of these all-optical networks. The most crucial impairments that degrade optical signals in optical networks include Chromatic Dispersion (CD), Polarization Mode Dispersion (PMD), Fibre Attenuation, Polarization Dependant Losses (PDL), Crosstalk (XT), Filter Concatenation (FC), Amplified Spontaneous Emission (ASE), Cross Phase Modulation (XPM), Four Wave Mixing (FWM) and Component Insertion Losses. These impairments severely compromise the quality of transmitted signals as they traverse the network such that the overall QoS may reach unacceptable levels, and thus result in high connection blocking rates.

In our work, we proposed a novel Q-factor evaluation tool that is essential in the routing and wavelength assignment decision-making process in order to ensure that the transmitted optical signal quality is not severely degraded. Our Q-factor estimation tool differs from the existing ones reviewed in literature because it incorporates the effects of XT and filter concatenation in its prediction. It is important to note that at bit-rates of 10 Gbit/s and above, XT and filter concatenation effects become well-pronounced and may not be ignored in the evaluation of transmitted signals Q-factors.

In addition, we proposed an impairment-aware routing and wavelength assignment algorithm (IA-RWA) that incorporates Q-factor estimation during operation. In contrast to existing approaches reviewed in the study, our approach employs the shortest-widest path (SWP)

algorithm to solve the routing sub-problem, and the first-fit with ordering (FFwO) algorithm to solve the wavelength assignment sub-problem.
In comparison with the shortest path routing and traditional impairment-aware approaches, our proposed algorithm clearly shows a marked reduction in the connection blocking probability.Another important milestone of our proposed algorithm is that it overtly outshines the existing IA-RWAs at high network speeds and loads for different network topologies.

An analytical model to compute the blocking probabilities for RWA with physical impairments in transparent networks was also proposed. Numerical examples are also provided to show the performance of the proposed model, and it is validated through the use of simulations. QoT-aware and QoT-guaranteed WA approaches are implemented in various networks to evaluate the performance of the model, and its validation is done through simulations. From the results, it was observed that at low traffic loads, the blocking probability of the analytical technique is lower than that obtained from the simulations. This is caused by the underestimation of the wavelength blocking probability that exists in real networks which is not appropriately captured in the analytical method. On the other hand, in the medium to high traffic conditions, the results obtained by the two approaches are almost the same. We can conclude that our proposed analytical method accurately predicts the behaviour of QoT-aware and QoT-guaranteed algorithms in both the traditional FF WA and FFwO WA.

On the topical issue of energy consumption in all-optical networks, we proposed several energy-aware and energy-efficient routing and wavelength assignment schemes to various scenarios. Our proposed *anycast* cluster-based approach shows that huge energy savings can be achieved, especially at high network loads. The results are particularly important in instances were certain clusters of nodes are switched off (sleep mode) at particular instances and scenarios.

Another energy-saving scheme that is based on energy-efficient dynamic sleep cycles was proposed. In this scheme, individual network nodes switch between ON and OFF states according to the volume of network traffic obtaining at any given instance. It can be observed that this approach leads to very enormous energy savings at generally low network loads since a significant number of nodes will have entered the “sleep mode”.

A novel Optimized Energy-Aware Lightpath Routing (OEA-LR) approach was also proposed that simultaneously considers both energy minimization and resource utilization as a unitary cost function. The results obtained show that the use of the OEA-LR strategy leads to higher average path lengths, compared to the approach where energy awareness is not taken into account. These results assert our expectation that, if path lengths are long, there is a likelihood that the network resources will be optimally utilized since traffic tend to traverse through already powered-on devices in the network. Thus, these results from the simulations confirm the competitive edge of the OEA-LR approach in terms of both energy and network utilization efficiencies.

An energy-efficient protection scheme that is subject to traffic variation was also proposed. In this approach, a 1+1 dedicated path protection scheme is considered since it ensures unparalleled availability of resources and enviable network resilience. Our proposed scheme shows that significant amounts of energy can be salvaged and can be as high as 29 % at off-peak periods as compared to the traditional 1+1 dedicated protection schemes.

An ingenious energy-efficient approach that utilizes solar energy was also proposed. In this approach, randomly selected nodes are powered alternately by both traditional and solar energy sources. It was observed that substantial amounts of non-renewable power could be saved and can be as high as 3000 kW depending on the time of the day and geographical location.

Lastly, an energy-efficient technique that employs Mixed Line Rates (MLR) was proposed and presented. This approach allows traffic that operates at different network speeds to coexist and traverse the same physical links. Simulations were once again used to check the efficiency and usefulness of the proposal, and it was observed that the approach promised to be a clear favourite of future green networks, mainly due to its elasticity. It was also noted that the deployment of MLR networks leads to appreciable and important energy savings in heterogeneous networks that essentially constitute modern and future high-speed networks. Since there is a strong correlation between energy savings and reduced opex, it is therefore prudent to ensure that future backbone networks are designed in a way that will enable them to effectively and efficiently support MLR.

6.2 Future Work

We intend to extend our work on the Q-factor estimation tool to include impairment effects due to Stimulated Brillouin Scattering (SBS) and Stimulated Raman Scattering (SRS) since the effects of these impairments become significant in future ultra-high-speed all-optical networks.

We also intend to thoroughly investigate the limitations and advantages of utilizing the "sleep mode" function in energy-efficient all-optical networks. The relationship between optical switching techniques and energy consumption in ultra-fast future MLR networks also needs to be explored in future studies.

Lastly, we also plan to investigate the impact of employing other renewable energy sources such as wind and tidal power in the powering of future backbone optical networks.

References

[1] A. Jirattigalachote, "Provisioning Strategies for Transparent Optical Networks Considering Transmission Quality, Security, and Energy Efficiency," PhD, KTH Information and Communication Technology, Stockholm, Sweden, 2012.

[2] R. Ramaswami, K. N. Sivarajan, and G. H. Sasaki, *Optical networks: A practical perspective*, 3rd ed. Boston, MA, United States: Morgan Kaufmann Publishers In, 2008.

[3] W. Van Heddeghem, S. Lambert, B. Lannoo, D. Colle, M. Pickavet, and P. Demeester, "Trends in worldwide ICT electricity consumption from 2007 to 2012," *Computer Communications*, vol. 50, pp. 64–76, Sep. 2014.

[4] F. Idzikowski, L. Chiaraviglio, R. Duque, F. Jimenez, and E. Le Rouzic, "Green Horizon: Looking at Backbone Networks in 2020 from the Perspective of Network Operators," in *IEEE International Conference on Communications (ICC)*, Budapest, Hungary, 2013.

[5] A. Andrae and T. Edler, "On global electricity usage of communication technology: Trends to 2030," *Challenges*, vol. 6, no. 1, pp. 117–157, Apr. 2015.

[6] C. Chan, A. Gygax, E. Wong, C. Leckie, A. Nirmalathas, and D. Kilper, "Methodologies for assessing the use-phase power consumption and greenhouse gas emissions of telecommunications network services," *Environmental science & technology.*, vol. 47, no. 1, pp. 485–92, Dec. 2012. [Online]. Available: https://www.ncbi.nlm.nih.gov/pubmed/23211093. Accessed: Oct. 5, 2014.

[7] R. S. Tucker, R. Parthiban, J. Baliga, K. Hinton, R. W. A. Ayre, and W. V. Sorin, "Evolution of WDM optical IP networks: A cost and energy perspective," *Journal of Lightwave Technology*, vol. 27, no. 3, pp. 243–252, Feb. 2009.

[8] J. Baliga, R. Ayre, K. Hinton, W. V. Sorin, and R. S. Tucker, "Energy consumption in optical IP networks," *Journal of Lightwave Technology*, vol. 27, no. 13, pp. 2391–2403, Jul. 2009.

[9] M. N. Dharmaweera, R. Parthiban, and Y. A. Sekercioglu, "Toward a power-efficient backbone network: The state of research," *IEEE Communications Surveys & Tutorials*, vol. 17, no. 1, pp. 198–227, 2015.

[10] D. C. Kilper *et al.*, "Power trends in communication networks," *IEEE Journal of Selected Topics in Quantum Electronics*, vol. 17, no. 2, pp. 275–284, Mar. 2011.

[11] W. Van Heddeghem, F. Idzikowski, W. Vereecken, D. Colle, M. Pickavet, and P. Demeester, "Power consumption modeling in optical multilayer networks," *Photonic Network Communications*, vol. 24, no. 2, pp. 86–102, Jan. 2012.

[12] R. Bolla, R. Bruschi, F. Davoli, and F. Cucchietti, "Energy efficiency in the future Internet: A survey of existing approaches and trends in energy-aware fixed network infrastructures," *IEEE Communications Surveys & Tutorials*, vol. 13, no. 2, pp. 223–244, 2011.

[13] A. P. Bianzino, C. Chaudet, D. Rossi, and J.-L. Rougier, "A survey of green networking research," *IEEE Communications Surveys & Tutorials*, vol. 14, no. 1, pp. 3–20, 2012.

[14] C. Lange, D. Kosiankowski, R. Weidmann, and A. Gladisch, "Energy consumption of telecommunication networks and related improvement options," *IEEE Journal of Selected Topics in Quantum Electronics*, vol. 17, no. 2, pp. 285–295, Mar. 2011.

[15] W. Vereecken *et al.*, "Power consumption in telecommunication networks: Overview and reduction strategies," *IEEE Communications Magazine*, vol. 49, no. 6, pp. 62–69, Jun. 2011.

[16] M. N. M. Warip, I. Andonovic, I. Glesk, P. Ehkan, F. A. A. Fuad, and M. E. E. S. Ahmed, "Energy efficient segmentation-link strategies for transparent IP over WDM core networks," *Journal of Communications*, vol. 9, no. 1, pp. 48–55, 2014.

[17] I. Tomkos *et al.*, "Impairment aware networking and relevant resiliency issues in all-optical networks," in *ECOC 2008*, Brussels, Belgium, 2008.

[18] A. Tzanakaki, K. Georgakilas, K. Katrinis, L. Wosinska, A. Jirattigalachote, and P. Monti, "Network performance improvement in survivable WDM networks considering

physical layer constraints," in *2009 11th International Conference on Transparent Optical Networks*, Institute of Electrical and Electronics Engineers (IEEE), 2009.

[19] L. Wosinska, A. Jirattigalachote, P. Monti, A. Tzanakaki, and K. Katrinis, "Lightpath routing considering differentiated physical layer constraints in transparent WDM networks," in *Asia Communications and Photonics Conference and Exhibition*, The Optical Society, 2009.

[20] R. Cardillo, V. Curri, and M. Mellia, "Considering transmission impairments in wavelength routed networks," in *Conference on Optical Network Design and Modeling, 2005.*, Milan, Italy: Institute of Electrical and Electronics Engineers (IEEE), 2005.

[21] C. Politi, V. Anagnostopoulos, C. Matrakidis, and A. Stavdas, "Physical layer impairment aware routing algorithms based on analytically calculated Q-factor," in *2006 Optical Fiber Communication Conference and the National Fiber Optic Engineers Conference*, Anaheim, Institute of Electrical and Electronics Engineers (IEEE), 2006.

[22] J. Hecht, *City of light: The story of fiber optics*, 1st ed. Oxford, New York: Oxford University Press, 1999.

[23] G. P. Agrawal, *Fiber-optic communication systems*, 2nd ed. New York, NY: John Wiley & Sons inc., 1997.

[24] J. P. G. Sterbenz *et al.*, "Resilience and survivability in communication networks: Strategies, principles, and survey of disciplines," *Computer Networks*, vol. 54, no. 8, pp. 1245–1265, Jun. 2010.

[25] M. Cvijetic and I. B. Djordjevic, *Advanced optical communications systems and networks*. Boston: Artech House Publishers, 2013.

[26] D. Chiaroni *et al.*, "Packet OADMs for the next generation of ring networks," *Bell Labs Technical Journal*, vol. 14, no. 4, pp. 265–283, Feb. 2010.

[27] T. S. El-Bawab, *Optical switching*. New York: Springer-Verlag New York, 2010.

[28] P. C. Becker, N. A. Olsson, J. R. Simpson, E. Snitzer, and I. P. Kaminow, *Erbium-doped fiber amplifiers: Fundamentals and technology*. San Diego: Academic Press, 1999.

[29] W.H. Cheng, Y.C. Huang, S.L. Huang, H. Taga, and Y.J. Chiu, "300-nm Broadband chromium-doped fiber amplifiers," in *Optical Fiber Communication Conference/National Fiber Optic Engineers Conference 2013*, The Optical Society, 2013.

[30] V. Bobrovs, S. Olonkins, A. Alsevska, L. Gegere, and G. Ivanovs, "Comparative performance of Raman-SOA and Raman- EDFA hybrid optical amplifiers in DWDM transmission systems," *International Journal of Physical Sciences Full Length Research Paper*, vol. 8, no. 39, pp. 1898–1906, 2013. [Online]. Available: http://www.academicjournals.org/article/article1383911284_Bobrovs%20et%20al.pdf. Accessed: Oct. 5, 2016.

[31] R. W. Lucky, *Raman amplifiers for telecommunications: Physical principles: V. 1*, M. Islam, Ed. New York: Springer-Verlag New York, 2004.

[32] R. H. Stolen, "Nonlinearity in fiber transmission," in *Proceedings of the IEEE*, Institute of Electrical and Electronics Engineers (IEEE), 1980, vol. 68, no. 10, pp. 1232–1236.

[33] F. M. Mustafa, A. A. M. Khalaf, and F. A. Elgeldawy, "Multi-pumped Raman Amplifier for Long-Haul UW-WDM Optical Communication Systems: Gain Flatness and Bandwidth Enhancements," in *15th International Conference on Advanced Communication Technology*, Institute of Electrical & Electronics Engineers (IEEE), 2013.

[34] G. M. Durães, A. C. B. Soares, W. F. Giozza, and J. A. S. Monteiro, "Best Shortest Lightpath Routing for Translucent Optical Networks," in *The Seventh International Conference on Systems and Networks Communications*, Lisbon, Portugal, 2012, pp. 143–150.

[35] S. Azodolmolky *et al.*, "A survey on physical layer impairments aware routing and wavelength assignment algorithms in optical networks," in *Computer Networks: The International Journal of Computer and Telecommunications Networking*, Elsevier

North-Holland, 2009, vol. 53, no. 7, pp. 926–944. [Online]. Available: http://dl.acm.org/citation.cfm?id=1518353. Accessed: Oct. 9, 2016.

[36] A. A. M. Saleh and J. M. Simmons, "All-optical Networking—Evolution, benefits, challenges, and future vision," in *Proceedings of the IEEE*, Institute of Electrical and Electronics Engineers (IEEE), 2012, vol. 100, no. 5, pp. 1105–1117.

[37] B. Ramamurthy, H. Feng, D. Datta, J. P. Heritage, and B. Mukherjee, "Transparent vs. Opaque vs. Translucent wavelength-routed optical networks," in *OFC/IOOC . Technical Digest. Optical Fiber Communication Conference, 1999, and the International Conference on Integrated Optics and Optical Fiber Communication*, Washington DC, Institute of Electrical and Electronics Engineers (IEEE), 1999.

[38] P. Wiatr, P. Monti, and L. Wosinska, "Green lightpath provisioning in transparent WDM networks: Pros and cons," in *2010 IEEE 4th International Symposium on Advanced Networks and Telecommunication Systems*, Institute of Electrical and Electronics Engineers (IEEE), 2010.

[39] K. Rottwitt, "Raman amplification in lightwave communication systems," in *Optical Fiber Telecommunications (OFC)*, San Diego, CA, 2000, vol. IV A.

[40] D. F. Welch *et al.*, "The realization of large-scale Photonic integrated circuits and the associated impact on fiber-optic communication systems," in *Journal of Lightwave Technology*, Institute of Electrical and Electronics Engineers (IEEE), 2006, vol. 24, no. 12, pp. 4674–4683.

[41] E. Temprana *et al.*, "Overcoming Kerr-induced capacity limit in optical fiber transmission," *Science*, vol. 348, no. 6242, pp. 1445–1448, Jun. 2015.

[42] M. Gagnaire and S. Zahr, "Impairment-aware routing and wavelength assignment in translucent networks: State of the art," *IEEE Communications Magazine*, vol. 47, no. 5, pp. 55–61, May 2009.

[43] P. Smith *et al.*, "Network resilience: A systematic approach," *IEEE Communications Magazine*, vol. 49, no. 7, pp. 88–97, Jul. 2011.

[44] Q. Rahman, S. Bandyopadhyay, and Y. Aneja, "Optimal regenerator placement in translucent optical networks," *Optical Switching and Networking*, vol. 15, pp. 134–147, Jan. 2015.

[45] G. Shen and R. Tucker, "Translucent optical networks: The way forward [Topics in optical Communications]," *IEEE Communications Magazine*, vol. 45, no. 2, pp. 48–54, Feb. 2007.

[46] P. Hlubina, M. Kadulová, and P. Mergo, "Chromatic dispersion measurement of holey fibres using a supercontinuum source and a dispersion balanced interferometer," *Optics and Lasers in Engineering*, vol. 51, no. 4, pp. 421–425, Apr. 2013.

[47] P. Pavon-Marino *et al.*, "Balancing multifibre and wavelength converter cost in wavelength routing networks," in *2008 34th European Conference on Optical Communication*, Institute of Electrical and Electronics Engineers (IEEE), 2008.

[48] M. Farahmand, D. Awduche, S. Tibuleac, and D. Atlas, ""Characterization and representation of impairments for routing and path control in all-optical networks," in *National Fiber Optic Engineers Conference (NFOEC)*, Dallas, TX, 2002.

[49] J. Strand and A. Chiu, "Impairments and other constraints on optical layer routing," 2002. [Online]. Available: draft-ietf-ipo-impairments-04.txthttp://citeseerx.ist.psu.edu/viewdoc/versions?doi=10.1.1.374.143.

[50] "Grid Job Routing Algorithms," in *Phosphorus–Deliverable D 5.3*, 2007. [Online]. Available: http://www.istphosphorus.eu/files/deliverables/Phosphorus-deliverable-D5.3.pdf.

[51] G. P. Agrawal, *Fiber-optic communication systems*, 4th ed. New York: Wiley-Blackwell (an imprint of John Wiley & Sons Ltd), 2010.

[52] B. Kose, R. Pimpinella, J. M. Castro, Y. Huang, and A. Novick, "Zero dispersion modes and its effects on characterization of MMF chromatic dispersion," in *Optical Fiber Communication Conference*, The Optical Society, 2015.

[53] I. P. Kaminov, T. Li, A. E. Willner, and I. P. Kaminow, *Optical fiber telecommunications V A: Components and subsystems [With CDROM]*, 5th ed. Amsterdam: Elsevier Science, 2008.

[54] L. Štěpánek, *Štěpánek: Chromatic Dispersion in optical Communications*, vol. 142, no. 2, 2012. [Online]. Available: http://pernerscontacts.upce.cz/26_2012/Stepanek.pdf. Accessed: Oct. 9, 2016.

[55] I. Tomkos, D. Vogiatzis, C. Mas, I. Zacharopoulos, A. Tzanakaki, and E. Varvarigos, "Performance engineering of metropolitan area optical networks through impairment constraint routing," in *IEEE Communications Magazine*, Institute of Electrical and Electronics Engineers (IEEE), 2004, vol. 42, no. 8, pp. S40–S47.

[56] S. Mundhe, S. Bhosale, and S. Shirodkar, "Evolution of Solitons in Optical Communication," *International Journal of Research in Advent Technology*, vol. 3, no. 12, Dec. 2015.

[57] X. Xu *et al.*, "Advanced modulation formats for 400-Gbps short-reach optical inter-connection," *Optics Express*, vol. 23, no. 1, p. 492, Jan. 2015.

[58] A. B. dos Santos, T. V. N. Coelho, M. J. Pontes, and D. D. Silveira, "A new experimental approach to second-order polarization mode dispersion analysis for optical communications systems," *Journal of Modern Optics*, vol. 61, no. 19, pp. 1582–1588, Aug. 2014.

[59] S. Norimatsu and M. Maruoka, "Accurate Q-factor estimation of optically amplified systems in the presence of waveform distortions," *Journal of Lightwave Technology*, vol. 20, no. 1, pp. 19–27, 2002.

[60] S. Wahls, S. T. Le, J. E. Prilepsk, H. V. Poor, and S. K. Turitsyn, "Digital backpropagation in the nonlinear Fourier domain," in *2015 IEEE 16th International Workshop on Signal Processing Advances in Wireless Communications (SPAWC)*, Institute of Electrical and Electronics Engineers (IEEE), 2015.

[61] M. E. McCarthy, M. A. Z. Al Kahteeb, F. M. Ferreira, and A. D. Ellis, "PMD tolerant nonlinear compensation using in-line phase conjugation," *Optics Express*, vol. 24, no. 4, p. 3385, Feb. 2016.

[62] X. Li *et al.*, "Electronic post-compensation of WDM transmission impairments using coherent detection and digital signal processing," *Optics Express*, vol. 16, no. 2, p. 880, 2008.

[63] T. Tanimura, M. Nölle, J. K. Fischer, and C. Schubert, "Analytical results on back propagation nonlinear compensator with coherent detection," *Optics Express*, vol. 20, no. 27, Dec. 2012.

[64] E. Torrengo *et al.*, "Experimental validation of an analytical model for nonlinear propagation in uncompensated optical links," *Optics Express*, vol. 19, no. 26, p. B790, Dec. 2011.

[65] E. Ip and J. M. Kahn, "Compensation of dispersion and Nonlinear Impairments using digital Backpropagation," *Journal of Lightwave Technology*, vol. 26, no. 20, pp. 3416–3425, Oct. 2008.

[66] Y. Kawaguchi, Y. Tamura, T. Haruna, Y. Yamamoto, and M. Hirano, "Ultra Low-loss Pure Silica Core Fiber," in *SEI Technical Review* (no. 80), 2015, pp. 50–55.

[67] F. Balasis, X. Wang, S. Xu, and Y. Tanaka, "Dynamic Physical Impairment-Aware Routing and Wavelength Assignment in 10/40/100 Gbps Mixed Line Rate Optical Networks," in *15th International Conference on Advanced Communication Technology*, PyeongChang, 2013.

[68] S. B. Alexander, *Optical communication receiver design*. London, WA: Institution of Electrical Engineers, SPIE Optical Engineering Press., 1997.

[69] A. H. Beshr, "Study of ASE noise power, noise figure and quantum conversion efficiency for wide-band EDFA," *Optik - International Journal for Light and Electron Optics*, vol. 126, no. 23, pp. 3492–3495, Dec. 2015.

[70] A. W. Naji, M. S. Z. Abidin, M. H. Al-Mansoori, A. R. Faidz, and M. A. Mahdi, "Experimental investigation of noise in double-pass erbium-doped fiber amplifiers," *Laser Physics Letters*, vol. 4, no. 2, pp. 145–148, Feb. 2007.

[71] N. Md Samsuri, S. W. Harun, and H. Ahmad, "Comparison of performances between partial double-pass and full double-pass systems in two-stage l-band EDFA," *Laser Physics Letters*, vol. 1, no. 12, pp. 610–612, Dec. 2004.

[72] Z. Q. Pan *et al.*, "Low-frequency noise suppression of a fiber laser based on a round-trip EDFA power stabilizer," *Laser Physics*, vol. 23, no. 3, p. 035105, Jan. 2013.

[73] X. Chen, P. R. Horche, and A. M. Minguez, "Optical signal impairment study of cascaded optical filters in 40 Gbps DQPSK and 100 Gbps PM-DQPSK systems," in *Optics and Photonics for Information Processing VII*, SPIE-Intl Soc Optical Eng, 2013.

[74] S. Azodolmolky, "Physical Impairments Aware Planning and Operation of Transparent Optical Networks," PhD, Universitat Politècnica de Catalunya, 2010.

[75] X. Chen, J. A. Martín Pereda, and P. R. Horche, "Signal penalties induced by different types of optical filters in 100Gbps PM-DQPSK based optical networks," *Optical Switching and Networking*, vol. 19, pp. 145–154, Jan. 2016.

[76] E. Giacoumidis, J. L. Wei, X. L. Yang, A. Tsokanos, and J. M. Tang, "Adaptive-Modulation-Enabled WDM impairment reduction in multichannel optical OFDM transmission systems for next-generation PONs," *IEEE Photonics Journal*, vol. 2, no. 2, pp. 130–140, Apr. 2010.

[77] J. M. Tang and K. A. Shore, "30-Gb/s signal transmission over 40-km directly modulated DFB-laser-based single-mode-fiber links without optical amplification and dispersion compensation," *Journal of Lightwave Technology*, vol. 24, no. 6, pp. 2318–2327, Jun. 2006.

[78] X. Liu, X. Wei, A. H. Gnauck, C. R. Doerr, and S. Chandrasekhar, "Analysis of loss ripple and its application to the mitigation of optical filtering penalty," *IEEE Photonics Technology Letters*, vol. 17, no. 1, pp. 82–84, Jan. 2005.

[79] Y. Tang and W. Shieh, "Filter concatenation impact on 107-Gb/s coherent optical OFDM system," in *2009 14th OptoElectronics and Communications Conference*, Institute of Electrical and Electronics Engineers (IEEE), 2009.

[80] E. Giacoumidis, I. Tomkos, and J. M. Tang, "Adaptive modulation-induced reduction in filter Concatenation impairment for optical OFDM metro/regional systems," *Journal of Optical Communications and Networking*, vol. 3, no. 7, pp. 587–593, Jun. 2011.

[81] M. Chochol, J. M. Fabrega, M. S. Moreolo, and G. Junyent, "Optical filter cascading effects in a phase modulated coherent optical OFDM transmission system based on Hartley transform," in *2012 14th International Conference on Transparent Optical Networks (ICTON)*, Institute of Electrical & Electronics Engineers (IEEE), 2012.

[82] H. Chotard, Y. Painchaud, A. Mailloux, M. Morin, F. Trepanier, and M. Guy, "Group delay ripple of cascaded Bragg grating gain flattening filters," *IEEE Photonics Technology Letters*, vol. 14, no. 8, pp. 1130–1132, Aug. 2002.

[83] G. Lenz, B. J. Eggleton, C. K. Madsen, C. R. Giles, and G. Nykolak, "Optimal dispersion of optical filters for WDM systems," *IEEE Photonics Technology Letters*, vol. 10, no. 4, pp. 567–569, Apr. 1998.

[84] S. E. Reza, N. Ahsan, S. Ferdous, R. K. Dhar, and M. J. Rahimi, "Analyses on the Effects of Crosstalk in a Dense Wavelength Division Multiplexing (DWDM) System Considering a WDM Based Optical Cross Connect (OXC)," *International Journal of Scientific & Engineering Research*, vol. 4, no. 1, Jan. 2013.

[85] Y. Shen, K. Lu, and W. Gu, "Coherent and incoherent crosstalk in WDM optical networks," *Journal of Lightwave Technology*, vol. 17, no. 5, pp. 759–764, May 1999.

[86] L. G. C. Cancela, J. L. Rebola, and J. J. O. Pires, "Implications of in-band crosstalk on DQPSK signals in ROADM-based metropolitan optical networks," *Optical Switching and Networking*, vol. 19, pp. 135–144, Jan. 2016.

[87] J. C. Attard, J. E. Mitchell, and C. J. Rasmussen, "Performance analysis of interferometric noise due to unequally powered interferers in optical networks," *Journal of Lightwave Technology*, vol. 23, no. 4, pp. 1692–1703, Apr. 2005.

[88] J. J. O. Pires and L. G. C. Cancela, "Estimating the performance of direct-detection DPSK in optical networking environments using Eigenfunction expansion techniques," *Journal of Lightwave Technology*, vol. 28, no. 13, pp. 1994–2003, Jul. 2010.

[89] M. R. Jimenez, R. Passy, M. A. Grivet, and J. P. von der Weid, "Computation of power penalties due to intraband crosstalk in optical systems," *IEEE Photonics Technology Letters*, vol. 15, no. 1, pp. 156–158, Jan. 2003.

[90] S. D. Dods and T. B. Anderson, "Calculation of bit-error rates and power penalties due to incoherent crosstalk in optical networks using Taylor series expansions," *Journal of Lightwave Technology*, vol. 23, no. 4, pp. 1828–1837, Apr. 2005.

[91] M. S. Islam and S. P. Majumder, "Bit error rate and cross talk performance in optical cross connect with wavelength converter," *Journal of Optical Networking*, vol. 6, no. 3, p. 295, 2007.

[92] T. Y. Chai, T. H. Cheng, S. K. Bose, C. Lu, and G. Shen, "Crosstalk analysis for limited-wavelength-interchanging cross connects," *IEEE Photonics Technology Letters*, vol. 14, no. 5, pp. 696–698, May 2002.

[93] Y. Fukada, "Probability density function of polarization dependent loss (PDL) in optical transmission system composed of passive devices and connecting fibers," *Journal of Lightwave Technology*, vol. 20, no. 6, pp. 953–964, Jun. 2002.

[94] N. Gisin and B. Huttner, "Combined effects of polarization mode dispersion and polarization dependent losses in optical fibers," *Optics Communications*, vol. 142, no. 1-3, pp. 119–125, Oct. 1997.

[95] B. Huttner and N. Gisin, "Anomalous pulse spreading in birefringent optical fibers with polarization-dependent losses," *Optics Letters*, vol. 22, no. 8, pp. 504–506, Apr. 1997.

[96] Y. Li and A. Yariv, "Solutions to the dynamical equation of polarization-mode dispersion and polarization-dependent losses," *Journal of the Optical Society of America B*, vol. 17, no. 11, pp. 1821–1827, Nov. 2000.

[97] A. Steinkamp, S. Vorbeck, and E. I. Voges, "Polarization mode dispersion and polarization dependent loss in optical fiber systems," in *Optical Transmission Systems and Equipment for WDM Networking III*, SPIE-Intl Soc Optical Eng, 2004.

[98] S. P. Singh and N. Singh, "Nonlinear effects in optical fibers: origin, management and applications," *Progress In Electromagnetics Research*, vol. 73, pp. 249–275, 2007.

[99] R. S. Luis and A. V. T. Cartaxo, "Analytical characterization of SPM impact on XPM-induced degradation in dispersion-compensated WDM systems," *Journal of Lightwave Technology*, vol. 23, no. 3, pp. 1503–1513, Mar. 2005.

[100] J. Zhao, K. Zhang, L. Wang, and Y. Wang, "Study of Q-factor estimation model based on multi-physical Impairments in transparent optical networks," *Journal of Communications*, vol. 7, no. 10, pp. 774–780, Oct. 2012.

[101] N. Sambo *et al.*, "Modeling and distributed provisioning in 10–40–100-Gb/s Multirate wavelength switched optical networks," *Journal of Lightwave Technology*, vol. 29, no. 9, pp. 1248–1257, May 2011.

[102] D. Nodop, C. Jauregui, D. Schimpf, J. Limpert, and A. Tünnermann, "Efficient high-power generation of visible and mid-infrared light by degenerate four-wave-mixing in a large-mode-area photonic-crystal fiber," *Optics Letters*, vol. 34, no. 22, p. 3499, Nov. 2009.

[103] D. Benedikovič, J. Litvík, M. Kuba, M. Dado, and J. Dubovan, "Influence of nonlinear effects in WDM system with non-equidistant channel spacing using different types of high-order PSK and QAM modulation formats," in *Optical Modelling and Design II*, SPIE-Intl Soc Optical Eng, 2012.

[104] M. Dossou, P. Szriftgiser, and A. Goffin, "Theoretical study of Stimulated Brillouin Scattering (SBS) in polymer optical fibres," in *Symposium IEEE/LEOS Benelux Chapter*, Twente, 2008.

[105] D. Cotter, "Stimulated Brillouin scattering in Monomode optical fiber," *Journal of Optical Communications*, vol. 4, no. 1, Jan. 1983.

[106] H. Akimaru, M. R. Finley, and Z. Niu, "Elements of the emerging broadband information highway," *IEEE Communications Magazine*, vol. 35, no. 6, Jun. 1997.

[107] M. Kakemizu and A. Chugo, "Approaches to Green Networks," *FUJITSU Science Technical Journal*, vol. 46, no. 4, pp. 398–403, 2009.

[108] A. A. M. Saleh, J. J. M. Simmons, and S. Member, "Evolution toward the next-generation core optical network," *Journal of Lightwave Technology*, vol. 24, no. 9, pp. 3303–3321, Sep. 2006.

[109] D. T. Neilson, "Photonics for switching and routing," *IEEE Journal of Selected Topics in Quantum Electronics*, vol. 12, no. 4, pp. 669–678, Jul. 2006.

[110] R. Parthiban, "Modeling and analysis of optical backbone networks," PhD, Department of Electrical and Electronic Engineering, University of Melbourne, Melbourne, 2004.

[111] M. N. Dharmaweera, "Towards a Green Optical Internet," PhD, School of Engineering, Monash University, 2014.

[112] A. Nag, M. Tornatore, and B. Mukherjee, "Energy-efficient and cost-efficient capacity upgrade in mixed-line-rate optical networks," *Journal of Optical Communications and Networking*, vol. 4, no. 12, p. 1018, Nov. 2012.

[113] J. Baliga, K. Hinton, and R. S. Tucker, "Energy consumption of the internet," in *Joint International Conference on Optical Internet and 32nd Australian Conference on Optical Fiber Technology (COIN-ACOFT)*, Sydney, Australia, 2007, pp. 1–3.

[114] E. Modiano, "Traffic grooming in WDM networks," *IEEE Communications Magazine*, vol. 39, no. 7, pp. 124–129, 2001.

[115] R. Dutta and G. N. Rouskas, "Traffic grooming inWDMnetworks: past and future," *IEEE Network*, vol. 16, no. 6, pp. 46–56, 2002.

[116] M. Xia, M. Tornatore, Y. Zhang, P. Chowdhury, C. Martel, and B. Mukherjee, "Greening the optical backbone network: A traffic engineering approach," in *2010 IEEE International Conference on Communications*, Institute of Electrical and Electronics Engineers (IEEE), 2010.

[117] M. Hasan, F. Farahmand, and J. Jue, "Energy-awareness in dynamic traffic grooming," in *Optical Fiber Communication Conference/National Fiber Optic Engineers Conference (OFC/NFOEC)*, San Diego, CA, USA, 2010, pp. 6–8.

[118] S. Zhang and D. Shen, "Energy efficient time-aware traffic grooming in wavelength routing networks," in *IEEE Global Telecommunications Conference (GLOBECOM)*, Miami, Florida, USA, 2010, pp. 1–5.

[119] S. Zhang, D. Shen, and C.-K. Chan, "Energy-efficient traffic grooming in WDM networks with scheduled time traffic," *Journal of Lightwave Technology*, vol. 29, no. 17, pp. 2577–2584, Sep. 2011.

[120] C. Labovitz, "The Internet after dark," 2009. [Online]. Available: http://ddos.arbornetworks.com/2009/08/the-internet-after-dark/.

[121] Cisco, "Cisco visual networking index: forecast and methodology, 2012-2017," 2013. [Online]. Available: http://www.cisco.com/en/US/solutions/collateral/ns341/ns525/ns537/ns705/ns827/white paper c11-481360.pdf.

[122] S. Nedevschi, J. Chandrashekar, J. Liu, B. Nordman, S. Ratnasamy, and N. Taft, "Skilled in the art of being idle: reducing energy waste in networked systems," in *6th USENIX symposium on Networked systems design and implementation*, Boston, USA, 2009, pp. 381–394.

[123] L. Chiaraviglio and M. Mellia, "Reducing power consumption in backbone networks," in *IEEE International Conference on Communications (ICC)*, Dresden, Germany, 2009, pp. 1–6.

[124] M. Gupta, S. Grover, and S. Singh, "A feasibility study for power management in LAN switches," in *12th IEEE International Conference on Network Protocols*, Berlin, Germany, 2004, pp. 361–371.

[125] C. Gunaratne, K. Christensen, and B. Nordman, "Managing energy consumption costs in desktop PCs and LAN switches with proxying, split TCP connections, and scaling of link speed," *International Journal of Network Management*, vol. 15, no. 5, pp. 297–310, 2005.

[126] J. Chabarek, J. Sommers, P. Barford, C. Estan, D. Tsiang, and S. Wright, "Power awareness in network design and routing," in *The 27th Conference on Computer Communications (INFOCOM)*, Phoenix, AZ, USA, 2008, pp. 457–465.

[127] Infinera, "Infinera introduces new line system, sets new standard for capacity,". [Online]. Available: http://www.infinera.com/j7/servlet/NewsItem?newsItemID=108. Accessed: 2008.

[128] P. Chowdhury, M. Tornatore, A. Nag, E. Ip, T. Wang, and B. Mukherjee, "On the design of energy-efficient mixed-line-rate (MLR) optical networks," *Journal of Lightwave Technology*, vol. 30, no. 1, pp. 130–139, Jan. 2012.

[129] P. Chowdhury, M. Tornatore, and B. Mukherjee, "On the energy efficiency of mixed-line-rate networks," in *Optical Fiber Communication Conference*, Optical Society of America, 2010.

[130] E. Le Rouzic *et al.*, "TREND towards more energy-efficient optical networks," in *17th International Conference on Optical Network Design and Modeling (ONDM)*, IEEE, 2013.

[131] OECD, "Free publications," 2016. [Online]. Available: http://www.iea.org/publications/freepublications/publication/keyworld2014.pdf. Accessed: Oct. 10, 2016.

[132] E. Gelenbe, K. Hussain, and V. Kaptan, "Simulating autonomous agents in augmented reality," *Journal of Systems and Software*, vol. 74, no. 3, pp. 255–268, Feb. 2005.

[133] G. Fettweis and E. Zimmermann, "ICT energy consumption - trends and challenges," in *The 11th International Symposium on Wireless Personal Multimedia Communications (WPMC 2008)*, Finnish Lapland, 2008.

[134] Y. Zhang, P. Chowdhury, M. Tornatore, and B. Mukherjee, "Energy efficiency in telecom optical networks," *IEEE Communications Surveys & Tutorials*, vol. 12, no. 4, pp. 441–458, 2010.

[135] C. Eyupoglu and M. A. Aydin, "Energy efficiency in backbone networks," in *Procedia - Social and Behavioral Sciences*, Elsevier BV, 2015, vol. 195, pp. 1966–1970.

[136] M. Meo, E. Le Rouzic, R. Cuevas, and C. Guerrero, "Research challenges on energy-efficient networking design," *Computer Communications*, vol. 50, pp. 187–195, Sep. 2014.

[137] Y. Fazili, A. Nafarieh, and W. Robertson, "Hybrid energy-aware and SLA-based routing mechanism over optical networks," in *Procedia Computer Science*, Elsevier BV, 2013, vol. 19, pp. 1151–1158.

[138] J. Baliga, R. Ayre, K. Hinton, W. V. Sorin, and R. S. Tucker, "Energy consumption in optical IP networks," *Journal of Lightwave Technology*, vol. 27, no. 13, pp. 2391–2403, Jul. 2009.

[139] C. Lange, D. Kosiankowski, D. von Hugo, and A. Gladisch, "Analysis of the energy consumption in telecom operator networks," *Photonic Network Communications*, vol. 30, no. 1, pp. 17–28, Mar. 2015.

[140] H. Mahmood and J. Jiang, "Modeling and control system design of a grid connected VSC considering the effect of the interface transformer type," *IEEE Transactions on Smart Grid*, vol. 3, no. 1, pp. 122–134, Mar. 2012.

[141] B. Nleya, A. Mutsvangwa, and M. Dewa, "A smart grid based algorithm for improving energy efficiency of large scale cooperating distributed systems," in *2016 IEEE PES PowerAfrica*, Institute of Electrical and Electronics Engineers (IEEE), 2016.

[142] R. S. Tucker, "Green optical Communications—Part I: Energy limitations in transport," *IEEE Journal of Selected Topics in Quantum Electronics*, vol. 17, no. 2, pp. 245–260, Mar. 2011.

[143] H. Song, "Long-Reach Passive Optical Networks," PhD, University of California, Davis, 2009.

[144] C. Develder, M. Pickavet, B. Dhoedt, and P. Demeester, "A power-saving strategy for Grids," in *Gridnets'08*, 2008. [Online]. Available: http://users.atlantis.ugent.be/cdvelder/papers/2008/develder2008gridnets.pdf. Accessed: Oct. 10, 2015.

[145] B. G. Balagangadhar, "QoS Aware Quorumcasting Over Optical Burst Switched Networks," PhD, Indian Institute of Science, 2008.

[146] M. Ezzahdi, S. Zahr, M. Koubaa, N. Puech, and M. Gagnaire, "LERP: A quality of transmission dependent Heuristic for routing and wavelength assignment in hybrid

WDM networks," in *Proceedings of 15th International Conference on Computer Communications and Networks*, Institute of Electrical and Electronics Engineers (IEEE), 2006.

[147] H. Zang, J. P. Jue, and B. Mukherjee, "A Review of Routing and Wavelength Assignment Approaches for Wavelength-Routed Optical WDM Networks," *Optical Networks Magazine*, pp. 47–60, Jan. 2000.

[148] I. Chlamtac, A. Ganz, and G. Karmi, "Lightpath communications: An approach to high bandwidth optical WAN's," *IEEE Transactions on Communications*, vol. 40, no. 7, pp. 1171–1182, Jul. 1992.

[149] P. Sakthivel and P. K. Sankar, "Dynamic multi-path RWA algorithm for WDM based optical networks," in *2014 International Conference on Electronics and Communication Systems (ICECS)*, Institute of Electrical & Electronics Engineers (IEEE), 2014.

[150] D. Eppstein, "Finding the k shortest paths," *SIAM Journal on Computing*, vol. 28, no. 2, pp. 652–673, Jan. 1998.

[151] S. Ramamurthy, "Optical Design of WDM Network Architectures," PhD, University of California, Davis, 1998.

[152] K. M. Chan and T. P. Yum, "Analysis of least congested path routing in WDM lightwave networks," in *Proceedings of INFOCOM '94 Conference on Computer Communications*, Institute of Electrical and Electronics Engineers (IEEE), 1994.

[153] S. Subramaniam and R. A. Barry, "Wavelength assignment in fixed routing WDM networks," in *Proceedings of ICC'97 - International Conference on Communications*, Institute of Electrical and Electronics Engineers (IEEE), 1997.

[154] S. Ansari and A. Ansari, "Comparative Analysis of Routing and Wavelength Assignment Algorithms used in WDM Optical Networks," *Research Journal of Applied Sciences, Engineering and Technology*, vol. 7, no. 13, pp. 2646–2654, 2014.

[155] M. Batayneh, D. A. Schupke, M. Hoffmann, A. Kirstädter, and B. Mukherjee, "Light-path level protection versus connection-level protection for carrier-grade ethernet in a

mixed-line-rate telecom network," in *Global Communications Conference (GLOBECOM '07)*, Washington, DC, Nov. 2007.

[156] B. Mukherjee, *Optical WDM networks*. New York, NY: Springer-Verlag New York, 2006.

[157] S. Pachnicke, T. Paschenda, and P. M. Krummrich, "Physical impairment based Regenerator placement and routing in translucent optical networks," in *OFC/NFOEC 2008 - 2008 Conference on Optical Fiber Communication/National Fiber Optic Engineers Conference*, Institute of Electrical and Electronics Engineers (IEEE), 2008.

[158] R. Cardillo, V. Curri, and M. Mellia, "Considering transmission impairments in configuring wavelength routed optical networks," in *2006 Optical Fiber Communication Conference and the National Fiber Optic Engineers Conference*, Institute of Electrical and Electronics Engineers (IEEE), 2006.

[159] J. He, M. Brandt-Pearce, Y. Pointurier, and S. Subramaniam, "QoT-Aware routing in impairment-constrained optical networks," in *IEEE GLOBECOM 2007-2007 IEEE Global Telecommunications Conference*, Institute of Electrical and Electronics Engineers (IEEE), 2007.

[160] J. He, M. Brandt-Pearce, and S. Subramaniam, "QoS-aware wavelength assignment with BER and Latency guarantees for Crosstalk limited networks," in *2007 IEEE International Conference on Communications*, Institute of Electrical and Electronics Engineers (IEEE), 2007.

[161] S. Zsigmond, G. Németh, and T. Cinkler, "Mutual Impact of Physical Impairments and Grooming in Multilayer Networks," in *ONDM'07 11th international IFIP TC6 conference on Optical network design and modeling*, Athens, Greece, 2007, pp. 38–47.

[162] A. Marsden, A. Maruta, and K. Kitayama, "Routing and wavelength assignment encompassing FWM in WDM lightpath networks," in *2008 International Conference on Optical Network Design and Modeling*, Institute of Electrical and Electronics Engineers (IEEE), 2008.

[163] J. He, M. Brandt-Pearce, Y. Pointurier, and S. Subramaniam, "Adaptive wavelength assignment using wavelength spectrum separation for distributed optical networks," in

2007 IEEE International Conference on Communications, Institute of Electrical and Electronics Engineers (IEEE), 2007.

[164] E. Salvadori *et al.*, "Signalling-based architectures for impairment-aware Lightpath set-up in GMPLS networks," in *IEEE GLOBECOM 2007-2007 IEEE Global Telecommunications Conference*, Institute of Electrical and Electronics Engineers (IEEE), 2007.

[165] X. Yang and B. Ramamurthy, "Dynamic routing in translucent WDM optical networks: The intradomain case," *Journal of Lightwave Technology*, vol. 23, no. 3, pp. 955–971, Mar. 2005.

[166] G. Markidis, S. Sygletos, A. Tzanakaki, and I. Tomkos, "Impairment aware based routing and wavelength assignment in transparent long haul networks," in *Optical Network Design and Modeling*, Athens, Greece, Springer Science + Business Media, 2007, pp. 48–57.

[167] S. Pachnicke, T. Paschenda, P. Krummrich, and Dortmund, "Assessment of a constraint-based routing algorithm for translucent 10Gbits/s DWDM networks considering fiber nonlinearities," *Journal of Optical Networking*, vol. 7, no. 4, pp. 365–377, Apr. 2008. [Online]. Available: http://www.opticsinfobase.org/abstract.cfm?URI=JON-7-4-365. Accessed: Jun. 15, 2015.

[168] P. Kulkarni, A. Tzanakaki, C. M. Machuka, and I. Tomkos, "Benefits of Q-factor based routing in WDM metro networks," in *31st European Conference on Optical Communications (ECOC 2005)*, Institution of Engineering and Technology (IET), 2005.

[169] G. Markidis, S. Sygletos, A. Tzanakaki, and I. Tomkos, "Impairment-constraint-based routing in Ultralong-Haul optical networks with 2R regeneration," *IEEE Photonics Technology Letters*, vol. 19, no. 6, pp. 420–422, 2007.

[170] X. Yang, L. Shen, and B. Ramamurthy, "Survivable lightpath provisioning in WDM mesh networks under shared path protection and signal quality constraints," *Journal of Lightwave Technology*, vol. 23, no. 4, pp. 1556–1567, Apr. 2005.

[171] F. Cugini, N. Andriolli, L. Valcarenghi, and P. Castoldi, "A novel signaling approach to encompass physical impairments in GMPLS networks," in *IEEE Global Telecommunications Conference Workshops, 2004. GlobeCom Workshops 2004.*, Dallas, Texas, Institute of Electrical and Electronics Engineers (IEEE), 2004, pp. 369–373.

[172] F. Cugini, F. Paolucci, L. Valcarenghi, and P. Castoldi, "Implementing a path computation element (PCE) to encompass physical impairments in transparent networks," in *OFC/NFOEC 2007 - 2007 Conference on Optical Fiber Communication and the National Fiber Optic Engineers Conference*, Institute of Electrical and Electronics Engineers (IEEE), 2007.

[173] A. Jukan and G. Franzl, "Path selection methods with multiple constraints in service-guaranteed WDM networks," *IEEE/ACM Transactions on Networking*, vol. 12, no. 1, pp. 59–72, Feb. 2004.

[174] A. M. Hamad and A. E. Kamal, "Routing and wavelength assignment with power aware multicasting in WDM networks," in *2nd International Conference on Broadband Networks, 2005.*, Boston, MA, Institute of Electrical and Electronics Engineers (IEEE), 2005.

[175] G. S. Pavani, L. G. Zuliani, H. Waldman, and M. Magalhães, "Distributed approaches for impairment-aware routing and wavelength assignment algorithms in GMPLS networks," *Computer Networks*, vol. 52, no. 10, pp. 1905–1915, Jul. 2008.

[176] T. J. Carpenter, R. C. Menendez, D. F. Shallcross, J. W. Gannett, J. Jackel, and A. C. Von Lehmen, "Cost-conscious impairment-aware routing," in *Optical Fiber Communication Conference, 2004*, San Diego, CA, 2004.

[177] Y. Huang, J. P. Heritage, and B. Mukherjee, "Connection provisioning with transmission impairment consideration in optical WDM networks with high-speed channels," *Journal of Lightwave Technology*, vol. 23, no. 3, pp. 982–993, Mar. 2005.

[178] E. Marin *et al.*, "Applying prediction concepts to routing on Semi-Transparent optical transport networks," in *2007 9th International Conference on Transparent Optical Networks*, Institute of Electrical and Electronics Engineers (IEEE), 2007.

[179] B. Ramamurthy, D. Datta, H. Feng, J. P. Heritage, and B. Mukherjee, "Impact of transmission impairments on the teletraffic performance of wavelength-routed optical networks," *Journal of Lightwave Technology*, vol. 17, no. 10, pp. 1713–1723, 1999.

[180] Y. Pointurier, M. Brandt-Pearce, T. Deng, and S. Subramaniam, "Fair QoS-Aware Adaptive routing and wavelength assignment in all-optical networks," in *2006 IEEE International Conference on Communications*, Institute of Electrical and Electronics Engineers (IEEE), 2006.

[181] F. W. Glover and M. Laguna, *Tabu search*, 3rd ed. Boston, MA: Kluwer Academic Publishers, 1997.

[182] S. Voß, *Meta-heuristics: the state of the art, in: Local Search for Planning and Scheduling*, A. Nareyek, Ed. Springer Science + Business Media, 2001, pp. 1–23.

[183] G. S. Pavani and H. Waldman, "Adaptive routing and wavelength assignment with power constraints using ant colony optimization," in *2006 International Telecommunications Symposium*, Institute of Electrical and Electronics Engineers (IEEE), 2006.

[184] K. Lee and M. A. Shayman, "Optical network design with optical constraints in multi-hop WDM mesh networks," in *Proceedings. 13th International Conference on Computer Communications and Networks (IEEE Cat. No.04EX969)*, Institute of Electrical and Electronics Engineers (IEEE), 2005.

[185] S. Azodolmolky, M. Klinkowski, E. Marin, D. Careglio, J. S. Pareta, and I. Tomkos, "A survey on physical layer impairments aware routing and wavelength assignment algorithms in optical networks," *Computer Networks*, vol. 53, no. 7, pp. 926–944, May 2009.

[186] M. Dorigo, T. Stützle, and T. Stutzle, *Ant colony optimization*. Cambridge, MA: Bradford Books, 2004.

[187] I. Karamitsos and C. Bowerman, "A resource reservation protocol with linear traffic prediction for OBS networks," *Advances in Optical Technologies*, vol. 2013, pp. 1–6, 2013.

[188] M. A. C. Lima, A. C. Cesar, and A. F. R. Araujo, "Optical network optimization with transmission impairments based on genetic algorithm," in *Proceedings of the 2003 SBMO/IEEE MTT-S International Microwave and Optoelectronics Conference - IMOC 2003. (Cat. No.03TH8678)*, Institute of Electrical and Electronics Engineers (IEEE), 2003, pp. 361–365.

[189] T. P. Valencia, A. M. H. Moncayo, and J. G. L. Perafan, "Cognitive Control Based on Genetic Algorithm for Routing and Wavelength Assignment in Optical OBS/WDM Networks," in *INNOV 2013: The Second International Conference on Communications, Computation, Networks and Technologies*, 2013.

[190] H. T. T. Binh and H. D. Ly, "Genetic algorithm for solving multilayer survivable optical network design problem," *International Journal of Machine Learning and Computing*, pp. 812–816, Dec. 2012.

[191] A. Muhammad, "Planning and provisioning strategies for optical core networks," PhD, Linkoping University, Sweden, 2015.

[192] E. Varvarigos, "An introduction to routing and wavelength assignment algorithms for fixed and flexgrid," in *Optical Fiber Communication Conference/National Fiber Optic Engineers Conference 2013*, The Optical Society, 2013.

[193] Y. Zhai, Y. Pointurier, S. Subramaniam, and M. Brandt-Pearce, "Performance of dedicated path protection in transmission-impaired DWDM networks," in *2007 IEEE International Conference on Communications*, Institute of Electrical and Electronics Engineers (IEEE), 2007.

[194] S. Pachnicke and P. M. Krummrich, "Constraint-based routing in path-protected translucent optical networks considering fiber nonlinearities and polarization mode dispersion," in *Optical Transmission, Switching, and Subsystems VI*, SPIE-Intl Soc Optical Eng, 2008.

[195] Y. Pointurier, "Cross-layer design of all-optical networks incorporating crosstalk effects," PhD, University of Virginia, 2006.

[196] T. Deng and S. Subramaniam, "Adaptive QoS routing in dynamic wavelength-routed optical networks," in *2nd International Conference on Broadband Networks, 2005.*, Institute of Electrical and Electronics Engineers (IEEE), 2005.

[197] K. Manousakis, P. Kokkinos, K. Christodoulopoulos, and E. Varvarigos, "Joint online routing, wavelength assignment and Regenerator allocation in translucent optical networks," *Journal of Lightwave Technology*, vol. 28, no. 8, pp. 1152–1163, Apr. 2010.

[198] T. Ivaniga and P. Ivaniga, "Evaluation of the bit error rate and Q-factor in optical networks," *IOSR Journal of Electronics and Communication Engineering*, vol. 9, no. 6, pp. 01–03, 2014.

[199] M. S. Hossain, S. Howlader, and R. Basak, "Investigating the Q-factor and BER of a WDM system in Optical Fiber Communication Network by using SOA," *International Journal of Innovation and Scientific Research*, vol. 13, no. 1, pp. 315–322, Jan. 2015.

[200] J. Zhao, S. Subramaniam, and M. Brandt-Pearce, "Intradomain and Interdomain QoT-Aware RWA for translucent optical networks," *Journal of Optical Communications and Networking*, vol. 6, no. 6, pp. 536–548, May 2014.

[201] C. D. Cantrell, "Transparent optical metropolitan-area networks," in *The 16th Annual Meeting of the IEEE Lasers and Electro-Optics Society, 2003. LEOS 2003.*, Institute of Electrical and Electronics Engineers (IEEE), 2003.

[202] D. Cavendish, A. Kolarov, and B. Sengupta, "Routing and wavelength assignment in WDM mesh networks," in *Globecom 2004*, 2004, pp. 1016–1022.

[203] E. Hyytiä and J. Virtamo, "Dynamic Routing and Wavelength Assignment Using First Policy Iteration," in *Fifth IEEE Symposium on Computers and Communications (ISCC 2000)*, 2000.

[204] A. Alyatama, "Wavelength decomposition approach for computing blocking probabilities in WDM optical networks without wavelength conversions," *Computer Networks*, vol. 49, no. 6, pp. 727–742, Dec. 2005.

[205] A. Girard, *Routing and Dimensioning in Circuit-switched Networks*. Addison Wesley, 1990.

[206] D. Jagerman, "Some properties of the erlang loss function," *Bell System Technical Journal*, vol. 53, pp. 525–551, 1974.

[207] "Small Network Equipment," in *Energy Star*. [Online]. Available: http://www.energystar.gov/index.cfm?c=new_specs.small_network_equip. Accessed: Mar. 11, 2015.

[208] B. G. Bathula, M. Alresheedi, and J. M. H. Elmirghani, "Energy Efficient Architectures for Optical Networks," in *IEEE London Communications Symposium*, 2009.

[209] B. G. Bathula and J. M. H. Elmirghani, "Green Networks: Energy Efficient Design for Optical Networks," in *Sixth IEEE International Conference on Wireless and Optical Communications Networks (WOCN2009)*, 2009.

[210] B. G. Bathula and J. M. H. Elmirghani, "Constraint-based Anycasting over optical burst switched networks," *Journal of Optical Communications and Networking*, vol. 1, no. 2, p. A35, Jun. 2009.

[211] X. Huang, Q. She, T. Zhang, K. Lu, and J. P. Jue, "Modelling and performance analysis of small group multicast with deflection routing in Optical Burst Switched networks," *IEEE Journal of Selected Areas in Communications*, vol. 26, no. 3, pp. 74–86, 2008.

[212] A. Muhammad, P. Monti, I. Cerutti, L. Wosinska, P. Castoldi, and A. Tzanakaki, "Energy-efficient WDM network planning with dedicated protection resources in sleep mode," in *2010 IEEE Global Telecommunications Conference GLOBECOM 2010*, Institute of Electrical and Electronics Engineers (IEEE), 2010.

[213] X. Dong, "Green Optical Networks," PhD, University of Leeds, Leeds, UK, 2012.

[214] R. Aparicio-Pardo, P. Pavon-Marino, and S. Zsigmond, "Mixed line rate virtual topology design considering nonlinear interferences between amplitude and phase modulated channels," *Photonic Network Communications*, vol. 22, no. 3, pp. 230–239, Jul. 2011.

List of Publications

[1] ***Andrew Mutsvangwa*** and Bakhe Nleya. Enhanced Congestion Management for OBS Network Performance Degradation Minimization. (*Under Review*, SAIEE Africa Research Journal 2016)

[2] Pule, B. Nleya and ***Andrew Mutsvangwa***. A Cluster Network Based Distributed Resource Management Scheme For OBS Networks. *In Proceedings of the Third International Conference on Advances in Computing, Communication & Engineering (ICACCE-2016)*, 28-29 November 2016. Durban, South Africa.

[3] ***Andrew Mutsvangwa***, B. Nleya, M. Gomba and N. Ngeama. Evaluation of End-to-End Latency for Segmented Bursts in OBS Networks. *In Proceedings of the Third International Conference on Advances in Computing, Communication & Engineering (ICACCE-2016)*, 28-29 November 2016. Durban, South Africa.

[4] ***Andrew Mutsvangwa*** and Bakhe Nleya. A study of the Performance of a Physical Layer Impairment-aware RWA. *In Proceedings of Southern Africa Telecommunication Networks and Applications Conference (SATNAC) 2016*, Fancourt, George, 04-07 September, 2016.

[5] Bakhe Nleya, & Jeaff Ngeama, ***Andrew Mutsvangwa***. Physical Impairments Aware Routing for Translucent Optical Networks. *In Proceedings of Southern Africa Telecommunication Networks and Applications Conference (SATNAC) 2016*, Fancourt, George, 04-07 September, 2016.

[6] ***Andrew Mutsvangwa***, Bakhe Nleya and Tshepiso Mooketsi. Secured Access Control Architecture Consideration For Hybrid Smart Grids. *IEEE's Power Energy Society International Conference*, 28 June -02 July, 2016. Livingstone, Zambia.

[7] Mendon Dewa, ***Andrew Mutsvangwa*** and Bakhe Nleya. Smart Grid Based Algorithm For Improving the Energy Efficiency of Large Scale Cooperating Distributed Systems. *IEEE's Power Energy Society International Conference*, 28 June -02 July, 2016. Livingstone, Zambia.

[8] Tshepiso Nicole Mooketsi, Bakhe Nleya, Mendon Dewa and ***Andrew Mutsvangwa***. A Secured Access Control Architecture Consideration For PLC based Smart Grids.

In Proceedings of Southern Africa Telecommunication Networks and Applications Conference (SATNAC) 2015.

[9] Ndadzibaya Gomba, Bakhe Nleya, and ***Andrew Mutsvangwa***. A Congestion Avoidance/Minimization Approach for Optical Burst Switched Backbone Networks. *In Proceedings of Southern Africa Telecommunication Networks and Applications Conference (SATNAC) 2015*.

[10] Ndadzibaya Gomba, Bakhe Nleya, ***Andrew Mutsvangwa***. Class Segmented Burst Assembling Approach in OBS Networks. *In Proceedings of the IEEE's International Conference*, 14-17 September 2015, Addis Ababa.

[11] Ndadzibaya Gomba, Bakhe Nleya, ***Andrew Mutsvangwa***. A Congestion Minimization Strategy for OBS Backbone Networks. *In Proceedings of the IEEE's International Conference*, 14-17 September 2015, Addis Ababa.

[12] Bakhe Nleya and ***Andrew Mutsvangwa***, (2014). QoS Considerations in OBS Switched Backbone Networks. *Global Journal of Computer Science and Technology*, Volume XIV, Issue V.